Title
RAS Signal Transduction: Insights from RIN1 Effector Pathway Studies

Permalink
https://escholarship.org/uc/item/97h9m62h

Author
Ting, Pamela

Publication Date
2015

Peer reviewed|Thesis/dissertation

UNIVERSITY OF CALIFORNIA

Los Angeles

RAS Signal Transduction: Insights from RIN1 Effector Pathway Studies

A dissertation submitted in partial satisfaction of the requirements

for the degree Doctor of Philosophy

in Biological Chemistry

by

Pamela YF Ting

2015

ABSTRACT OF THE DISSERTATION

RAS Signal Transduction: Insights from RIN1 Effector Pathway Studies

by

Pamela YF Ting

Doctor of Philosophy in Biological Chemistry

University of California, Los Angeles, 2015

Professor John Colicelli, Chair

The small G protein, RAS, transduces signals from receptor tyrosine kinases at the plasma membrane to the interior of the cell, mediating cell proliferation, differentiation, apoptosis and senescence. Guanine nucleotide exchange factors (GEFs) and GTPase activating proteins (GAPs) tightly regulate RAS activation. Dysregulation of this process through activating mutations in RAS is responsible for 16% of all human tumors. Prior research has focused on regulation of RAS activity by GEFs and GAPs, but recently scientists have begun to uncover a role for posttranslational modifications in RAS regulation. In Chapter Two we describe the identification of a novel ABL tyrosine phosphorylation site on RAS (RAS-Y^{137}) that allosterically regulates RAS activation and effector binding. Furthermore, phosphorylation at this site is significantly enhanced by overexpression of the RAS effector RIN1, which binds to and

activates its effector ABL. This suggests that RAS-stimulated RIN1 can drive ABL-mediated RAS modification and regulation in a novel feedback circuit.

In response to activation by RAS binding, RIN1 signals through two downstream effectors – the small GTPase RAB5 and the non-receptor tyrosine kinase ABL – and mediates endocytosis and cytoskeleton remodeling. Consistent with this role, RIN1 localizes to the cytoplasm and can be recruited to the plasma membrane by activated RAS. However, previous studies have sporadically reported nuclear localization of RIN1. Chapter Three describes the novel cell-cycle dependent nuclear localization of RIN1. RIN1 nuclear localization peaks in G2 phase, and is regulated by three nuclear localization sequences and three serine residues. Multidimensional protein identification technology (MudPIT) analysis found that during G2 phase nuclear RIN1 binds to chaperones, nucleic acid binding proteins and ribonucleoproteins. These data suggest a novel pathway by which this RAS effector influences signal transduction from the plasma membrane to the nucleus.

RIN1 binding to its effector ABL relieves ABL autoinhibition and stimulates its kinase activity. Importantly, RIN1 also binds to the leukemogenic fusion protein, BCR-ABL1. Although BCR-ABL1 is considered to be constitutively active, previous work in the lab has demonstrated that RIN1 enhances BCR-ABL1 kinase activity and accelerates BCR-ABL1-induced leukemias in mice. We extend these studies in Chapter Four, examining the requirement for RIN1 in BCR-ABL1 leukemias. We demonstrate that RIN1 is required for BCR-ABL1 bone marrow transformation *ex vivo* and that RIN1 silencing sensitizes drug-resistant cells to the tyrosine kinase inhibitor imatinib. However, we found that RIN1 is not required for BCR-ABL1-induced leukemias in mice, suggesting that while BCR-ABL1 remains responsive to RIN1, this interaction is not required for leukemogensis.

That RIN1 silencing increases sensitivity to the ABL kinase inhibitor imatinib, even in drug-resistant cells, suggested that small molecule inhibitors of the RIN1::BCR-ABL1 interaction might be an effective therapy in combination with existing kinase active site-directed inhibitors. Chapter Five describes the design and implementation of a TR-FRET-based high throughput screen to identify inhibitors of this protein-protein interaction, as well as the identification of two lead scaffolds.

The dissertation of Pamela YF Ting is approved.

Peter A. Edwards

Harvey R. Herschman

Jorge Z. Torres

John Colicelli, Committee Chair

University of California, Los Angeles

2015

TABLE OF CONTENTS

LIST OF FIGURES AND TABLES

CHAPTER 1

CHAPTER 2

CHAPTER 3

CHAPTER 4

CHAPTER 5

ACKNOWLEDGEMENTS

THANK YOU, first and foremost, to my dissertation advisor, Dr. John Colicelli. John has tirelessly supported, encouraged and guided me through graduate school. He has been incredibly kind, patient, calm and generous in giving me space to learn and make mistakes. I am particularly grateful to John for being such an attentive advocate of my growth as a scientist. He has facilitated many collaborations, helped me to sharpen my oral and written communication skills and has made it a habit to pass along interesting papers and talks. And finally, thanks to John, the font on my slides will always be legible from the back of the room, I will always use the word "data" properly as a plural noun, and I will remember to write SRC instead of c-src.

THANK YOU to my committee members: Dr. Peter Edwards, Dr. Harvey Herschman, Dr. Jorge Torres and Dr. Hong Wu for their encouragement and guidance. I am grateful that they have so generously shared their time and expertise. I feel very fortunate to have had these scientists serve on my committee.

THANK YOU to all of my lab and podmates for creating a fun, positive and supportive working environment. I am indebted to Christine, Kavitha, Daniel, Andrew and Judy for preserving my sanity and will always treasure our relationships, our SEAS runs and cake days.

THANK YOU to my friends and family for all their love and care. To Mark, Katrina, Faith, Grace, Ian, Noele, Kostas, Mommy, Daddy and Vicki – thank you for believing in me.

THANK YOU to my past advisors for encouraging my interests in research and science. Dr. Fu-Ming Tao gave me my first taste of research as a high school student. Dr. Lu Chen gave me the opportunity to learn in her lab as an undergrad, and has continued to share her wisdom with me over the years. Dr. Jason Aoto patiently taught me lab techniques when I was an undergrad, and encouraged me to understand the underlying science. Lu and Jason gave me an

incredible foundation on which to build during graduate school, and I am grateful that they invested their time in me.

Finally, THANK YOU to all the incredible co-authors that I've had the great fortune of working with and learning from during my time at UCLA:

Chapter Two is a version of [Ting PY, Johnson CW, Fang C, Vashisht AA, Cao X, Wohlschlegel JA, Graeber TG, Mattos C and Colicelli J. *ABL phosphorylation of HRAS alters intrinsic hydrolysis and effector binding*. Manuscript in preparation.] Dr. Carla Mattos and Christian Johnson performed the hydrolysis and crystallography experiments. Dr. Thomas Graeber and Dr. Cathy Fang identified the RAS-Y^{137} phosphorylation site by mass spectrometry. Dr. James Wohlschlegel and Dr. Ajay Vashisht used MuDPIT to identify RAS-interacting proteins. Dr. Xiaoqing Cao identified RAS as an ABL substrate and started the project.

Chapter Three is a version of [Ting PY, Vashisht AA, Wohlschlegel JA, Colicelli J. *Cell cycle dependent nuclear localization of the RAS effector RIN1*. Manuscript in preparation] Dr. James Wohlschlegel and Dr. Ajay Vashisht used MuDPIT to identify G2 phase-specific nuclear RIN1 binding partners. Edward Chang and Elaine Tam enthusiastically cloned many of the RAS and RIN1 constructs.

Chapter Four is a version of [Thai M, Ting PY, McLaughlin J, Cheng D, Muschen M, Witte ON, Colicelli J. *ABL Fusion Oncogene Transformation and Inhibitor Sensitivity are Mediated by the Cellular Regulator RIN1*. Leukemia, 2011. 25, 290-300]. Dr. Minh Thai generously allowed me to work with and learn from him on this project during my first year in the lab. Minh created the expression constructs and lentivirus stocks and performed immunostaining, immunoprecipitation, immunoblotting and *ex vivo* bone marrow experiments. Dr. Owen Witte, Dr. Jami McLaughlin and Donghui Cheng performed bone marrow

PAMELA YF TING – BIOGRAPHICAL SKETCH

EDUCATION

University of California, Los Angeles   Sept. 2008-present
Candidate for Doctorate of Philosophy, Biological Chemistry

University of California, Berkeley   Aug. 2004-May 2008
Bachelor of Arts in Molecular and Cell Biology, Immunology

PUBLICATIONS

Ting PY, Damoiseaux R, Titz B, Bradley KA, Graeber TG, Fernandez-Vega V, Bannister TD, Chase P, Nair R, Scampavia L, Hodder P, Spicer TP, Colicelli J. Identification of small molecules that disrupt ABL interaction with positive regulator RIN1 by high throughput screening. (revised and resubmitted)

John Colicelli, **Pamela Y. Ting** and Christine Janson. RIN Family Proteins (RIN1, RIN2, and RIN3). Encyclopedia of Signaling Molecules. Ed. Sangdun Choi. Springer New York, 2012. 1681-1685

Thai M, **Ting PY**, McLaughlin J, Cheng D, Müschen M, Witte ON, Colicelli J. ABL fusion oncogene transformation and inhibitor sensitivity are mediated by the cellular regulator RIN1. *Leukemia*, **25**(2): 290-300 (2011)

Aoto J, Nam CI, Poon MM, **Ting P** and Chen L. Synaptic signaling by all-trans retinoic acid in homeostatic synaptic plasticity. *Neuron,* **60**(2): 308-20 (2008)

Maghsoodi B, Poon MM, Nam CI, Aoto J, **Ting P**, Chen L. Retinoic acid regulates RARalpha-mediated control of translation in dendritic RNA granules during homeostatic synaptic plasticity. *Proc Natl Acad Sci U S A,* **105**(41): 16015-20 (2008)

Aoto J, **Ting P**, Maghsoodi B, Xu N, Henkemeyer M and Chen L. Postsynaptic ephrinB3 promotes shaft glutamatergic synapse formation. *Journal of Neuroscience,* **27**(28): 7508-19 (2007)

Manuscripts in preparation:

Ting PY, Johnson CW, Cao X, Fang C, Vashisht AA, Wohlschlegel JA, Graeber TG, Mattos C, Colicelli J. ABL phosphorylation of HRAS alters intrinsic hydrolysis and effector binding.

Ting PY, Vashisht AA, Wohlschlegel JA, Colicelli J. Cell cycle-dependent nuclear localization of the RAS effector RIN1.

RESEARCH EXPERIENCE

Graduate Student Researcher, UCLA   Sept. 2008-present
Advisor: Dr. John Colicelli, Professor and Vice Chair, Department of Biological Chemistry
Adopted diverse technical approaches to study the function of the RAS-RIN1-ABL signaling pathway in cell proliferation and cell cycle control, as well as its dysregulation in cancer.

Undergraduate Student Researcher, UC Berkeley 2005-2008
Advisor: Dr. Lu Chen, Department of Molecular and Cell Biology, Neurobiology
Applied lentiviral-mediated genomic manipulation of primary hippocamapal neurons and electron microscopy methods to study the mechanism of synapse formation and homeostatic synaptic plasticity.

High School Student, California State University, Fullerton 2003-2004
Advisor: Dr. Fu-Ming Tao, Department of Chem and Biochemistry, Physical Chemistry
Utilized computational quantum chemistry techniques to demonstrate the effect of explicit water molecules in selectively stabilizing peptide conformations, a result that has important implications for improving computational protein structure prediction.

AWARDS

Whitcome Fellow, UCLA Molecular Biology Institute 2012-2013

Cell and Molecular Biology Training Grant, UCLA 2009-2012

UCLA Department of Biological Chemistry Presentation Award 2011

American Chemical Society 227th National Mtng Physical Chemistry Poster Award 2004

SELECTED ORAL PRESENTATIONS

Biological Chemistry Seminar, Los Angeles, CA 2012
Chemical probes to interrogate RIN1-ABL Signaling

UCLA Department of Biological Chemistry Retreat, Lake Arrowhead, CA 2011
Regulation of RAS signaling by a novel tyrosine phosphorylation

SELECTED POSTER PRESENTATIONS

American Association for Cancer Research Annual Meeting, Washington DC 2013
RIN1 suppresses apoptosis in melanoma cells

Cambridge Healthtech Institute Drug Discovery Chemistry, San Diego, CA 2012
Chemical probes to interrogate RIN1-ABL Signaling

JCCC HTS in Signal Transduction and Translational Medicine, Los Angeles, CA 2011
RIN1::ABL1 protein interaction inhibitors

American Chemical Society 227th National Meeting, Anaheim, CA 2004
Effects of explicit water molecules on the structure and stability of alanine dipeptide conformers: a density functional study

CHAPTER 1. INTRODUCTION

1.1 RAS DISCOVERY, FUNCTION AND REGULATION

RAS discovery

The discovery of RAS emerged from studies of acutely transforming retroviruses isolated from rats. In 1964 Jennifer Harvey discovered the Harvey murine sarcoma virus after observing that a preparation of a murine leukemia virus taken from a leukemic rat rapidly induced formation of sarcomas in newborn rats (1). This was followed in 1967 by the discovery of the Kirsten murine sarcoma virus (2). In 1973 Scolnick provided evidence that the Kirsten virus resulted from transduction of normal cellular rat sequences and hypothesized that it was from this that its transforming properties arose (3). This principle of the cellular origin of retroviral oncogenes was demonstrated by Bishop and Varmus in 1976 (4), a discovery for which they were later awarded the Nobel Prize. In the early 1980s Scolnick and colleagues published studies identifying the cellular counterparts of the viral genes (5,6) and establishing many of the fundamental properties of RAS such as guanine nucleotide binding and membrane association (7).

RAS structure

The RAS proteins HRAS, KRAS and NRAS are founding members of the Ras superfamily comprising over 150 members that share a conserved structure and GDP/GTP-regulated biochemistry (reviewed in (8)). RAS is made up of five alpha helices and six beta sheets. GTP-binding and hydrolysis are mediated by five conserved regions, or G boxes, designated G-1 to G-5. These five sequence regions are critical in guanine nucleotide exchange and hydrolysis, each serving distinct functions in nucleotide binding and coordination of a Mg^{2+} ion that is important for hydrolysis (reviewed in (9)).

Guanine nucleotide exchange and hydrolysis

In the inactive state, GDP is bound. Exchange of GDP for GTP induces conformational changes in two flexible chains known as Switch I and Switch II, creating the effector binding domains of activated RAS. GTP hydrolysis returns RAS to its inactive conformation. The intrinsic GTPase rate of RAS proteins is low (4.2×10^{-4} s^{-1} for HRAS [10]), but can be stimulated by GTPase activating proteins (GAPs) such as RASA1 (a.k.a. p120RasGAP) [11,12]. RASA1 inserts the side chain of Arg^{789} into the active site of RAS to neutralize the developing charge on the gamma phosphate of GTP and thereby stabilizing the transition state. Switch II is stabilized by RASA1 binding, allowing Gln^{61} to stabilize the nucleophilic water molecule and contribute to the stability of the transition state [13].

Guanine nucleotide exchange factors (GEFs) catalyze the exchange of GDP for GTP, a slow process that would otherwise be rate-limiting. This occurs via displacement of the Switch I region, thus opening up the nucleotide-binding site, as well as displacement of Switch II, which alters the environment of the binding site in such a way that binding of the nucleotide and its associated magnesium ion are no longer favored [14]. Release of GDP enables the loading of GTP, which is present in 10-fold excess [15]. Four subfamilies of GEFs have been identified, each featuring specificity and diversity in expression and regulation (reviewed in [16]).

RAS signaling and effectors

By 1984, Stacey and Kung had demonstrated that RAS induced transformation of NIH3T3 fibroblasts and was sufficient to stimulate entry of quiescent cells into the cell cycle [17]. The following year, Mulcahy and colleagues gave the first indication that RAS functioned downstream of receptor tyrosine kinases (RTKs) by demonstrating that microinjection of anti-RAS neutralizing antibodies blocked proliferation of NIH 3T3s that had been induced to

proliferate by growth factor treatment (18). In the early 1990s, a series of genetic studies in *Drosophila melanogaster* identified a putative nucleotide exchange factor, son of sevenless (SOS), that functioned downstream of receptor tyrosine kinases (19,20), and demonstrated that SOS functioned as an activator of RAS (21). The adapter Growth factor receptor-bound protein 2 (GRB2) was subsequently found to associate with tyrosine phosphorylated RTKs via its SH2 domain (22) and SOS via two SH3 domains (23,24), thus linking RAS activation to RTK signaling.

The signal from activated RTKs, passed from adapters to GEFs, to activate RAS, is subsequently translated further downstream through RAS binding to its effectors (Figure 1-1). To date, more than 10 families of effectors have been described, through which RAS modulates proliferation, differentiation, senescence and apoptosis (reviewed in (25)). RAF1 was the first effector of RAS to be identified. Like RAS, RAF was cloned from a murine retrovirus and shown to efficiently transform NIH 3T3 cells (26). In 1991, Kolch and colleagues demonstrated that RAF1 was required for NIH 3T3 transformation by HRAS or KRAS (27) and in 1993 four groups reported that RAF specifically interacts with activated RAS (28-31). Activation of RAF activity by RAS binding leads to signaling through the MEK-ERK pathway, resulting in transcription and regulation of cell proliferation and differentiation (reviewed in (32)). The RAF-MEK-ERK pathway is often mutationally activated in cancers (reviewed in (33)).

Another well-characterized RAS effector is phosphatidylinositol-3-OH kinase (PI3K), which mediates cell survival and proliferation. RAS interacts with the catalytic subunit of PI3K (34), leading to increased kinase activity and recruitment of AKT to the plasma membrane (35). The PI3K/AKT1/mTOR pathway is also frequently mutated in human cancers (36).
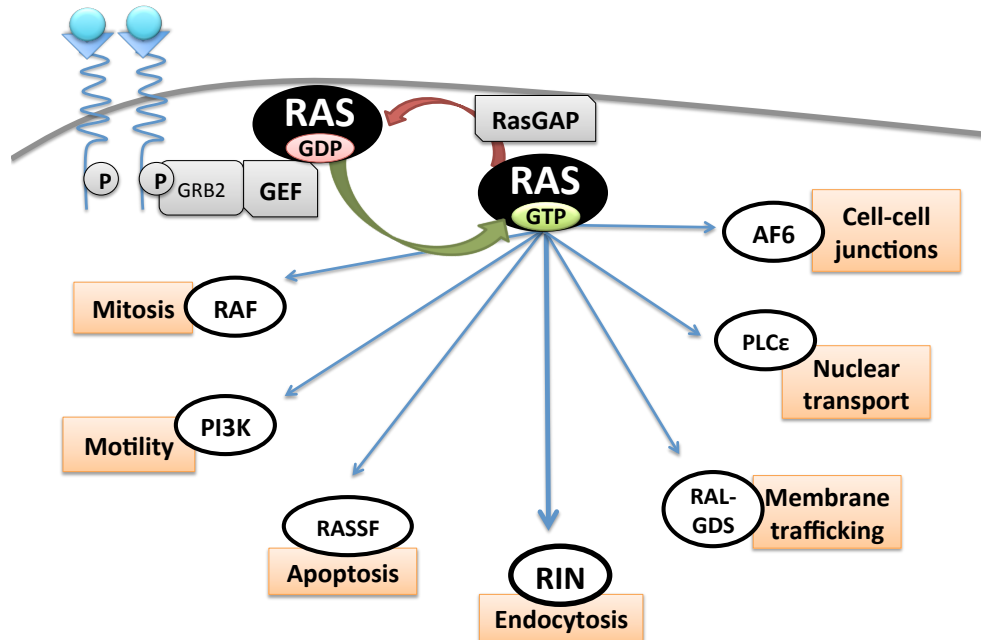
Figure 1-1. RAS activation and signaling. RAS is activated in response to ligand binding to receptor tyrosine kinases at the plasma membrane. Phosphorylated receptor tyrosine kinases recruit the adapter GRB2, which also binds to SOS, a guanine nucleotide exchange factor (GEF) for RAS. RAS-GTP binds to many families of effectors that mediate different cellular functions. RAS signaling is turned off by hydrolysis of GTP to GDP, a process that can be catalyzed by GTPase activating proteins (GAP).

RAS also interacts with RIN, a mediator of endocytosis and cytoskeleton remodeling that is discussed further in Chapter 1.2. Additional effectors include RAL-GEFs (exchange factors that activates RAL proteins) (37), TIAM (exchange factors that activates RAC proteins) (38), RASSF (tumor suppressors) (39) and PLCε (40).

RAS in cancer and other diseases

In the 1970s, Hill and Hillova, and later Wigler and colleagues, demonstrated a technique that allowed the introduction of foreign DNA into mammalian cells by calcium phosphate precipitation (41,42). This enabled scientists to search for suspected oncogenes in the DNA of tumor cells, by examining their ability to induce transformation of NIH 3T3 cells. The first report was published in 1979 when Weinberg and colleagues demonstrated that DNA from rat cell lines transformed by chemical carcinogens could induce foci in NIH3T3 (43). This was

followed by reports of transmissible activated transforming genes from the human EJ bladder carcinoma cell line (44), as well as leukemia, lung and colon cancer cell lines (45,46).

In 1982 three groups reported that the transforming gene isolated from the EJ human bladder carcinoma was the same as the Harvey sarcoma virus oncogene which had first been isolated in 1964 by Jennifer Harvey (47-49). This was rapidly followed by the discovery that a single point mutation, resulting in the incorporation of valine instead of glycine at position 12, was responsible for the transforming properties of HRAS (50-52). This mutation blocks the arginine finger of GAP, making HRAS^{G12V} insensitive to GAP-stimulation of hydrolysis (13,53).

RAS is frequently mutated in human tumors, with an average pan-RAS mutation incidence of 16%. However, mutations occur more frequently in some isoforms than in others. KRAS is the most frequently mutated isoform in most cancers. For example, 90% of pancreatic tumors have mutations in KRAS. NRAS mutations are associated with hematopoietic cancers, while HRAS mutations in tumors are relatively rare. Although most mutations occur at codons 12 and 61, each isoform has a codon mutation bias. For example, 80% of KRAS mutations occur at codon 12. 60% of NRAS tumors harbor mutations at codon 61, while 35% have mutations at codon 12. HRAS has an approximately 50%/40% split between mutations at codons 12 and 61, respectively (54). Overexpression of *HRAS, KRAS* and *NRAS* transcripts is seen in some cancers (55), although this has not been correlated with prognosis. *RAS* amplification has also been detected, although this does not appear to be a common mechanism in cancer (56,57).

Germline *RAS* mutations also contribute to hereditary familial developmental syndromes. These germline mutations are generally less activating than those found in tumors, and can also effect higher guanine exchange dissociation rates (reviewed in (58)). Mutations in *HRAS* cause Costello syndrome, characterized by delayed development and mental retardation, as well as

other abnormalities (59). *RAS* mutations are also associated with Noonan syndrome, a genetic disorder that prevents normal development of many parts of the body. However, Noonan syndrome is genetically heterogeneous and can also be caused by mutations in many components of the RAS-RAF-MEK-ERK signaling pathway including SOS1, KRAS, NRAS and RAF1 (60).

Posttranslational modification of RAS

The first posttranslational modifications of RAS to be described arose out of studies aimed at determining the alterations that allowed RAS to become membrane-bound. The earliest clue came in 1984 when Willumsen and Lowy used deletion mutants to demonstrate that the C-terminus of RAS is required for transformation, membrane association and lipid binding (61). This was followed by studies identifying RAS palmitoylation (62), methylation (63) and in 1989, farnesylation (64,65). RAS terminates with a consensus CAAX sequence that specifies a series of sequential posttranslational modifications consisting of prenylation, proteolysis and methylation (reviewed in (66)). These modifications make RAS hydrophobic at the C terminus, thus mediating a low affinity association with the endomembrane (67,68). One (NRAS and KRAS-4A) or two (HRAS) cysteine residues can also be palmitoylated (69), a requirement for RAS trafficking to the plasma membrane (70). The acylation cycle is dynamic, and regulates RAS localization and activity (71). Unlike the other RAS isoforms, KRAS-4B association with the plasma membrane is mediated by a lysine-rich region in the C-terminal hypervariable domain (72). This association can be disrupted by PKC phosphorylation of S^{181}, causing KRAS-4B to lose association with the plasma membrane and move to the endomembrane (73).

Recently, several other posttranslational modifications of RAS have been reported. C^{118} of RAS can be nitrosylated, leading to enhanced guanine nucleotide exchange (74). Monoubiquitination of K^{147} leads to enhanced GTP loading, as well as enhanced binding to PI3K

6

and RAF (75). HRAS Thr^{144}/Thr^{148} phosphorylation by GSK3β leads to polyubiquitylation and proteasome-mediated degradation (76). In 2014, the first tyrosine phosphorylation was reported on RAS. RAS-Y^{32} phosphorylation by SRC reduces binding to RAF, while increasing binding to GTPase-activating proteins and the rate of GTP hydrolysis (77). Chapter Two describes the discovery of another novel tyrosine phosphorylation site on RAS (Y^{137}), its phosphorylation by ABL, regulation by RIN1 and implications for RAS structure and function.

1.2 RIN FAMILY OF PROTEINS

Discovery of RIN1, a RAS effector

In 1991, RAF1 was demonstrated to be required for NIH 3T3 transformation by HRAS and KRAS (27), and it was later the first RAS effector to be identified (28-31). In the same year, Colicelli, Wigler and colleagues reported three cDNAs that could specifically suppress the heat shock-sensitive phenotype of *Saccharomyces cerevisiae* strains expressing an activated *RAS* gene (78). Han and Colicelli reported direct and specific binding of one of the cDNA-encoded proteins to RAS, in 1995, and the gene was named *RIN1* (RAS interaction/interference) (79).

RIN family proteins

The RIN family of proteins consists of four members: RIN1 (79), RIN2 (80), RIN3 (81) and RINL (82). On the far C-terminal end they share a RAS association domain, which mediates binding to activated RAS (83). Binding is enhanced when RAS is GTP-bound (79) and the affinity is relatively high ($K_d \approx 22$ nM for RIN1-RAS), on par with RAF1-RAS binding affinity (84). Upstream of the RAS association domain in the C-terminus, the RIN family proteins contain a Vps9 domain that stimulates RAB5 guanine nucleotide exchange (85). On the amino-terminus, RIN family members encode an SH2 domain, as well as a proline-rich motif which mediates binding to SH3 domains (86).

The RIN proteins coordinate their various domains to modulate receptor endocytosis and signaling in diverse cell types (80,85,87-95). Dysregulation of RIN family members contributes to many diseases. Overexpression (96-100) or silencing (101,102) of RIN1 is associated with cancer. Homozygous frameshift mutations that reduce RIN2 expression cause a collection of connective tissue disorders termed RIN2 syndrome (103-105). RIN3 polymorphisms are associated with Paget's disease of bone, a metabolic bone disease (106,107), as well as lower limb bone mineral density (108). A recent genome wide association study also implicated variations in the RIN3 loci in late-onset Alzheimer's disease risk (109).

RIN1 expression and regulation

The most well characterized RIN family member is RIN1. RIN1 is strongly expressed in forebrain neurons (86,110), and moderately expressed in hematopoietic (111) and epithelial cells (112). Silencing or overexpression of RIN1 is associated with many types of cancer. RIN1 overexpression in bladder urothelial carcinoma (96), non-small cell lung cancer (97,98), gastric adenocarcinoma (99) and melanoma (100), is associated with poor prognosis and lymph node metastasis. However, in other types of cancer including hepatocellular carcinoma (101) and breast cancer (102), *RIN1* is silenced. In breast tumor cell lines this is accomplished by overexpression of the transcription repressor SNAI1, as well as DNA methylation within the promoter and first exon of *RIN1* (102). Re-expression of RIN1 inhibited anchorage-independent growth in soft agar, as well as initiation and progression of tumorigenesis. SNAI1 is thought to be responsible for regulated expression of *RIN1* in neurons and epithelial cells (113).

Rin1$^{-/-}$ mice are viable but exhibit neuronal defects including enhancements in amygdala long-term potentiation, elevated amygdala-dependent aversive memory (110) and deficits in

latent inhibition and fear extinction (114). Mammary epithelial cells from *Rin1*^{-/-} mice exhibit accelerated cell adhesion and increased motility compared to wild-type cells (112).

RIN1 in endocytosis and cell migration

RIN1 binds activated RAS following growth factor-mediated activation of RTKs at the plasma membrane (84). This binding recruits RIN1 from its residence in the cytoplasm, to the plasma membrane (84), where it mediates endocytosis and trafficking of RTKs (Fig.1-2). This is accomplished by RIN1 coordination of several different functions and binding partners. The Vps9 domain of RIN1 mediates activation of the small GTPase RAB5, which facilitates receptor endocytosis and early endosome fusion (85). RIN1 also binds to the non-receptor tyrosine kinase ABL, and stimulates its kinase activity to modulate actin remodeling, thus coupling endocytosis
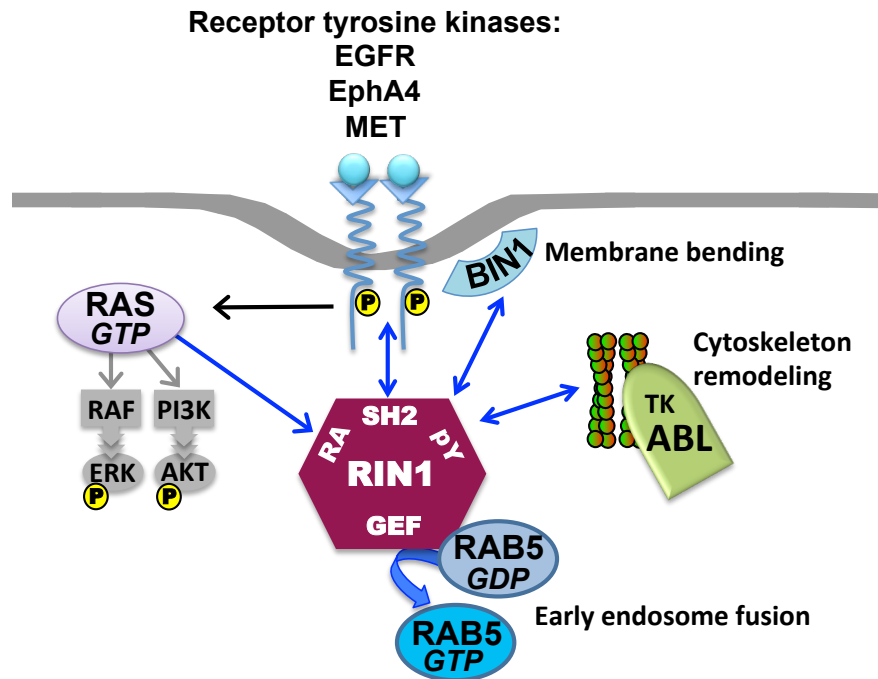
Figure 1-2. RIN1 mediates receptor tyrosine kinase endocytosis. Binding to activated RAS recruits RIN1 to the plasma membrane, where it coordinates its different domains to mediate endocytosis of activated RTKs. RIN1 can bind directly to phosphorylated receptors through its SH2 domain. RIN1 associates with the membrane bending protein BIN1, as well as with ABL to stimulate cytoskeleton remodeling. RIN1 also has GEF activity for RAB5, a small GTPase that regulates early endosome fusion.

with cytoskeleton remodeling (95). Endocytosis can also be modulated by RIN1 recruitment of the membrane bending protein BIN1 (95), direct binding of the RIN1-SH2 domain to tyrosine phosphorylated RTKs (115), and association with STAM, a component of the ESCRT-1 complex which mediates late stage RTK trafficking to lysosomes (116). RIN1 has been implicated in the endocytosis and regulation of RTKs including EGFR (115), IL3R (94) IR (117), EphA4 (91) and MET (92), and functions as a host cell factor in *Listeria monocytogenes* infection (93).

RIN1 binding to and stimulation of ABL kinase activity also regulates growth factor-directed cell migration (112). This process involves both receptor endocytosis and actin remodeling, and requires the ability of RIN1 to coordinate both functions through RAB5 activation and ABL stimulation (118). PKD regulates cell migration, in part, by phosphorylation of RIN1 at S^{292}, which affects RIN1 stimulation of ABL activity (119).

RIN1 subcellular localization

In accordance with its functions in endocytosis and cytoskeleton remodeling, RIN1 is localized in the cytoplasm and can be recruited to the plasma membrane by activated RAS (79,84). Cytoplasmic retention is mediated by 14-3-3 binding (86), in a manner dependent on phosphorylation of RIN1-S^{351} (84). However, nuclear localization of RIN1 has been sporadically observed and reported over the years (96,100,116,119). Chapter Three identifies the cell cycle-dependent nuclear localization of RIN1, its regulation by three nuclear localization sequences and three serine residues, and its nuclear binding partners.

1.3 ABL1, BCR-ABL1 and kinase inhibitors

ABL1 Discovery

As with RAS, the discovery of ABL also had its roots in the study of oncogenic murine retroviruses. In 1970 Herbert Abelson isolated a murine retrovirus that induced leukemia, and it

was later named for him (120). Several years later, in 1976, Bishop and Varmus demonstrated the cellular origin of a retroviral oncogene from a different virus, the Rous sarcoma virus (4). This pioneering work on what came to be known as SRC, as well as the identification of SRC as a protein kinase (121), significantly influenced studies of the Abelson murine leukemia virus. In 1978, Witte and Baltimore identified the protein product encoded by the Abelson murine leukemia virus (122). This was followed shortly by identification of the normal cellular analogue (123), tyrosine phosphorylation of the protein (124) and its protein tyrosine kinase function (125).

ABL structure and function

The ABL family is comprised of two members: ABL1 and ABL2, which share several conserved sequences and structural domains. On the amino-terminus, the proteins have an SH3, an SH2 and a tyrosine kinase domain that are over 90% identical. They also share an N-terminal glycine residue that is myristoylated (126). On the carboxy-terminus, both kinases have a conserved F-actin binding domain (127) as well as a series of P-x-x-P motifs that mediate binding to SH3 domain-containing proteins including CRK (128), ATM (129) and p53 (130). However, the two kinases also possess their own distinct features. ABL1 has G-actin binding (127) and DNA binding domains (131), while ABL2 has a second F-actin binding domain (132). ABL1 also has three nuclear localization sequences (NLSs) (133) and one nuclear export sequence (NES) (134), which allows ABL1 to shuttle between the cytoplasm and nucleus, while ABL2 lacks these sequences and is confined to the cytoplasm.

ABL1 and ABL2 coordinate their different domains to regulate cell proliferation, survival and motility. In the cytoplasm, their F-actin binding domain and tyrosine kinase activity are involved in regulation of actin remodeling. The CRK and CAS family proteins, regulators of

11

cell attachment and motility, are well-studied ABL substrates which share the preferred ABL target site (L,I,V)-pY-x-x-P. The actin remodeling function of ABL also contributes to receptor endocytosis, and many RTKs and endocytic proteins, including RIN1, are phosphorylated by ABL (reviewed in (135)). ABL1 is unique in its involvement in the DNA damage response, and many substrates are known mediators of DNA repair. ABL is required for proper activation of ATM and ATR, as well as proper execution of DNA repair (reviewed in (136)).

Regulation of ABL1 kinase activity

ABL1 activity is normally tightly regulated by a complex set of intramolecular interactions that conformationally restrain the kinase domain. The SH3 and SH2 domains on the N-terminus bind to the face of the kinase domain and allosterically clamp the kinase domain in a conformation with low catalytic activity (137). Binding of the myristoyl group to a deep hydrophobic pocket at the base of the kinase domain is critical to achieve and stabilize the inhibited conformation (138), as is an N-terminal "cap" that binds in several regions across the molecule (139). Additionally the SH3-SH2 connector and SH2-kinase domain linker are also important for autoinhibition (reviewed in (140)).

In the inhibited conformation, the activation loop folds into the active site, blocking substrate and ATP binding (137). Phosphorylation of Y^{412} in the activation loop stabilizes the active conformation of ABL1 (141), as does phosphorylation of Y^{245} of the SH2-kinase domain linker, which the SH3 domain binds to in the inhibited conformation (142). This phosphorylation can occur by SRC-family kinases (143) or in *trans* by other ABL kinase molecules (141). Intermolecular interactions with protein partners that bind the ABL-SH3 and -SH2 domains can also activate ABL. These binding interactions with partners such as RIN1 (144) and CBL (145) release the SH3-SH2 domain clamp from the kinase domain and stimulate kinase activity. Kinase

12

activity can be downregulated by recruitment of phospho-tyrosine phosphatases (146), or by ubiquitylation and subsequent degradation (147).

Discovery of BCR-ABL1

Regulation of ABL activity is of particular interest due to oncogenic activation of ABL1 in chronic myelogenous leukemia (CML), through chromosome translocation and fusion to BCR. In 1960, Nowell and Hungerford were studying whether human leukemias could be characterized by chromosomal abnormalities when they observed an odd, shortened chromosome in two male patients with CML (148). As abnormalities had not been detected by other groups, the findings were published cautiously and with the suggestion that the small chromosome might actually be an altered Y chromosome (149). Samples from females, as well as improved techniques, subsequently identified the "minute" chromosome as chromosome 22 (150), and it was named the Philadelphia chromosome. More than a decade later, Janet Rowley used new staining techniques to track chromosome segments and discovered that the Philadelphia chromosome was the result of a translocation between chromosomes 9 and 22 (151).

In the early 1980s, study of the Philadelphia chromosome collided with a new movement to find the cellular homologs of retroviral oncogenes and map them to chromosomes. In 1979, Witte identified ABL as the normal cellular homolog of the protein encoded by the Abelson murine leukemia virus (123), and in 1982, *ABL* was localized to human chromosome 9 by Heisterkamp and colleagues (152). Separately, Annelies de Klein was investigating the Philadelphia chromosome, in particular whether it contained material from chromosome 9 (reviewed in (153)). Taking advantage of the recent identification of *ABL* on chromosome 9, de Klein, Heisterkamp and colleagues used *ABL* hybridization probes to study *ABL* involvement in

translocation. Surprisingly, they found that *ABL* was present not on the 9q+ chromosome, but on the Philadelphia chromosome, the first suggestion of a role for ABL in CML (154).

BCR-ABL1 regulation

Three different forms of BCR-ABL1 have been identified, differing on the precise translocation breakpoints. The hallmark of CML is p210 BCR-ABL1, which also appears in some cases of B-cell acute lymphocytic leukemia (B-ALL) (155,156). Other forms include p185 BCR-ABL1, which is present in 20-30% of B-ALL cases (157), and p230 BCR-ABL1 (158). BCR-ABL1 is constitutively active due to loss of the amino-terminal myristoyl group and a portion of the cap sequence from ABL1 (139), as well as addition of coiled-coil oligomerization domains from BCR (159). This dysregulated kinase activity is responsible for cell transformation by BCR-ABL1 (160), giving rise to unregulated growth of white blood cells.

BCR-ABL1 regulates a variety of signaling molecules that promote cell proliferation and suppress apoptosis, as well as hematopoietic factors and cytoskeletal proteins. However, for the majority of these signaling molecules, it is unclear whether they contribute to cell transformation, and opposing effects are often reported (reviewed in (161)). BCR-ABL1 does, however, transmit proliferative signals downstream via RAS activation (162). Inactivation of RAS signaling by expression of either a GAP for RAS or a dominant negative form, completely blocks transformation (163).

Kinase inhibition of BCR-ABL1

In the 1990s, several protein kinases including BCR-ABL1, EGFR and PKC, were targeted for development of selective inhibitors because of their dysregulation in cancer. Scientists at Ciba-Geigy (now Novartis) developed the ABL kinase inhibitor STI571 (a.k.a. imatinib, a.k.a. Glivec) using a rational design approach. In the course of screening for inhibitors

of PKC, they had identified a promising compound (a phenylaminopyrimidine derivative) that inhibited PKC and PDGF-R (164). During optimization it was observed that substitutions could be made that conferred inhibitory activity against tyrosine kinases, and abolished PKC inhibitory activity. STI571 was the best compound in the series, and was subsequently selected for clinical development (reviewed in (165)). In 1996, Druker and Lydon reported that the compound specifically inhibited cellular proliferation and tumor formation by BCR-ABL1 expressing cells (166). Several years later in 2001, Druker and Sawyers reported the results of the phase I clinical trial, finding that 53 of 54 patients achieved complete hematologic response. This demonstrated the essential role of BCR-ABL1 kinase activity in CML and the potential for targeted therapies (167).

Despite the efficacy and success of imatinib in targeting BCR-ABL1, many patients treated in the blast crisis phase of the disease ultimately develop resistance and relapse. This drug resistance is associated with reactivation of BCR-ABL1 signal transduction, either by single amino acid mutations or by BCR-ABL1 gene amplification (168). Second generation kinase inhibitors were later developed that are not only more potent than imatinib, but also retain activity against 14 of 15 imatinib-resistant BCR-ABL1 mutants. The only mutant resistant to imatinib, dasatinib and nilotinib is T315I (169,170). Most recently, another kinase inhibitor, ponatinib, was described which could suppress BCR-ABL1 T315I activity (171,172), although it is still subject to inactivation by compound mutations (172,173).

RIN1 and BCR-ABL1

The RAS effector RIN1 binds to ABL, relieving autoinhibition and stimulating kinase activity (144). This interaction is mediated by binding of a proline rich domain on RIN1 to ABL-SH3, phosphorylation of RIN1-Y[36] by ABL and its subsequent association with ABL-SH2 (86).

RIN1 also binds to and positively regulates BCR-ABL1, which retains the SH3/SH2 autoinhibitory domains that mediate RIN1 binding (111) (Figure 1-3). Binding of RIN1 enhances the oncogenic activity of BCR-ABL1 in hematopoietic cells and accelerates BCR-ABL1-induced leukemias in mice (111).
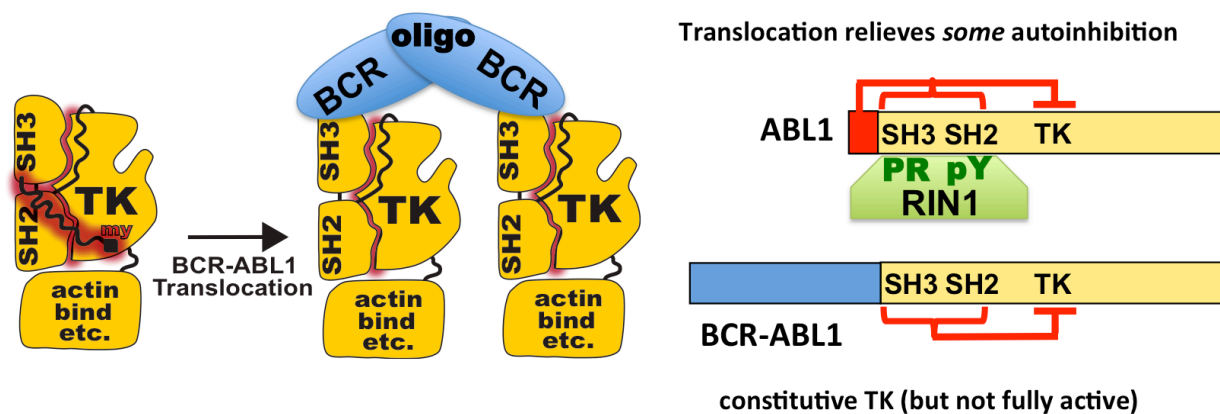
Figure 1-3. Constitutively active BCR-ABL1 retains SH3-SH2 autoinhibitory regions. BCR-ABL1 translocation results in loss of the ABL amino-terminal myristoyl group and cap sequence, and addition of BCR oligomerization domains, resulting in a constitutively active kinase. However, BCR-ABL1 retains the SH3-SH2 autoinhibitory domains. RIN1 binds to ABL SH3-SH2, relieving ABL autoinhibition and stimulating ABL kinase activity.

In Chapter Four we study the requirement for RIN1 in BCR-ABL1 transformation and leukemogenesis, as well as its role in modulating BCR-ABL1 sensitivity to imatinib. Using growth factor independence assays, we demonstrated that RIN1 was required for BCR-ABL1 transformation of murine bone marrow cells. Additionally, RIN1 silencing increased sensitivity to imatinib, even in leukemia cells carrying the imatinib-resistant mutant BCR-ABL1^{T315I} (174). Based on these data we hypothesized that blocking the stimulatory interaction of RIN1 with BCR-ABL1 might decrease kinase activity and offer an alternative mechanism to target BCR-ABL1-driven leukemias. In Chapter Five we describe the design, validation and implementation of a high throughput screen to identify small molecule inhibitors of the RIN1-ABL1 interaction, resulting in the identification of two lead scaffolds.

CHAPTER 2. ABL PHOSPHORYLATION OF HRAS ALTERS INTRINSIC HYDROLYSIS AND EFFECTOR BINDING

[Original Aricle: Ting PY, Johnson CW, Fang C, Vashisht AA, Cao X, Wohlschlegel JA, Graeber TG, Mattos C and Colicelli J. *ABL phosphorylation of HRAS alters intrinsic hydrolysis and effector binding.* **Manuscript in preparation]**

2.1 ABSTRACT

RAS proteins are signal transduction gatekeepers that mediate cell growth, proliferation, survival and differentiation through interactions with multiple effector proteins. The RAS effector RIN1 activates its own downstream effectors, RAB5 and ABL, to modulate receptor endocytosis and cytoskeleton remodeling. To identify ABL substrates that are unique and enriched on this RAS-to-RIN1 signal transduction axis, we compared cells over-expressing different combinations of ABL, RIN1 and RAS. Proteomic analysis revealed several novel phosphotyrosine peptides, including HRAS-pY^{137}. Here we report that ABL family tyrosine kinases can phosphorylate tyrosine 137 of H-, K-, and N-RAS. Increased RIN1 levels enhanced ABL activity and HRAS-Y^{137} phosphorylation, suggesting that RAS-stimulated RIN1 can drive ABL-mediated RAS modification in a feedback circuit. The structures of HRAS^{Y137F} and HRAS^{Y137E} showed conformation changes radiating from the mutated residue. Although consistent with Y137 participation in some type of HRAS allosteric control, the mutations did not alter intrinsic GTP hydrolysis rates *in vitro*. However, HRAS-Y^{137} phosphorylation appeared to enhance HRAS signaling capacity in cells, as measured by association of phosphorylated HRAS^{G12V} with the RAF1 effector protein. These data suggest that RAS tyrosine phosphorylation at Y^{137} may alter protein conformation and effector binding, providing a mechanism for effector-initiated modulation of RAS signaling.

2.2 INTRODUCTION

The vertebrate family of RAS small GTPases is comprised of three members, HRAS, NRAS and KRAS, which function as molecular switches that transduce signals from cell surface receptors to the cytoplasm. RAS is activated by the exchange of GDP for GTP, a process that is catalyzed by guanine nucleotide exchange factors (GEFs) (175,176). Activated RAS can bind to a diverse group of effectors that regulate cell growth, proliferation, survival and differentiation (reviewed in (177)). Specificity and biological relevance of each effector is primarily determined by relative binding affinity and local concentration (reviewed in (178)). GTP hydrolysis returns RAS to an inactive conformation. The intrinsic GTPase rate of RAS proteins is low (3.4×10^{-4} s^{-1} for NRAS) (10), but greatly enhanced by GTPase activating proteins (GAPs) such as RASA1 (a.k.a. p120RASGAP) (179,180). RAS activation status is normally under tight regulation. Indeed, constitutive activating RAS mutations are among the most common driver mutations in human cancers (54).

Several posttranslational modifications contribute to RAS regulation. All three RAS proteins are proteolytically clipped and methylated in conjunction with attachment of a carboxy-terminal prenyl group (64). In HRAS, NRAS and the KRAS-4A isoform, one or two cysteine residues upstream of the prenyl addition site are palmitoylated to further stabilize binding to the plasma membrane (62,64), where receptors and upstream activators reside. Other posttranslational modifications of RAS include monoubiquitylation of Lys^{147}, which enhances GTP loading and increases RAS affinity for the effectors RAF1 and PI3K (75). HRAS Thr^{144}/Thr^{148} phosphorylation by GSK3β leads to polyubiquitylation and proteasome-mediated degradation (76). Phosphorylation of S^{181} of KRAS-4A causes dissociation from the plasma

membrane and is required for tumor growth (73,181), and RAS nitrosylation at Cys^{118} promotes guanine nucleotide exchange (74).

Activated RAS binds a RAS association domain in the carboxy terminus of RIN1 (84,86,182), which transduces downstream signals that modulate receptor endocytosis, cell adhesion and cell migration (95,112,118,183). This is achieved, in part, by RIN1 binding to and stimulating the non-receptor tyrosine kinases ABL1 and ABL2 (112,144). RAS-RIN1-ABL complexes can be detected by several methods including immunoprecipitation (112). The interaction between RIN1 and ABL is initiated by low-affinity binding between a proline-rich motif on RIN1 and the SH3 domain of ABL. ABL subsequently phosphorylates RIN1-Y^{36}, which then binds to the ABL-SH2 domain, resulting a stable divalent interaction (86,111). RIN1 binding stimulates ABL kinase activity by de-repression of an autoinhibitory conformation (144). ABL tyrosine kinases preferentially phosphorylate proteins involved in cell motility, adhesion, endocytosis and DNA damage response, and show specificity for the consensus target sequence Y-x-x-P (reviewed in (135)).

Enhanced ABL signaling is implicated in a wide range of neoplasias (reviewed in (161)), and BCR-ABL1 fusion proteins are the causative genetic abnormality in chronic myelogenous leukemia and many cases of acute lymphocytic leukemia (184,185). BCR fusion confers constitutive kinase activity, but BCR-ABL1 activity is further enhanced by RIN1's de-repression effect. RIN1 binding to BCR-ABL1 is necessary for bone marrow cell transformation to growth factor independence *ex vivo*, and RIN1 silencing sensitizes leukemia cells to the ABL tyrosine kinase inhibitor imatinib (174). In addition, RIN1 is upregulated and associated with poor prognosis in many tumor types including melanoma (100), gastric adenocarcinoma (99), non-small cell lung cancer (97) and bladder urothelial carcinoma (96).

To determine how RAS-RIN1 signaling affects ABL activity and substrate specificity, we used phosphoproteomics to compare cells transfected with different combinations of RAS, RIN1 and ABL2. Unexpectedly, we identified the novel tyrosine phosphorylation site HRAS-pY^{137}. Here we report that ABL can phosphorylate HRAS on Y^{137} *in vitro* and when over-expressed in 293T cells. Phosphorylation is enhanced by HRAS palmitoylation. HRAS-pY^{137} phosphorylation levels were also increased by RIN1 over-expression, consistent with RIN1 involvement in this post-translational modification pathway. The contributions of Tyr^{137} to RAS function were demonstrated by structural analysis and by quantified binding of activated RAS (with or without Y^{137} phosphorylation) to the effector protein RAF1.

2.3 RESULTS

ABL phosphorylates HRAS on tyrosine 137

To better understand how RAS-RIN1 signal transduction regulates ABL activity and substrate specificity, we used proteomic analysis to compare phosphopeptide profiles from cells transfected with ABL2+RIN1 or ABL2+RIN1+HRAS^{G12V} (constitutively active RAS). Cells transfected with ABL2 alone served as a baseline control. The ABL2 isoform of ABL was used because it co-localizes with RIN1 in the cytoplasm (ABL1 is primarily nuclear). We detected the previously unreported phosphopeptide HRAS-pY^{137} in samples from cells transfected with ABL2, RIN1 and HRAS^{G12V} constructs, but not in matched cells without HRAS^{G12V} (Table 2-1).

We hypothesized that Y^{137} phosphorylation could serve as a feedback modification of HRAS for several reasons. First, the signal intensity suggested that phosphorylation at this site is relatively efficient. Second, the residues surrounding HRAS-Y^{137} conform to the ABL target site consensus sequence Y-x-x-P (Figure 2-1A), consistent with a direct ABL substrate. Third, of eight tyrosines conserved in mammalian, fly and worm RAS proteins, Tyr^{137} is the only one not

Substrate	pY site	A	AR	ARR
RIN1	36	8.2×10^6	3.8×10^8	1.4×10^8
FKBP4	220	9.3×10^6	7.5×10^7	5.1×10^7
HRAS	137	-	-	1.3×10^9
HRAS	96	-	1.4×10^4	2.2×10^6
ENO2	43	1.8×10^7	4.7×10^7	1.3×10^7

Table 2-1. Mass spectrometry analysis of tyrosine-phosphorylated peptides. 293T cells were transfected with ABL2 (A), ABL2 + RIN1 (AR) or ABL2 + RIN1 + HRAS (ARR) and phosphotyrosine peptides were enriched and analyzed by mass spectrometry. The most enriched peptides are listed. The data are representative of three independent experiments.

also found in yeast (Figure 2-1A), consistent with Tyr^{137} serving as a phospho-regulatory site that evolved in conjunction with tyrosine kinases. Our data (Table 2-1) also included the previously validated ABL substrates RIN1-pY^{36} and ENO2-pY^{43}, as well as a novel ABL-dependent phosphopeptide, FKBP4-pY^{220}. HRAS-pY^{96}, which can be phosphorylated by the closely related kinase SRC *in vitro* (77)*,* also appeared in our dataset .

We next generated a phospho-specific antibody to HRAS-pY^{137} and tested its specificity using 293T cells that over-expressed ABL2 with HRAS or $HRAS^{Y137F}$. The antibody recognized wild-type HRAS, but not the HRAS mutant with phenylalanine at position 137 (Figure 2-1B). This antibody was also used to quantify *in vitro* kinase assays demonstrating that purified HRAS is phosphorylated in an ABL-dependent manner. This result (Figure 2-1C) is consistent with HRAS serving as a direct ABL substrate.

When wild type ABL2 was replaced with a kinase dead mutant of ABL2 ($ABL2^{K319R}$) in the 293T cell assay, HRAS phosphorylation, could not be detected (Figure 2-1D). Treatment of cells with the ABL tyrosine kinase inhibitors imatinib and dasatinib also decreased HRAS-pY^{137} (Figure 2-1E), arguing against the contribution of contaminating kinases. All three RAS isoforms
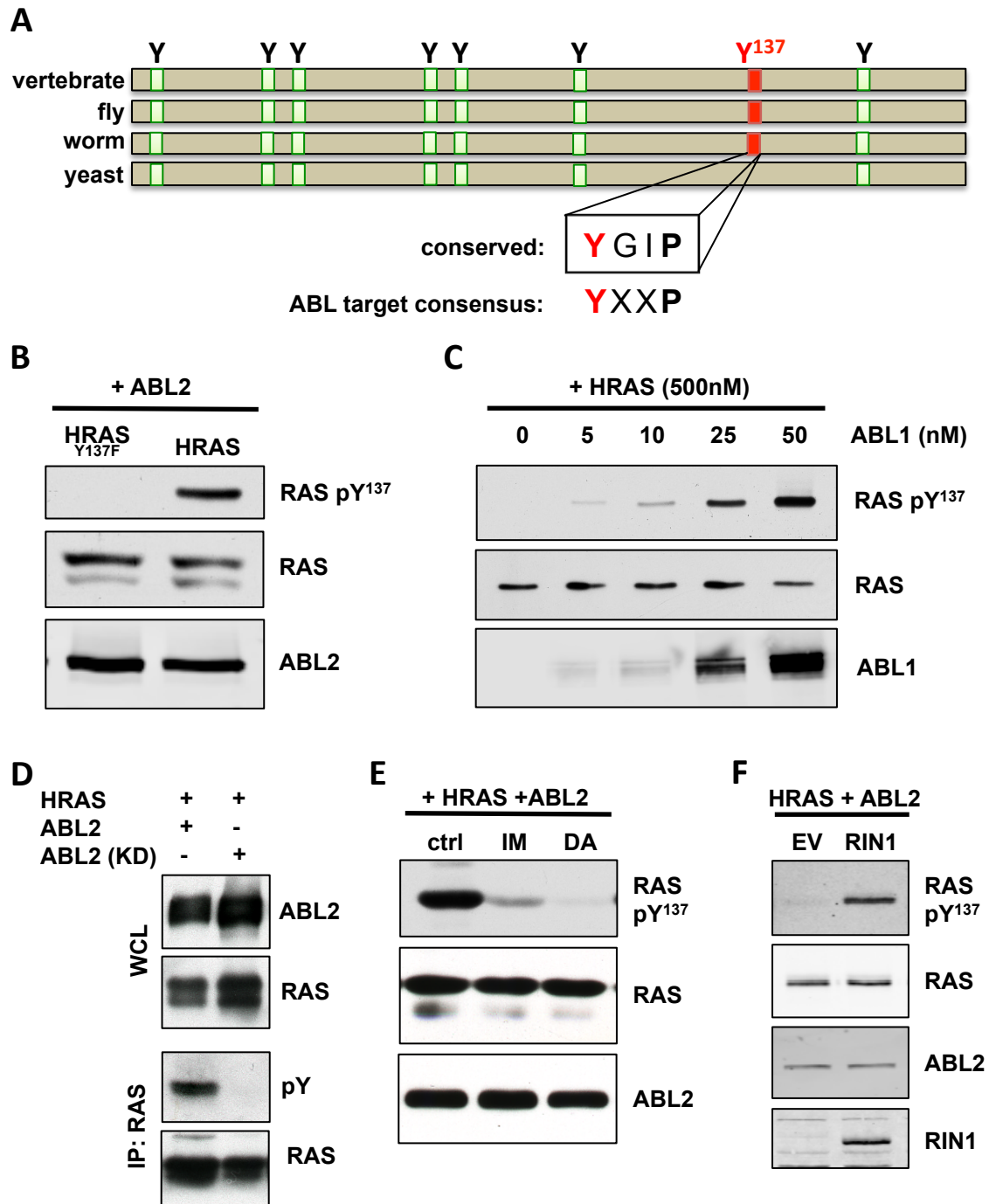
Figure 2-1. ABL phosphorylates HRAS on Tyr[137]. All immunoblot images are representative of at least two independent experiments. (A) Schematic alignment of tyrosine residues in vertebrate, fly, worm and yeast RAS. (B) A phospho-specific antibody against RAS-pY[137] was developed and tested in 293T cells transfected with ABL2 and HRAS or HRAS[Y137F]. (C) *In vitro* kinase assay performed with 500nM purified HRAS and increasing concentrations of ABL1. (D, E, F) 293T cells transfected and analyzed for tyrosine-phosphorylated HRAS. In (D), HRAS and ABL2 or a kinase-dead mutant, ABL2[K319R] (ABL2 KD). In (E), HRAS and ABL2, and treated with imatinib (IM) or dasatinib (DA). In (F), HRAS, ABL2 and empty vector (EV) or RIN1.

22

could be phosphorylated at Tyr[137] by ABL2 (Figure 2-S1A), and both ABL isoforms could phosphorylate HRAS (Figure 2-S1B), indicating a functional conservation across isoforms. Importantly, RIN1 over-expression significantly increased HRAS-pY[137] (Figure 2-1F), suggesting that RAS-RIN1-mediated ABL stimulation feeds back to regulate RAS by tyrosine phosphorylation.
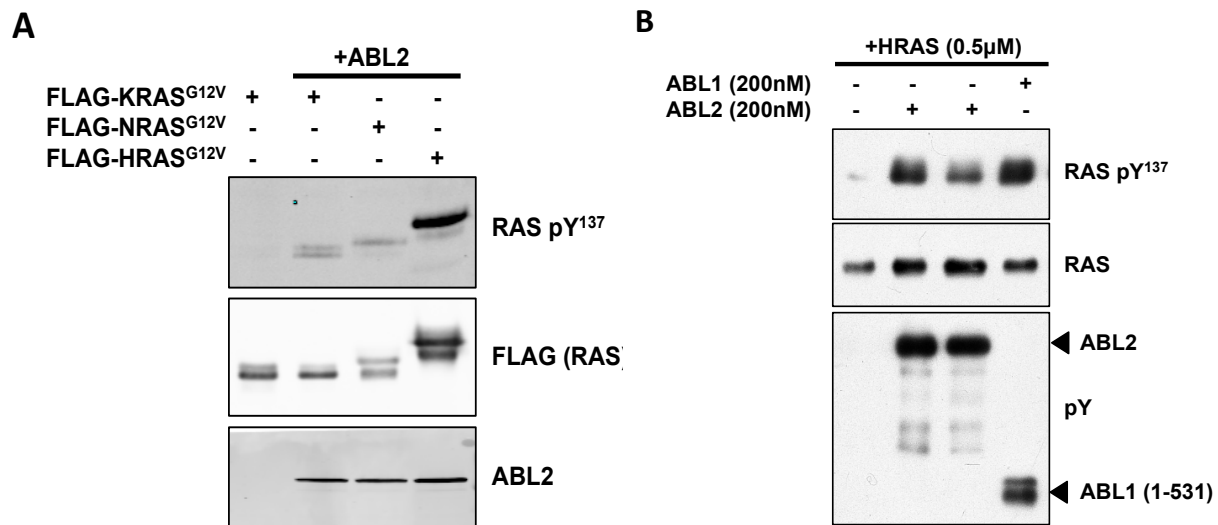
Figure 2-S1. All three RAS isoforms can be phosphorylated, and both ABL isoforms can phosphorylate HRAS. (A) 293T cells were transfected with ABL2 and FLAG-tagged KRAS[G12V], NRAS[G12V] or HRAS[G12V]. (B) *In vitro* kinase assay with 0.5 μM HRAS and 200 nM ABL1(1-531) or ABL2.

ABL phosphorylates active and inactive HRAS

In light of the evidence that RIN1 mediates HRAS phosphorylation, we considered whether guanine nucleotide binding (i.e., activation state) might influence the efficiency of HRAS phosphorylation. 293T cells were transfected with ABL2 and wild-type HRAS, which is primarily GDP-bound due to the slow intrinsic rate of GDP release following hydrolysis (10), or oncogenic HRAS[G12V], which is primarily GTP-bound due to a disabled hydrolysis function and loss of GAP responsiveness (186). Both wild type HRAS and HRAS[G12V] were phosphorylated at

similar levels on Tyr[137] (Figure 2-2A). Likewise, in an *in vitro* kinase assay, HRAS could be phosphorylated regardless of whether it was loaded with GDP or the non-hydrolyzable GTP analog GTPγS (Figure 2-2B).
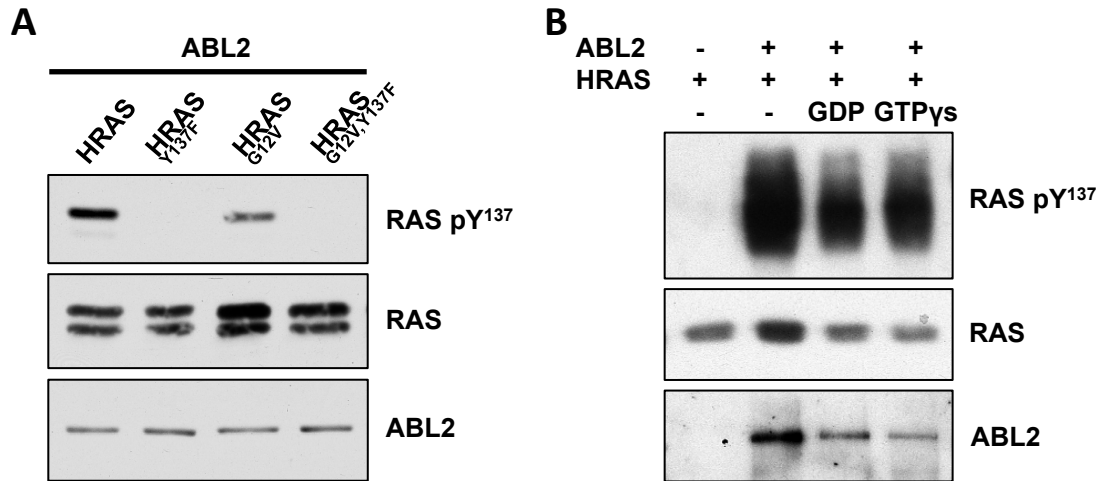
Figure 2-2. ABL2 can phosphorylate GDP- and GTP-bound HRAS. (A) 293T cells transfected with ABL2 and wild-type HRAS (primarily GDP-bound) or HRAS[G12V] (primarily GTP-bound), with corresponding Y137F controls. The immunoblot images are representative of two independent experiments. (B) *In vitro* kinase assay with 200nM ABL2 and 2μM HRAS loaded with GDP or GTPγs.

HRAS-Y[137] phosphorylation is enhanced by RAS palmitoylation

HRAS palmitoylation on cysteines 181 and 184 mediates stable attachment to the plasma membrane. To examine the effect of acylation on HRAS phosphorylation we treated cells with 2-bromopalmitate, an inhibitor of protein palmitoylation enzymes (187). Blocking palmitoylation resulted in decreased HRAS-pY[137] levels (Figure 2-3A). To rule out the possibility that broad inhibition of palmitoylation might influence HRAS phosphorylation indirectly, we created a palmitoylation-defective mutant HRAS[C181S/C184S]. When expressed with ABL2, the palmitoylation-defective mutant exhibited significantly less phosphorylation compared to wild-type HRAS (Figure 2-3B). Together, the results suggest that HRAS palmitoylation facilitates Y[137] phosphorylation.
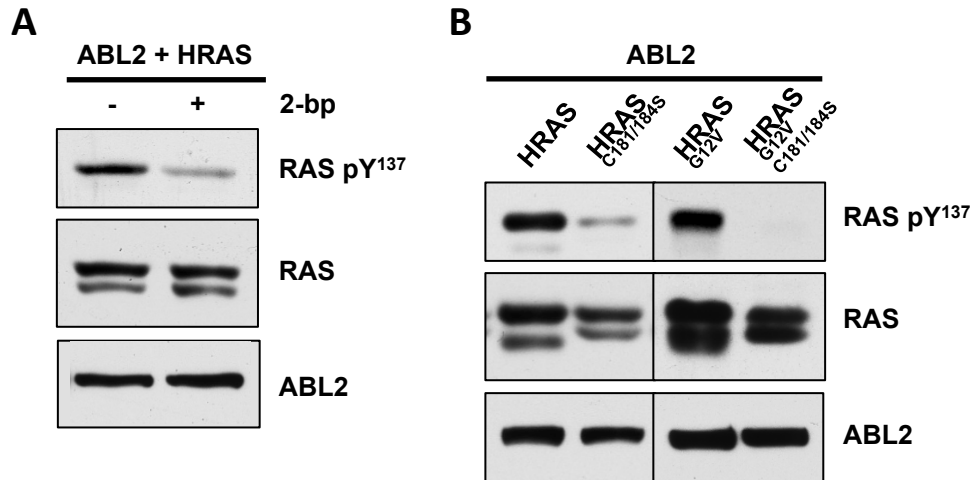
Figure 2-3. Palmitoylation enhances HRAS-Y^{137} phosphorylation. The immunoblot images are representative of two independent experiments. (A) 293T cells transfected with ABL2 and HRAS and treated with 100μM 2-bromopalmitate for 24 hours. (B) 293T cells transfected with HRAS or palmitoylation mutant HRAS$^{C181S/C184S}$, in wild-type and G12V background. Analyzed for Tyr^{137}-phosphorylated HRAS.

HRAS-Y^{137} mutations alter RAF1-dependent intrinsic hydrolysis

We next examined whether Y^{137} phosphorylation altered the rate of GTP hydrolysis, a property fundamental to RAS regulation. RAS proteins have a relatively weak GTPase activity that is enhanced in cells by GAP proteins. Many oncogenic RAS cancer mutations, such as RAS^{G12V}, lead to significantly slower rates of intrinsic hydrolysis as well as reduced responsiveness to GAPs, resulting in persistence of the GTP-bound active RAS conformation (188). We determined k_{cat} in single turnover assays for HRAS, HRAS^{Y137E}, and HRAS^{Y137F}, both alone and in the presence of excess RAF1-RBD (*R*AS *B*inding *D*omain), which binds primarily to RAS protein segments called Switch I and Switch II. The construct used for wild type and mutant RAS proteins in these experiments contained residues 1-166 (all but the C-terminal 23 amino acids). Switch I and II are disordered prior to effector binding (189), but the interaction with RAF1-RBD imposes a stable switch I fold while switch II remains disordered (190).

Hydrolysis measurements in the presence of RAF1-RBD revealed the effect of Y137 modification on switch II, which is allosterically connected to helices 3 and 4 through a water-mediated H-bonding network leading from an allosteric site containing Y137 to catalytic residue Q61 (Figure 2-4A). This network promotes a disordered-to-ordered transition in switch II, completing the active site. While neither mutant produced a significant change in rate compared to HRAS in our single-turnover assays (Figure 2-4B), the HRAS^{Y137E} mutant hydrolyzed GTP at a rate that was 80% of the wild type HRAS rate in the presence of RAF1-RBD. Note that for HRAS^{Y137E} the rate does not change upon RAF1-RBD binding, while the wild type showed a 1.2 fold increase in intrinsic hydrolysis in the presence of RAF1-RBD relative to the uncomplexed protein.
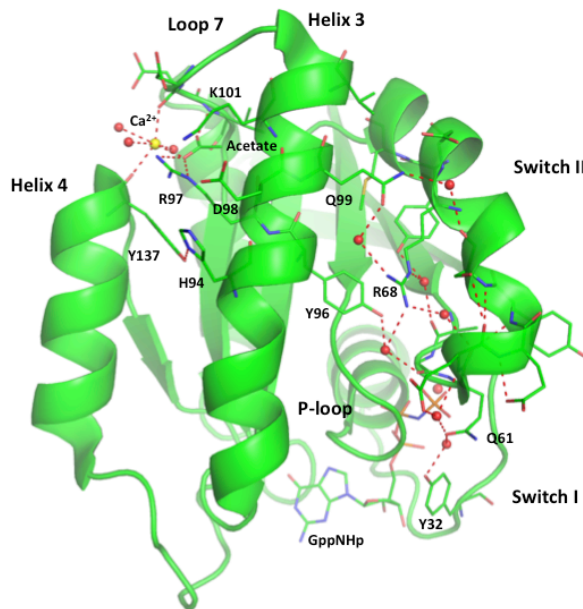
A

B

| kobs | 2.30E-02 | 2.79E-02 | 2.18E-02 | 2.20E-02 | 2.32E-02 | 2.59E-02 |
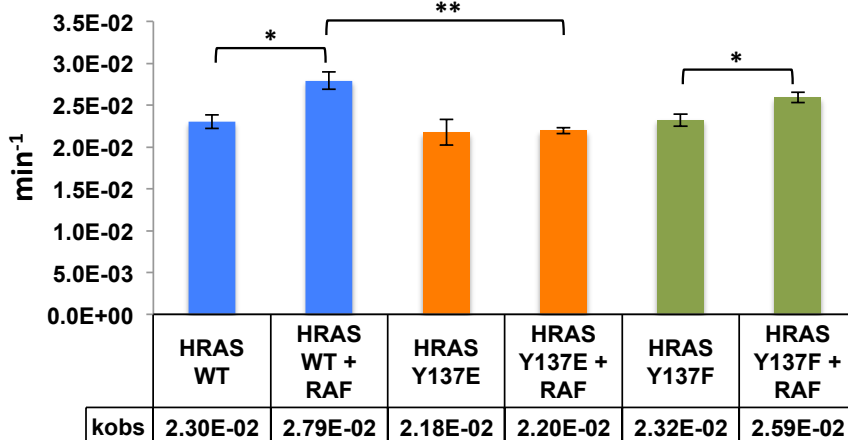
Figure 2-4. Y137E mutation alters instrinsic hydrolysis rate in the presence of RAF1-RBD. (A) Y137 is allosterically connected to Switch I and Switch II by an extensive hydrogen-bonding network. (B) Single turnover intrinsic hydrolysis assays using purified HRAS, with and without RAF1-RBD. * = p-value < 0.05. ** = p-value < 0.01.

HRAS-Y[137] mutations result in long-range conformation effects

To better understand the results of Y137 phosphorylation and its effect on HRAS biochemistry, we purified and crystallized truncated HRAS[Y137E] and HRAS[Y137F] (residues 1-166) bound to a non-hydrolyzable GTP analogue, GppNHp. HRAS[Y137E] and HRAS[Y137F] crystallized with symmetry of the space group P3$_2$21 and with one molecule in the asymmetric unit. The tyrosyl moiety of Y137 of HRAS packs along the aliphatic portion of the R97 side chain and participates in a hydrophobic pocket beneath the allosteric site while simultaneously forming an H-bond with H94. Thus in HRAS, Y137 packs in the protein core, and at the same time bridges helix 3 and 4.

In the Y137E mutant (Figure 2-5A), the aliphatic portion of R97 drops into the cavity occupied by a phenyl ring in the wild type protein, while the R97 guanidinium group forms a salt bridge with the side chain of E137. At the same time, K101 swings down so that its amino group resides in the R97 guanidinium group position of wild type RAS. The repositioned K101 also forms a salt bridge with E137. In the Y137 substitution, the side chain of H94 in helix 3 is somewhat disordered with B-factors around 45 A^2, and helix 4 shifts away from helix 3 to accommodate this reorganization. The active site superimposes well on both structures (Y137E and wild type), even though the N-terminal end of switch II is disordered in the mutant. The allosteric site contains a water molecule that is within good H-bonding distance from both the side chain of E137 and its backbone carbonyl group. The E137-R97 salt bridge may explain the small reduction in GTPase rate seen for HRAS[Y137E] in the presence of RAF1-RBD.

When RAF is bound to RAS, we expect intrinsic hydrolysis to be controlled by an allosteric mechanism, whereby a shift of helix 3 and loop 7 increases switch II stability. This shift of helix 3 is described as a transition from a disordered switch II (T state) to an ordered

switch II (R state), where switch I is already stabilized by RAF1 binding (191). The shift from T- to R-state in HRAS requires that R97 extend out toward the solvent to reduce packing in the hydrophobic pocket and allow helix 3 more room to shift toward helix 4. In HRAS[Y137E] the aliphatic portion of R97 reaches deeper into the hydrophobic core than in the wild type structure (Figure 2-5A), potentially keeping helix 3/loop7 shifted toward switch II, which is poorly ordered as a consequence. Our results suggest that HRAS[Y137E] favors the T-state, which might explain why this mutant has a reduced k_{obs} compared to wild type in single-turnover hydrolysis assays in the presence of RAF1-RBD.

In the RAS[Y137F] mutant (Figure 2-5B), F137 drops its position toward the hydrophobic core consisting of L133, I93, F90 and V113. H94 has become part of this core, with its ring roughly perpendicular to the phenyl ring of F137, although electron density for this residue is not continuous for the side chain. R97 shifts accordingly to stack over F137, and K101 is again near the R97 guanidinium position in the wild type structure. Two crystallographic water molecules are found near the allosteric site. HRAS[Y137F] is similar to HRAS[Y137E] with respect to a poorly ordered switch II. However, the phenylalanine substitution effect on the allosteric site is less prominent than the glutamate substitution, and HRAS[Y137F] may therefore better accommodate the helix 3 shift needed for intrinsic hydrolysis. F137 maintains the same conformation as Y137 in HRAS, while the rest of the allosteric site and helix 3 superimposes nicely with HRAS. This is consistent with our kinetic data for HRAS[Y137F], which showed little difference in the single turnover hydrolysis rate compared to HRAS. Comparison of HRAS[Y137F] and HRAS[Y137E] suggests that the GTPase rate change in the effector-bound form of the glutamate mutant is due to a more constrained helix 3 associated with the allosteric switch mechanism.
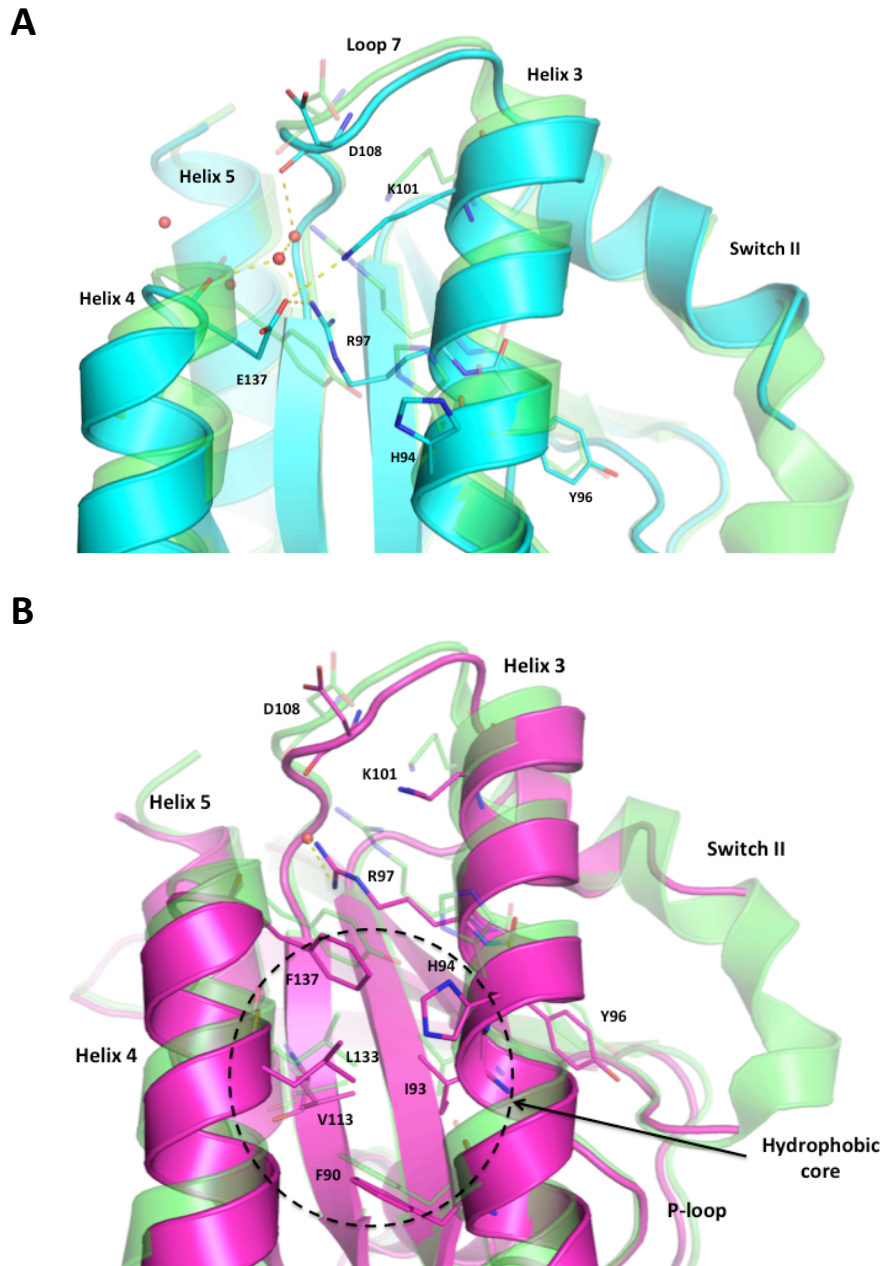
Figure 2-5. Structure of HRAS^{Y137E} and HRAS^{Y137F} superimposed on HRAS. (A) HRAS^{Y137E} (blue) superimposed on HRAS (green). (B) HRAS^{Y137F} (pink) superimposed on HRAS (green).

Although it was not possible to obtain large quantities of the phosphorylated protein for structural biology experiments, information from the wild type and mutant structures have provided insights into the possible effects of Y137 phosphorylation. This bulky, highly charged covalent modification would most likely interact with R97 and/or with K101, as seen for the

29

Y137E mutant. However, unlike the mutant, it would be expected to completely prevent the shift in helix 3 toward helix 4, which is necessary for hydrolysis in the presence of RAF (191,192). Therefore, RAS^{Y137} phosphorylation is likely to severely attenuate GTP hydrolysis activity.

RAF1-RBD binds with higher affinity to HRAS-pY^{137} than to unphosphorylated HRAS

To examine the consequence of tyrosine phosphorylation on HRAS signal transduction we probed binding to RAF1, a well established RAS effector, using 293T cells over-expressing both ABL2 and HRAS^{G12V}. A portion of the whole cell lysate was reserved and the remaining material was incubated with bacterially purified GST-RAF1-RBD, which encodes the RAS-binding domain (RBD) that interacts preferentially with activated (GTP-bound) RAS. In this protocol activated RAS in a cell extract binds to RAF1-RBD and the complex can be pulled down using glutathione sepharose beads. Inactive (GDP-bound) RAS has much lower affinity for the RBD construct. Equal ratios of RAF1-RBD pull down material to whole cell lysate (WCL) were run in separate lanes on an SDS-PAGE gel and immunoblotted for total RAS or RASpY^{137}. If tyrosine phosphorylation of RAS had no effect on hydrolysis rates, we would expect the same amount of RAF1 binding, and hence the same signal ratio (RAF1-RBD/WCL), for both RAS and RASpY^{137} immunoblots (Figure 2-6A). However, the immunoblots showed a 5-fold increase in this ratio when using the anti-RASpY^{137} probe compared to the anti-RAS (total RAS) probe (Figure 2-6B). This result is most easily explained by preferential binding of RAF1 to RAS^{G12V}pY^{137} compared to unphosphorylated RAS^{G12V} (Figure 2-6B).

We used activated RAS^{G12V} to obtain a detectable ratio of GTP-bound RAS in our lysates, as wild type RAS is found almost entirely in the GDP-bound state in lysed cells. Figure 2-6B indeed shows some unphosphorylated RAS^{G12V} could be detected in complex with RAF-RBD. The significantly higher amount of RAS^{G12V} pY^{137} bound to RAF1 in Figure 2-6B is

consistent with a higher proportion of cellular RAS^{G12V} pY^{137} in the GTP-bound state, compared to unphosphorylated RAS. Unfortunately, we have been unable to purify sufficient amounts of phosphorylated RAS to test this directly. However, our results are consistent with the Y137 mutant structure analyses that support an allosteric role for Y137 and suggest that a phosphate group at this position should produce a significant decrease in the rate of GTP hydrolysis.
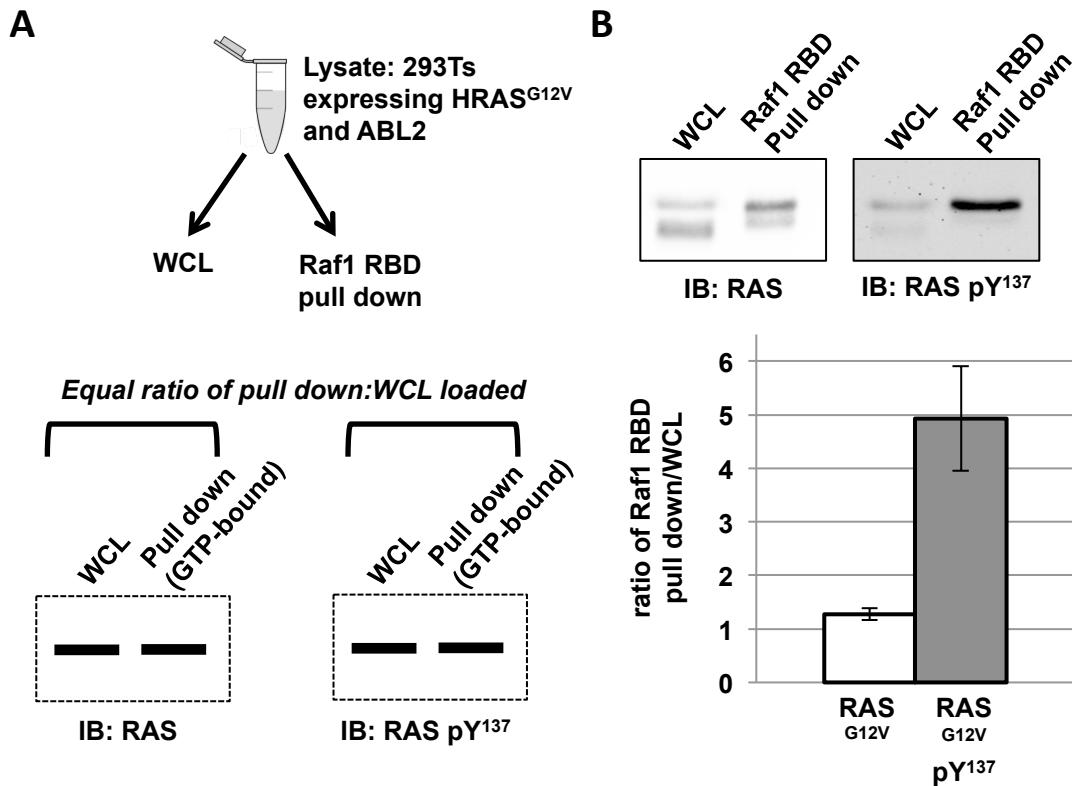
Figure 2-6. Tyr^{137}-phosphorylated HRAS binds with higher affinity to Raf1-RBD than unphosphorylated HRAS. (A) Schematic of experimental design. 293Ts transfected with ABL2 and HRAS^{G12V} are lysed. Part of the whole cell lysate (WCL) is reserved, while the remaining lysate is incubated with GST-Raf1-RBD for a pull down. Equal ratios of pull down to WCL are examined by immunoblot against RAS and RASpY^{137}. If pY^{137} has no effect on Raf1 binding, the ratio of pull down to WCL would be expected to be the same whether analyzed anti-RAS or anti-RASpY^{137}. (B) Raf1-RBD pull down as described in (A). Results were averaged from five independent experiments. p-value = 0.001 (two-tailed equal variant Student's *t*-test)

HRAS-pY[137] binds to RASA1-SH2

Many signal transduction pathways use tyrosine phosphorylation to increase binding affinity for SH2 domains. We therefore considered the possibility that RAS tyrosine phosphorylation conferred new interaction capabilities, and searched for SH2 domains that might bind RASpY[137]. We used a scoring matrix-assisted ligand identification (SMALI) program to predict binders based on pTyr[137] flanking sequences (193). Intriguingly, this non-biased approach identified the carboxy-terminal SH2 domain of RASA1, a GAP that stimulates GTP hydrolysis by RAS proteins.
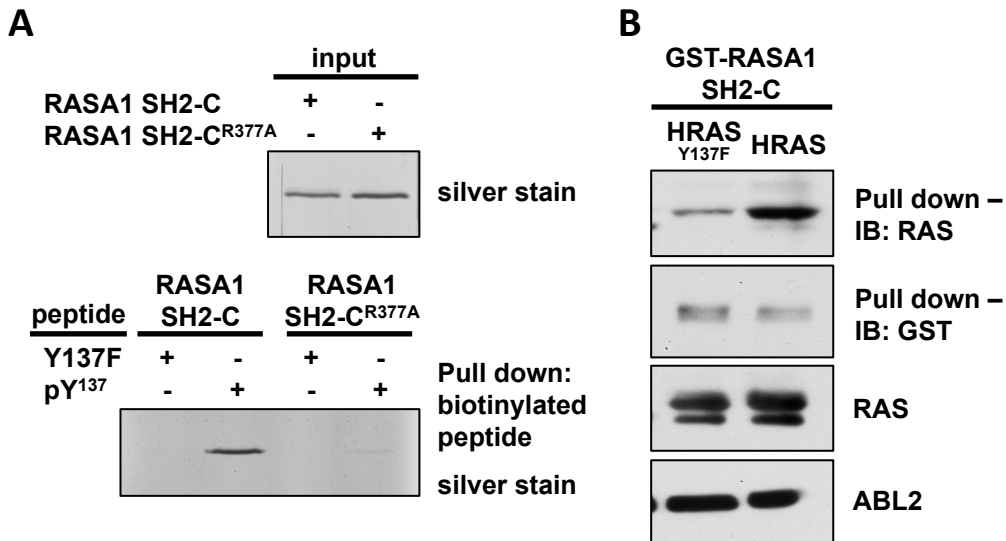
Figure 2-7. HRAS-pY[137] binds to RASA1 C-terminal SH2 domain. (A) biotinylated peptide pull-down of RASA1-SH2C (top). RASA1-SH2C loading control, visualized by silver stain (bottom). Biotinylated pY[137] or Y137F control peptides were incubated with RASA1-SH2C or RASA1-SH2C[R377A] and pulled down with avidin beads. Samples were resolved by SDS-PAGE and visualized by silver staining. (B) 293T cells were transfected with ABL2 and HRAS or HRAS[Y137F]. Cell extract was incubated with 2.5 μg purified GST-RASA1-SH2C and pulled down with glutathione sepharose beads.

We examined the possibility that HRAS-pY[137] binds to the RASA1 C-terminal SH2 domain, using biotinylated RAS peptides and a RASA1 SH2-C domain purified from bacteria. A peptide encoding pY[137] and its flanking sequences efficiently pulled down RASA1 SH2-C, but a mutant peptide with phenylalanine in position 137 was unable to do so (Figure 2-7A). As a

control we employed a RASA1 SH2-C arginine mutation known to impair phosphotyrosine binding (194). Consistent with dependence on a standard SH2 docking arrangement, the pY^{137} peptide pulled down significantly less RASA1 SH2-C^{R377A} than wild type RASA1 SH2-C (Figure 2-7A). Using a reciprocal experimental design, GST-RASA1 SH2-C pulled down more HRAS than $HRAS^{Y137F}$ from cell lysate. These results are consistent with RASA1 SH2-C binding to tyrosine phosphorylated HRAS (Figure 2-7B) and suggested a conditional but stable association between RASA1 and tyrosine phosphorylated RAS proteins.

2.4 DISCUSSION

Despite more than three decades of intense research into RAS protein structure and function, researchers have only recently begun uncovering how RAS post-translational modifications regulate this paradigmatic small GTPase. Here, we report the tyrosine phosphorylation of HRAS-Y^{137} by ABL kinases *in vitro* and in cultured human cells. This post-translational modification is enhanced by over-expression of RIN1, a direct RAS effector and ABL activator expressed in many epithelial, hematopoietic and central nervous system cells (79,110,113). The RIN1 carboxy terminal domain binds to activated RAS while the RIN1 amino terminal region binds to ABL tyrosine kinases, and RIN1 connects RAS with ABL proteins in cultured cells (112). We also note that RAS-Y^{137} resides in a consensus ABL target site conserved in species that express this tyrosine kinase. These data suggest that RIN1 facilitates RAS tyrosine phosphorylation by bringing it in close proximity to an ABL tyrosine kinase catalytic domain. Modulation of RAS tyrosine phosphorylation by RIN1 would represent a novel mechanism for RAS regulation whereby effector binding can result in feedback phosphorylation (Figure 2-8).
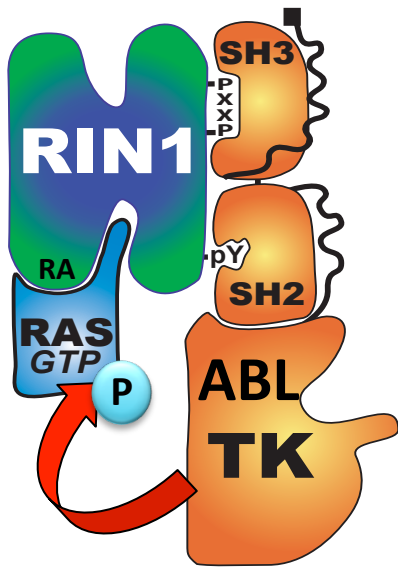
Figure 2-8. HRAS phosphorylation model. RIN1 mediates phosphorylation of RAS by convening ABL and RAS in close proximity. RIN1 binds to ABL through a proline rich domain (PxxP) and pY^{36} binding to ABL SH3 and SH2, respectively. RIN1 binds to RAS through a C-terminal RAS association domain (RA).

To better understand the biological effects of RAS tyrosine phosphorylation by ABL, we searched for endogenous RAS proteins with this modification. We examined diverse conditions while focusing our search on three categories: (1) neurons, where HRAS, RIN1 and ABL are highly expressed, (2) cancer cell lines with constitutively active BCR-ABL or $NRAS^{G12V}$ and (3) growth factor-stimulated epithelial cell lines stimulated with growth factors that activate HRAS, RIN1 and ABL. However, we were unable to identify endogenous RAS-pY^{137} by immunoblot using a phospho-specific antibody or by searching published mass spectrometry datasets. This may not be surprising, as regulatory tyrosine phosphorylations are both infrequent and transient, comprising only about 0.04% of total protein phosphorylation in cells. Tyrosine kinase oncogenes can increase this to about 0.3% (195), but this likely involves an extension of kinase target range and activation of secondary tyrosine kinases.

Because of the difficulty in purifying phosphorylated HRAS, we were unable to directly measure the intrinsic hydrolysis rate of HRAS-pY^{137}. However, conservative mutation of Tyr^{137} to phenylalanine had no detectable effect on the single turnover hydrolysis rate. This was not unexpected, given the minimal structure perturbations in $HRAS^{Y137F}$ relative to wild type HRAS. Mutation of Tyr^{137} to glutamate, which mimics the negative charge of a phosphate group, resulted in a single turnover rate that was 80% of wild type in the presence of RAF1-RBD. Structural analysis reveals changes in the allosteric site due to the negatively charged glutamate

34

that result in a partial disruption of the allosteric switch mechanism associated with the timing of the RAS::RAF1 complex. This conformation shift is consistent with the observed reduction in hydrolysis rate. A bulky phosphate group on Tyr[137] would be expected to exacerbate this effect and further impair intrinsic GTP hydrolysis. If, as predicted, phosphorylation impairs hydrolysis and prolongs the GTP-bound state, this could explain in part why HRAS[G12V]pY[137] was pulled down more efficiently than HRAS[G12V] by the RAF1-RBD effector construct. It remains possible, however, that Tyr[137] phosphorylation triggers allosteric changes in GTP-bound RAS that enhance its affinity for RAF1-RBD.

We provide evidence that HRAS-pY[137] can bind stably to the C-terminal SH2 domain of RASA1, a GAP for RAS. Although it is unclear how this affects RASA1 function and RAS signaling, an intriguing possibility is that a RASpY[137]::RASA1 interaction could modify RASA1 activity and, by extension, the GTP hydrolysis capacity of RAS proteins. This could produce a regulatory circuit in which tyrosine phosphorylation of activated RAS could both hamper intrinsic GTP hydrolysis and modulate the influence of GAPs. Only cells with readily available RIN1 and cytoplasmic ABL would be subject to this form of signal inflection.

To expand our search for proteins that bind pY[137] directly, or that bind a conformation stabilized by pY[137], we used multidimensional protein identification technology (MudPIT) to analyze 293T cells over-expressing ABL2 with HRAS[G12V] or HRAS[G12V/Y137F]. HRAS[G12V] and HRAS[G12V/Y137F] both co-immunoprecipitated with the effector protein RAF1, and no quantitative difference was detected. Surprisingly, the most abundant protein to co-immunoprecipitate with either HRAS mutant was KRAS (Table 2-S1). While RAS homodimers have recently been reported (196,197), this is the first report of binding between different RAS isoforms. We also

pulled down several 14-3-3 isoforms that bound preferentially to HRAS[G12V], but not HRAS[G12V/Y137F] (Table 2-S2).

Protein	HRAS G12V/Y137F				HRAS G12V			
	NSAF	spectra	unique peptides	coverage	NSAF	spectra	unique peptides	coverage
HRAS	37963.933	2570	49	79.9%	48100.408	2691	38	77.8%
KRAS	14520.835	983	26	50.8%	10420.861	583	15	50.8%
RABGGTA	571.182	116	31	40.0%	601.776	101	23	33.5%
RPS16	478.065	25	7	28.1%	138.834	6	4	18.5%
RPL23	279.190	14	5	37.9%	313.698	13	3	30.7%
ZNF615	175.687	46	2	2.9%	402.067	87	2	1.0%
PHB	205.287	20	9	30.9%	347.765	28	9	39.0%
PHB2	233.436	25	9	33.1%	225.973	20	6	23.7%
RABGGTB	134.956	16	7	15.1%	204.126	20	6	16.0%
SLC25A5	187.376	20	8	20.1%	79.356	7	3	11.4%
ATP5B	84.443	16	9	24.6%	70.248	11	6	17.6%
ENO1	51.464	8	4	10.6%	62.273	8	3	12.0%
HADHA	73.182	20	11	18.0%	39.849	9	5	10.7%
GCN1L1	71.078	68	33	13.7%	18.972	15	9	4.8%
RAF1	51.702	12	10	20.4%	10.427	2	2	4.2%

Table 2-S1. HRAS[G12V/Y137F] and HRAS[G12V]-interacting proteins identified by MuDPIT. HRAS[G12V/Y137F] and HRAS[G12V] were expressed in 293T cells with ABL2, immunoprecipitated, and interacting proteins were identified by multidimensional protein identification technology.

Protein	HRAS G12V/Y137F				HRAS G12V			
	NSAF	spectra	unique peptides	coverage	NSAF	spectra	unique peptides	coverage
YWHAZ	0				179.256	13	5	24.9%
SNRPD1	0				170.334	6	2	27.7%
YWHAB	0				164.795	12	3	15.0%
YWHAQ	0				151.678	11	3	15.1%
YWHAG	0				136.773	10	3	15.0%
RPL27A	0				114.131	5	2	14.2%
RPL32	0				100.097	4	2	17.8%
ATP5A1	0				67.199	11	8	17.4%
HSPB1	0				65.918	4	2	12.7%
HADHB	0				28.509	4	3	6.5%
PGGT1B	0				26.883	3	2	5.8%
BFSP2	0				16.281	2	2	7.0%
SEC61A1	0				14.194	2	2	4.4%
KPNB1	0				11.569	3	2	2.7%
RANBP2	0				2.096	2	2	0.9%

Table 2-S2. HRAS[G12V]-interacting proteins identified by MuDPIT. HRAS[G12V/Y137F] and HRAS[G12V] were expressed in 293T cells with ABL2, immunoprecipitated, and interacting proteins were identified by multidimensional protein identification technology.

Tyr^{137} is notably distant from the RAS nucleotide-binding site, as well as the switch I and switch II components of the effector binding region. However, the main chain carbonyl and side chain of Y^{137} participate in a hydrogen bond network that stretches across the molecule to stabilize Switch II in the crystal structure of HRAS with calcium acetate bound near Y^{137} (190). Additionally, recent analysis of multiple solvent crystal structures and computational solvent mapping identified Y^{137} as a member of an allosteric hot spot on H-Ras (198). Our data support the hypothesis that residues remote from the active site, such as Y^{137}, can allosterically modulate RAS function. The crystal structures of HRAS^{Y137E} and HRAS^{Y137F} shed additional light on how RAS post-translational modifications could function as allosteric triggers that influence nucleotide hydrolysis and effector binding.

2.5 MATERIALS AND METHODS

Expression constructs

pcDNA3 ABL2, ABL2^{K319R} (kinase-dead), RIN1, HRAS and HRAS^{G12V} have previously been described (112). pcDNA3 HRAS$^{C181S/C184S}$ palmitoylation mutants were made by amplifying HRAS with forward primer 5'-ATATGCGGCCGAATTCATGACGGAATATAAGCTGGTGGTGGTGGGC-3' and a reverse primer encoding the mutations: 5'-ATATCTCGAGTCAGGAGAGCACACACTTGCTGCTCATGCTGCCGGGGCCACTCTCATC-3'. V5-tagged HRAS was constructed by digesting at the N-terminus and inserting annealed oligos encoding the v5 tag (5'-GGC AAA CCG ATC CCG AAT CCG CTG CTG GGC CTG GAC TCT ACC-3'). HRAS and HRAS^{Y137F} fragments were generated by PCR using primers containing flanking AttB1 and AttB2 sites and cloned into pDONR221 (Invitrogen). These fragments were then subcloned into pcDNA5-FRT/TO-3xHA-3xFLAG.

pFastBac ABL1(1-531) and ABL2 have previously been described (144). pDEST15 RASA1-C SH2 was a gift of Dr. Shawn Li, University of Western Ontario. The R377A mutation was made by site directed mutagenesis using forward primer 5'-GCAGTTTTCTTGTGGCGCCCTCAGATAATACTCC-3' and complementary reverse primer. pGEX-KG-RafRBD (1-149) was a gift of Frank McCormick, University of California, San Francisco. pProExHT-HRAS was a gift of John Kuriyan, University of California, Berkeley. The Y137E mutation was made by site directed mutagenesis using forward primer 5'-GACCTCGCCCGAAGCGAAGGCATCCCCTACATCG-3' and complementary reverse primer. The Y137F mutation was made by site directed mutagenesis using forward primer 5'-CTCGCCCGAAGCTTCGGCATCCCCTAC-3' and complementary reverse primer.

Protein expression and purification

ABL1 and ABL2 were produced in Sf9 insect cells and purified as previously described (144). GST-tagged RASA1-SH2C, RASA1-SH2C^{R377A} and RAF1-RBD were expressed in BL21 bacteria and purified as follows. Bacteria were grown at 37C to OD 0.6, induced with 1mM IPTG and grown at 37C for three hours. Cultures were pelleted, then resuspended in wash buffer (20mM Tris pH8.0, 250mM NaCl, 10% glycerol, 0.01% Triton, protease inhibitors) and sonicated. Lysates were clarified by centrifugation at 15,000xg for 20 minutes at 4°C. Supernatant was rotated with glutathione sepharose beads (GE Life Sciences) for 1 hour at 4°C. Beads were washed over a column four times with wash buffer, then eluted with increasing concentrations of reduced glutathione (5-40mM). Proteins were dialyzed in 50mM Tris pH 8, 50mM NaCl, 1mM DTT and 10% glycerol. Protein concentration was determined by Bradford, and aliquots were frozen at -80°C until use.

His-tagged HRAS, HRAS^{Y137F} and HRAS^{Y137E} were expressed in BL21 bacteria and purified as follows. Bacteria were grown to OD 2.5, then diluted 1:1 with fresh LB. Cultures were induced with 1mM IPTG and grown at 18°C overnight. After pelleting, cells were resuspended in lysis buffer (2.65mM NaH$_2$PO$_4$, 47.35mM Na$_2$HPO$_4$, 500mM NaCl, 20mM imidazole) and sonicated. Lysates were clarified by centrifugation at 15,000xg for 30 minutes at 4°C. Supernatant was rotated with Ni-NTA beads (Qiagen) for 1 hour at 4°C. Beads were washed over a column four times with lysis buffer, then eluted with increasing concentrations of imidazole (150-500mM). Proteins were dialyzed in 25mM Tris pH8.0, 50mM NaCl and stored as above.

Cell culture and reagents

293T cells were cultured in DMEM (Media Tech) with 10% fetal bovine serum (Hyclone) and 1% penicillin streptomycin (Invitrogen). All transfections were performed using Polyfect (Qiagen). Imatinib and dasatinib treatment were performed at 500nM drug for 12 hours, followed by an additional 500nM drug and incubation for 30 minutes before lysing in NP-40 buffer.

Flp-In^{TM} T-REX^{TM}-293 cells (Invitrogen) expressing 3xHA-3xFLAG-HRAS and 3xHA-3xFLAG-HRAS^{Y137F} were generated using the Flp-In system (Invitrogen) according to the manufacturer's directions.

Immunoprecipitation and Immunoblotting

Antibodies used and their sources were – ABL1 1:1000 (Santa Cruz Biotechnology, sc-131), ABL2 1:1000 (Santa Cruz Biotechnology, sc-6356), FLAG 1:3000 (Sigma-Aldrich, F1804) phosphotyrosine 4G10 1:1000 (Millipore, 05-321), RAS 1:10,000 (Novus Bio, EP1125Y), RIN1 1:1000 (mouse mAb, clone C9E11, Colicelli lab, AbPro), v5 1:3000 (Life

Technologies, R960-25). A peptide encoding pY[137] (Ac-AQDLARSpY[137]GIPYI-Ahx-C-amide) was used to generate anti-RAS-pY[137] rabbit polyclonal antibodies that were used 1:500. Antibodies were purified from bleeds by incubating with protein A beads. To eliminate antibodies that bind unphosphorylated Y[137] or the flanking sequence, antibodies were negatively selected over an unphosphorylated peptide (Ac-AQDLARSY[137]GIPYI-Ahx-C-amide), then negatively selected again over bacterially purified GST-HRAS (1-166). Secondary antibodies included sheep-anti-mouse-HRP 1:3000 (Amersham Biosciences, NA931), goat-anti-rabbit-HRP 1:3000 (Kirkegaard and Perry, 4741506), goat-anti-rabbit-IRDye 800 1:5000 (Li-Cor Biosciences, 926-32211) and goat-anti-mouse-IRDye 680 1:5000 (Li-Cor Biosciences, 926-32220).

Mass spectrometry and phosphopeptide identification by fragmentation spectra sequencing and chromatography alignment

HEK 293T cells were cultured in DMEM with 10% FBS and 1% Pen/Strep. Cells were transfected with pcDNA3 RIN1, pcDNA3 ABL2 and/or pcDNA3 HRAS[G12V] using Polyfect (Qiagen). Cells were lysed by sonication in urea buffer (8 M urea, 50 mM Tris-HCl pH 7.5, 1 mM vanadate). Phosphotyrosine peptide were immunoprecipitated with anti-phosphotyrosine antibodies (Millipore, clone 4G10) using 2×10^8 cells as previously described (199).

Phosphorylated peptides were analyzed by LC-MS/MS using an autosampler coupled with Nano2DLC pump (Eksigent) and LTQ-Orbitrap (Thermo Fisher Scientific). The samples were loaded onto an analytical column (10 cm ×75 μm i.d.) packed with 5 μm Integrafit Proteopep2 300 Å C18 (New Objective). Peptides were eluted into the mass spectrometer using a HPLC gradient of 5−40% Buffer B in 45 min followed by a quick gradient of 40−90% Buffer B in 10 min, where Buffer A contains 0.1% formic acid in water and Buffer B contains 0.1%

formic acid in acetonitrile (Ultima Gold, Fisher Scientific). Mass spectra were collected in positive ion mode using the Orbitrap for parent mass determination and the LTQ for data-dependent MS/MS acquisition of the top five most abundant peptides. Each sample was analyzed twice (replicate runs), and in each run, one-half of the sample was injected.

MS/MS fragmentation spectra were searched with SEQUEST (Version v.27, rev. 12, Thermo Fisher Scientific) against a database containing the human International Protein Index (IPI) protein database (ftp.ebi.ac.uk). Search parameters included carboxyamidomethylation of cysteine as static modification. Dynamic modifications included phosphorylation on tyrosine, and oxidation on methionine. Results derived from database searching were filtered using the following criteria: Xcorr >1.0(+1), 1.5(+2), 2(+3); peptide probability score <0.001; dCn >0.1; and mass accuracy <5 ppm (parts per million) with Bioworks version 3.2 (Thermo Electron Corp.). We estimated the false-positive rate of sequence assignments at 0.5% on the basis of a composite target-reversed decoy database search strategy (200). The Ascore algorithm was used to more accurately localize the phosphate on the peptide (http://ascore.med.harvard.edu) (201). As is common in data-dependent MS2 fragmentation sequencing, some peptides identified by sequencing in one sample may not be sequenced or identified in another sample even if the peak is present. Peptide peaks sequenced in some samples but not in others were located in the remaining samples by aligning the chromatogram elution profiles by means of a dynamic time warping algorithm (202). An extended explanation of the strategy used in this work, and example performance results, can be found in the supporting information of Zimman *et al* (199).

In vitro kinase assays

Purified ABL and GST-HRAS were incubated in a kinase buffer (100mM NaCl, 10mM Tris pH7.5, 1mM DTT, 10mM $MgCl_2$, 500µM ATP, 100µM Na_3VO_4, 100µM NaF) for 15

minutes at 30°C. To load HRAS with GDP or GTPγs, purified GST-HRAS was incubated with 5mM DTT, 4mM EDTA and 10x molar excess of nucleotide on ice. After 1.5 hours, 10mM MgCl₂ was added and the reaction was incubated on ice for an additional 30 minutes.

RAS peptide pull down

Biotinylated RAS peptides were synthesized by 21st Century Biochemicals and encoded pY[137] (Biot-Ahx-LARS(pY)GIPFIE-amide) or Y137F (Biot-Ahx-LARSFGIPFIE-amide) surrounded by flanking sequences. For the pull downs, 10μg of peptide was mixed with 10μg of GST-RASA1-SH2C in 300μL of NP-40 buffer and rotated at 4C for 4 hours. 50μL of 50% avidin slurry was then added to each tube, and rotated for 2 hours at 4°C. Beads were washed 4x with NP-40, then boiled in SDS-PAGE sample buffer.

Silver staining was performed by fixing the gel in 40% ethanol, 10% acetic acid while shaking for 1 hour. After draining the fixing solution, sensitizing solution (30% ethanol, 0.2% sodium thiosulphate, 6.8% sodium acetate) was added and the gel shaken for 30 minutes. The gel was then washed 3x with water, for 5 minutes each time. Silver nitrate solution (0.25% silver nitrate in water) was added and the gel was shaken for 20 minutes. After washing 2x with water (1 minute each time), developing solution (2.5% sodium carbonate, 0.015% formaldehyde) was added and the gel was shaken until brown, smokey precipitate appeared. The solution was then replaced with fresh developer solution, continuing until the desired intensity of spots was achieved, at which time the developer solution was drained and 5% acetic acid stop solution was added for 10 minutes. The gel was then washed 3x with water (5 minutes each time) and the image acquired.

Hydrolysis assays

The single turnover hydrolysis rate experiments were done using C-terminally truncated HRAS, HRAS[Y137E] and HRAS[Y137F] (residues 1-166) (203). Briefly, 5µM of HRAS and mutants were loaded with 50mM γ^{32}P-GTP for 5 minutes at 37˚C (buffers in reference). The nucleotide-exchanged protein was then diluted 5-fold with hydrolysis buffer pre-heated to 30˚C, bringing protein and nucleotide concentrations to 1µM and 10nM, respectively. Reactions proceeded for 100 minutes. CPM was converted to fmols of P_i and self-normalized to 100%. The half-time ($t_{1/2}$) for hydrolysis reaction were determined using the curve-fitting program ProFit (http://www.quansoft.com), and k_{obs} determined as the reciprocal of $t_{1/2}$. Reactions including Raf were done in the presence of 5µM Raf-RBD.

Crystallization and structure determination of Y137 mutants

C-terminal truncated HRAS, HRAS[Y137E] and HRAS[Y137F] (residues 1-166) were purified as previously published (203) and the bound GDP was exchanged for the nucleotide analogue Guanylyl-imidodiphosphate (GppNHp) in stabilization buffer (20mM HEPES, 50mM NaCl, 20mM $MgCl_2$, and either 10mM or 1mM DTT) (204). Protein was concentrated, flash frozen, and stored at -80˚C. Reagents and materials for crystallization were purchased by Hampton Research, Inc. Crystals grew in 24-well plates with reservoir volumes of 425µL to 625µL. HRAS[Y137E] was crystallized in hanging drops containing 2µL protein at a concentration of 12.4 mg/mL in stabilization buffer and 2µL of reservoir solution consisting of 152mM $Ca(OAc)_2$, 24.8% PEG 3350, and 4.8% stabilization buffer at pH 7.5. For HRAS[Y137F] crystallization of the protein was at a concentration 20.7 mg/mL and the reservoir contained 139mM $Ca(OAc)_2$, 22.6% PEG 3350, and 13% stabilization buffer at pH 7.5. Both proteins crystallized with symmetry of the space group $P3_221$. Data were collected at the Advanced Photon Source (APS) at the Southeast Regional Collaborative Access Team (SER-CAT) synchrotron beamline at a

temperature of 100 K with X-rays wavelength of 1.0 Å. Data were processed with HKL2000 (205). The coordinates with PDB code 1CTQ were used for phasing with molecular replacement method, followed by refinement and model building using the PHENIX suite of programs (206) and with COOT (207).

MudPIT analysis to identify RAS associated proteins

Flp-In[TM] T-REX[TM]-293 cells with tetracycline-inducible 3xHA-3xFLAG-HRAS and 3xHA-3xFLAG-HRAS[Y137F] were transduced with a lentivirus encoding ABL2. Cells were harvested by trypsinization and lysed in FLAG buffer (100 mM Tris-HCl 8.0, 150 mM NaCl, 5 mM EDTA, 5% glycerol, 0.2% NP-40, 1 mM DTT, PMSF, pepstatin, leupeptin, sodium fluoride, sodium orthovanadate) while rotating at 4°C for 45 minutes. Clarified lysate was incubated with EZview Red Anti-FLAG M2 Affinity gel (Sigma-Aldrich) at 4°C for 2 hours. Beads were then washed 4x with FLAG buffer and 2x with detergent-free FLAG buffer. Proteins were eluted sequentially using 250 µg/mL 3xFLAG peptide (Sigma-Adrich).

Immunopurified protein complexes were reduced, alkylated and digested by the sequential addition of lys-C and trypsin proteases as described earlier (208). The digested peptide mixture was fractionated online using strong-cation exchange and reverse phase chromatography and eluted directly into a LTQ-Orbitrap mass spectrometer (Thermofisher) (208,209). MS/MS spectra were collected and subsequently analyzed using the ProLuCID and DTASelect algorithms (210,211) . Protein and peptide identifications were further filtered with a false positive rate of less than 5% as estimated by a decoy database strategy (212). Normalized spectral abundance factor (NSAF) values were calculated as described and multiplied by 10^5 to improve the readability (213).

RAF1-RBD pull down

293Ts were plated 6×10^5 cells/well in a 6-well plate. 24 hours post plating, cells were transfected with pcDNA3 ABL2 and pcDNA3 HRAS^{G12V}. 48 hours post-transfection, cells were lysed in 20mM Tris pH7.4, 150mM NaCl, 5mM MgCl$_2$, 1% Triton X-100, 1mM DTT. Cells were incubated on ice for five minutes, then the lysate was clarified by centrifuging for 10 minutes at 15,000xg. A sample of whole cell lysate was reserved for immunoblotting. Meanwhile, 4μg of purified Raf1-RBD was incubated with 30μL of glutathione sepharose in lysis buffer and rotated for 1 hour at 4°C. Beads were washed twice with lysis buffer to remove excess Raf1-RBD. Clarified lysate was added to the beads and incubated for 1 hour at 4°C. Beads were washed three times in lysis buffer, then resuspended in SDS-PAGE sample buffer and boiled.

CHAPTER 3. CELL CYCLE-DEPENDENT NUCLEAR LOCALIZATION OF THE RAS EFFECTOR RIN1.

3.1 ABSTRACT

RIN1 is a RAS effector protein that modulates receptor tyrosine kinase signaling and down-regulation by coordinately activating RAB5 GTPases and ABL tyrosine kinases. In order to perform these functions, RIN1 localizes primarily in the cytoplasm and at the plasma membrane. Intriguingly, however, immunofluorescence and immunohistochemical data from prior studies suggest that RIN1 sometimes localizes in the nucleus. We found that in multiple human cell lines RIN1 accumulates in the nucleus during S phase of the cell cycle, reaching a peak in G2, before being excluded in early G1. We determined that nuclear localization is directed by three nuclear localization sequences (NLSs), and regulated by phosphorylation-dependent binding to 14-3-3 proteins. Multidimensional protein identification technology (MudPIT) analysis found that during G2 phase nuclear RIN1 binds to chaperones, nucleic acid binding proteins and ribonucleoproteins. This research identifies the cell-cycle dependent nuclear localization of RIN1 and suggests a novel pathway by which this RAS effector influences signal transduction from the plasma membrane to the nucleus.

3.2 INTRODUCTION

As a RAS effector, RIN1 binds activated RAS and transduces the signal downstream. The binding affinity is high (K_d = 22nM), on par with RAF1 binding to RAS (79,84), and is mediated by a RAS association domain encoded in the RIN1 carboxy-terminus (86). Through other distinct domains, RIN1 coordinates the small GTPase RAB5 and the non-receptor tyrosine kinase ABL, to mediate endocytosis, cytoskeleton remodeling and cell migration. A Vps9p catalytic GEF domain on RIN1 activates the small GTPase RAB5 and regulates receptor tyrosine kinase endocytosis and signaling (85,95,116). Endocytosis can also be regulated by direct binding of RIN1-SH2 to phosphorylated EGFR (115). Binding of RIN1 to the SH3 and SH2 domains of ABL stimulates ABL kinase activity (144), and inhibits epithelial cell adhesion and migration (112).

RIN1 is highly expressed in the brain (86,110), where it acts as an inhibitory modulator of neuronal plasticity in aversive memory formation (110,114). Expression can also be detected in hematopoietic (111) and epithelial cells (112). In breast cancer, RIN1 acts as a tumor suppressor, and its expression is reduced (102). However, in many other tumors including colorectal, non-small cell lung, bladder urothelial, gastric and melanoma, RIN1 is overexpressed and high expression is associated with poor prognosis and metastasis (96-100,214). Overexpression of RIN1 accelerates leukemogenesis (111), and RIN1 is required for transformation of bone marrow cells ex vivo by BCR-ABL (174), the causative genetic abnormality in chronic myelogenous leuekemia. RIN1 also acts as a host-cell factor for pathogenic bacterial invasion (93,215).

Like other RAS effectors such as RAF1 (216), RIN1 is localized in the cytoplasm and recruited to the plasma membrane by activated RAS (79,84). Binding to 14-3-3 retains RIN1 in

the cytoplasm (86), in a manner dependent on phosphorylation of RIN1-S[351] (84). However, sporadic observations of RIN1 nuclear localization have been mentioned in the literature (96,100,116,119). In an effort to clarify this, we sought to determine the conditions under which RIN1 is in the nucleus. Here we describe the cell-cycle dependent nuclear localization of RIN1, its regulation by nuclear localization sequences (NLSs) and serine residues, and a set of novel nuclear binding partners. The cell cycle dependent nuclear localization of this endocytic protein and RAS effector suggest a novel function in mediating signal transduction.

3.3 RESULTS

RIN1 accumulates in the nucleus during G2 phase

Data from previous studies revealed strong nuclear RIN1 staining in a small subset of asynchronously proliferating cells, suggesting that nuclear entry might be cell cycle-regulated. To examine this hypothesis, we studied HeLa cells over-expressing RIN1 under the control of a tetracycline-responsive promoter. The cells were either allowed to grow asynchronously, or chemically arrested at various cell cycle phases, and subcellular localization of RIN1 was visualized by immunofluorescence (Figure 3-1A). RIN1 was excluded from the nucleus in early G1 phase, enriched in the nucleus during S phase and its nuclear localization peaked in G2 phase. While nearly 100% of cells in early G1 had primarily cytoplasmic localization of RIN1, this dropped to 30% in S phase, and 5% in G2 phase. In parallel, cells with strong nuclear RIN1 staining increased from 0 in early G1, to more than 60% in G2-phase arrested cells (Figure 3-1B).

To exclude the possibility that strong nuclear localization of RIN1 during G2 phase might be an artifact of chemical treatment with RO-3306, cells were arrested at the G1/S interface using double thymidine and allowed to proceed synchronously through the cell cycle. At the time

of release, less than 2% of cells had strong RIN1 nuclear localization. This gradually increased, until peaking at 6-9 hours post-release from double thymidine (Figure 3-S1A), time points that are consistent with G2 phase of the cell cycle as assessed by flow cytometry (Figure 3-S1B).

Cell fractionation of HeLa cells confirmed that endogenous RIN1 localizes to the nucleus during S phase, and is largely excluded during G1 phase (Figure 3-1C). We observed cell-cycle dependent nuclear localization of exogenously expressed RIN1 in several other cell lines we examined including an NRAS-mutant melanoma line, M296, as well as the mammary epithelial cell line MCF10A (Figure 3-S2).
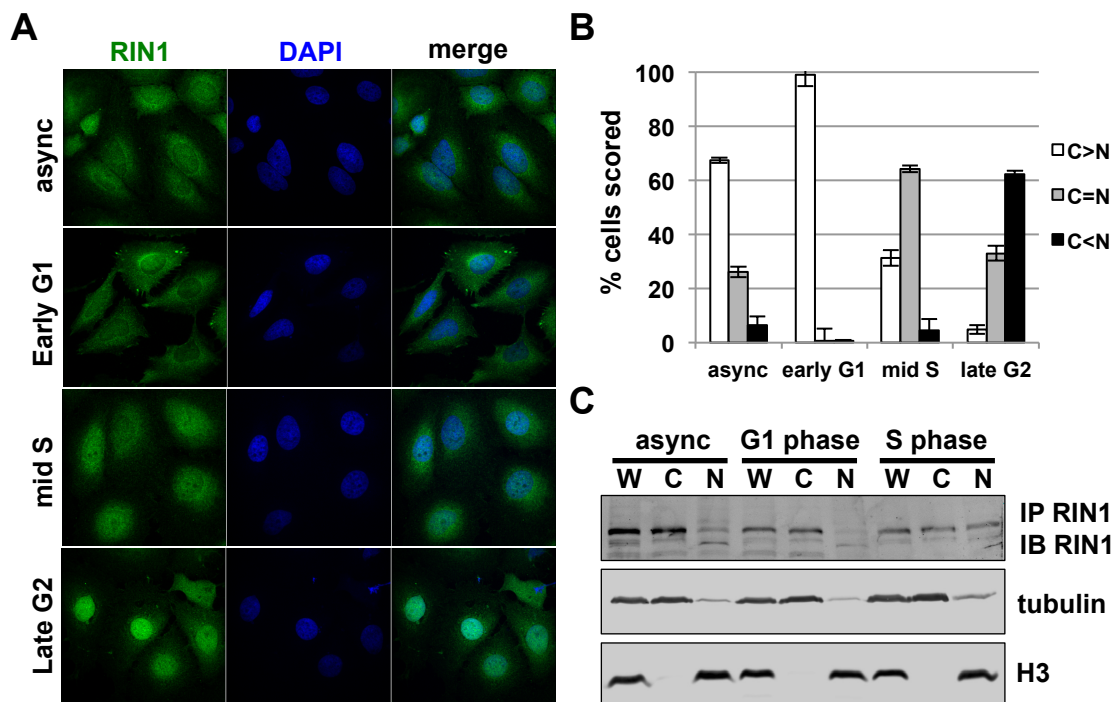

Figure 3-1. RIN1 translocates to the nucleus during S phase and G2. (A) HeLa cells overexpressing doxycycline-inducible RIN1 and growing asynchronously or arrested in early G1 (lovastatin), mid S (double thymidine + release) and late G2 (RO-3306) were fixed and stained with anti-RIN1 (green) and DAPI (blue) to visualize the nucleus. Representative images are shown. (B) Cells were scored for RIN1 signal intensity in the cytoplasm (C) vs. nucleus (N). >200 cells were counted blindly per condition, and the results are averaged from 2 independent experiments. Error bars = standard deviation. (C) Subcellular fractionation of asynchronous, early G1 (lovastatin) and mid S (double thymidine + release) HeLa cells. Subcellular localization of endogenous RIN1 was detected by immunoprecipitation followed by immunoblotting. Tubulin and histone H3 were used as subcellular markers of the cytoplasm and nucleus, respectively. W, whole cell lysate; C, cytoplasm; N, nucleus. The experiment was performed twice independently, and a representative immunoblot is shown.
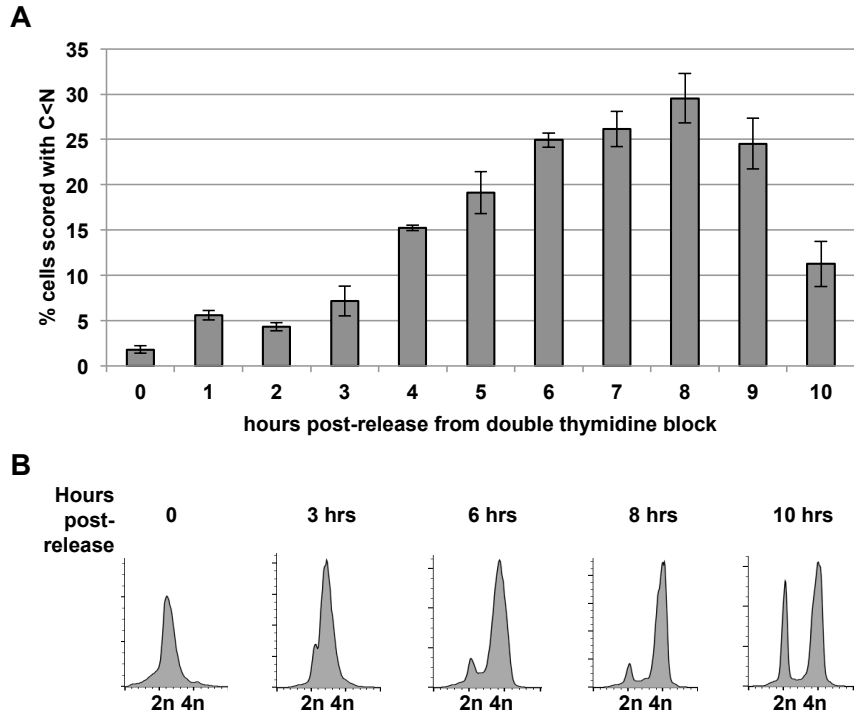
A

B

Figure 3-S1. RIN1 nuclear localization peaks 6-9 hours post-release from double thymidine arrest. (A) HeLa cells overexpressing RIN1 were synchronized at G1/S using double thymidine, then released. Cells were fixed at each hour post-release and stained with anti-RIN1 and DAPI to visualize the nucleus. Cells were scored for RIN1 signal intensity in the cytoplasm (C) vs. nucleus (N), and the percentage of cells scored with cytoplasmic staining intensity lower than nuclear (C<N) is plotted. >200 cells were counted blindly per condition, and the results are averaged from 2 independent experiments. Error bars = standard deviation. (B) HeLa cells were synchronized at G1/S using double thymidine, then released. Cells were fixed at selected intervals post-release, stained with propidium iodide, and evaluated by flow cytometry to assess cell cycle progression. The plots shown are representative of three independent experiments.
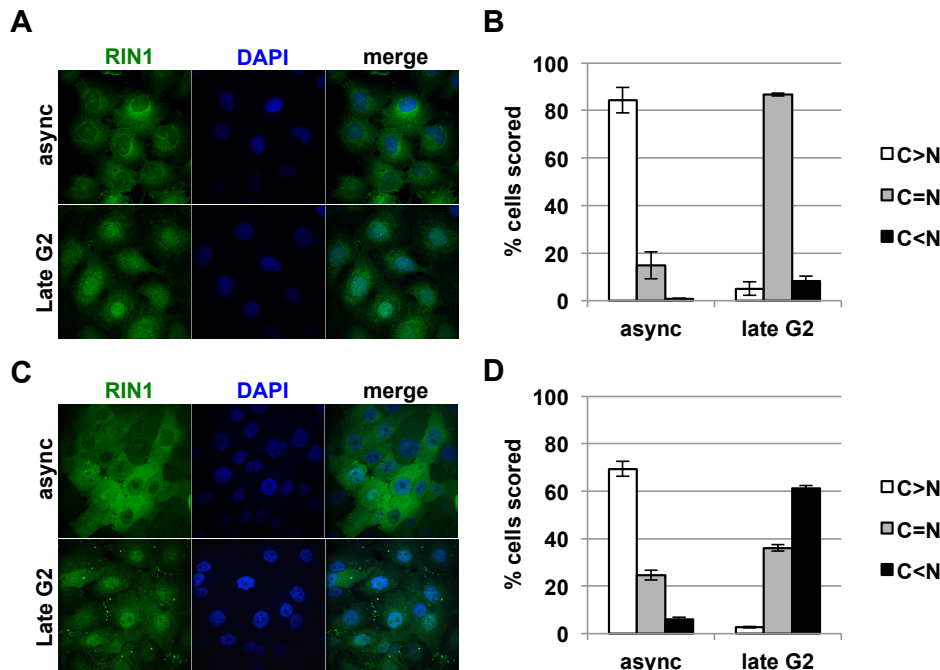
A

B

C

D

Figure 3-S2. RIN1 is enriched in the nucleus during late G2 phase in M296 and MCF10A cells. (A) M296 cells were cultured with doxycycline to induce overexpression of RIN1. Asynchronously growing or late G2-arrested (RO-3306) cells were fixed and stained with anti-RIN1 (green) and DAPI (blue) to visualize the nucleus. Representative images are shown. (B) M296 cells were scored for RIN1 signal intensity in the cytoplasm (C) vs. nucleus (N). >200 cells were counted blindly per condition, and the results are averaged from 2 independent experiments. Error bars = standard deviation. (C) MCF10A were cultured with doxycycline to induce overexpression of RIN1, and were treated as in (A). (D) MCF10A cells were scored as in (B).

Three serine residues regulate nuclear localization of RIN1

We hypothesized that RIN1 localization is regulated by 14-3-3 proteins, cytoplasmic partners RIN1 (84). 14-3-3 proteins regulate nuclear translocation of many proteins (217), including some implicated in cell cycle regulation such as p27(Kip1) (218) and cdc25 (219,220). By sequence analysis, we identified three serine residues whose flanking sequences conform to the consensus 14-3-3 binding site R-x-x-pS (pS=phospho-serine) (221). One, S351, has previously been described as a 14-3-3 binding site on RIN1 and the corresponding mutant RIN1^{S351A} has been previously characterized (84,95,183). The other two sites are S291 and S292.

Mutation of the consensus serines at all three sites to alanine residues shifted RIN1 localization to the nucleus (Figure 3-2A). In an asynchronous population of cells, less than 3% of cells exhibited strong nuclear localization of RIN1. However, the RIN1^{S351A} mutant strongly localized to the nucleus in nearly 40% of cells, and the triple serine mutant, RIN1$^{S291/292/351A}$, in nearly 60% of cells (Figure 3-2B). These serine mutants also showed reduced binding to 14-3-3 in a co-immunoprecipitation experiment (Figure 3-2C), suggesting that 14-3-3 binding may contribute to RIN1 cytoplasmic localization.
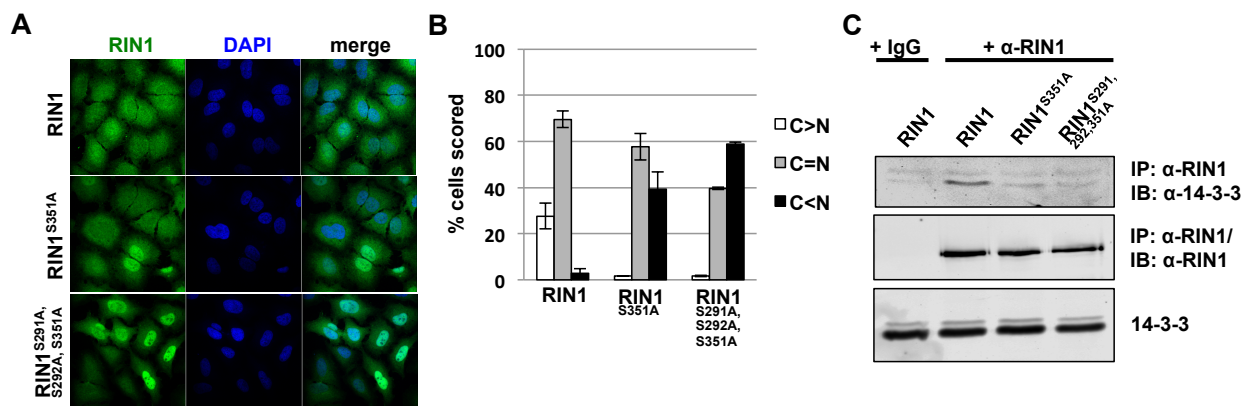
Figure 3-2. Three serine residues mediate subcellular localization. (A) Asynchronous HeLa cells overexpressing doxycycline-inducible RIN1, RIN1^{S351A} or RIN1$^{S291/292/351A}$ were fixed and stained with anti-RIN1 (green) and DAPI (blue) to visualize the nucleus. Representative images are shown. (B) Cells were scored for RIN1 signal intensity in the cytoplasm (C) vs. nucleus (N). >200 cells were counted blindly per condition, and the results are averaged from 2 independent experiments. Error bars = standard deviation. (C) HeLa cells expressing RIN1, RIN1^{S351A} or RIN1$^{S291/292/351A}$ were lysed and

immunoprecipitated with anti-RIN1 or IgG. IP samples were immublotted for pan 14-3-3 and RIN1, and the whole cell lysate immunoblotted for 14-3-3. The immunoblots shown are representative of two independent experiments.

RIN1 nuclear localization is mediated by three NLSs

We used sequence analysis to identify three putative nuclear localization sequences (NLSs), one of which (^{237}KREK) conforms to an NLS consensus sequence K-K/R-X-K/R (222). Two additional sequences (^{342}RRR and ^{451}RLRRR) fit a looser NLS pattern of short arginine strings (Figure 3-3A). Similar arginine-rich sequences have been implicated in nuclear localization (217,223). Mutation of all three NLSs (RIN1$^{\text{NLS1,2,3m}}$) blocked nuclear localization of RIN1 during G2 phase (Figure 3-3B). While approximately 55% of G2-arrested HeLa cells exhibited strong nuclear localization of RIN1, less than 1% of RIN1$^{\text{NLS1,2,3m}}$-expressing cells had strong RIN1 nuclear localization (Figure 3-3C). The triple NLS mutant expressed at similar levels as the wild-type protein (Figure 3-S3A) and could bind to the known RIN1 binding partners RAS and 14-3-3 (Figure 3-S3B).

Single and combination mutations indicated that while each of the three NLSs contributes to RIN1 nuclear localization, ^{451}RLRRR (NLS3) appears to be the most important determinant of localization. Mutation of NLS1 produced mild alterations in localization that were apparent only in an asynchronous population of cells, but not when the cells were arrested in S or G2 phase (Figure 3-S4). However, mutation of NLS1 and 3 was sufficient to induce a significant change in localization, and additional mutation of NLS2 only slightly increased the effect (Figure 3-S5).
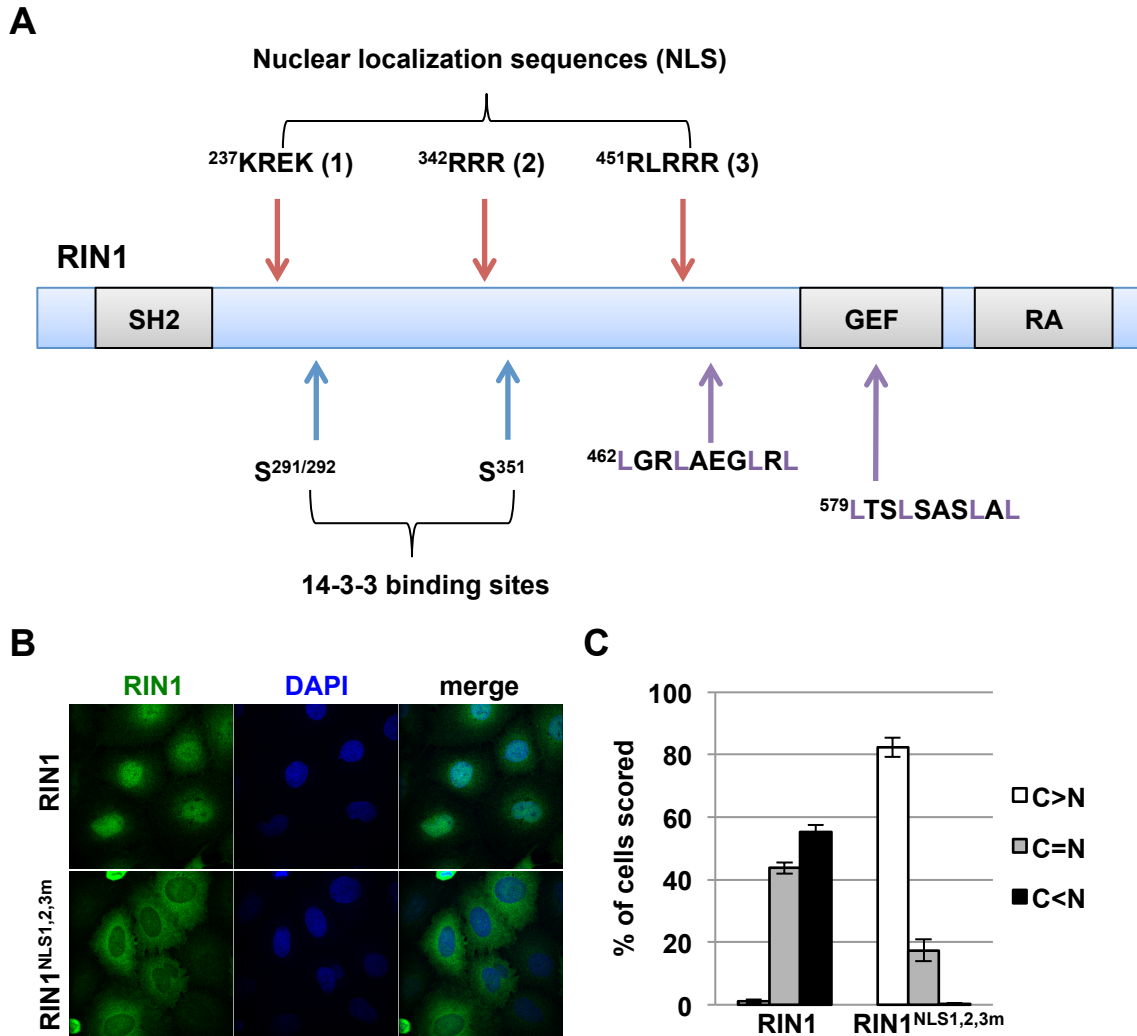
Figure 3-3. Mutation of three putative NLSs blocks nuclear localization of RIN1. (A) Schematic representation of RIN1. RIN1 has three putative nuclear localization sequences: [237]KREK (designated NLS[1]), [342]RRR (NLS[2]) and [451]RLRRR (NLS[3]), as well as two putative CRM1-dependent nuclear export sequences conforming to the consensus motif LxxLxxxLxL. SH2, SRC homology domain 2; GEF, Vps9 domain that catalyzes guanine nucleotide exchange; RA, RAS association domain. (B) HeLa cells expressing RIN1 or RIN1 with mutations in all three putative NLSs (RIN1[NLS1,2,3m]) were arrested in late G2 phase using RO-3306. They were then fixed and stained with anti-RIN1 (green) and DAPI (blue) to visualize the nucleus. Representative images are shown. (C) Cells were scored for RIN1 signal intensity in the cytoplasm (C) vs. nucleus (N). >200 cells were counted blindly per condition, and the results are averaged from 2 independent experiments. Error bars = standard deviation.
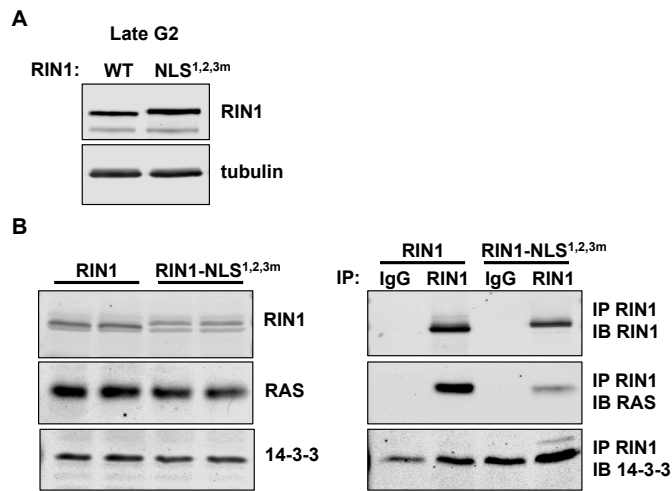
Figure 3-S3. RIN1-NLS^{1,2,3m} expression and binding to RAS and 14-3-3. (A) HeLa cells were cultured with doxycycline to induce overexpression of RIN1 or RIN1-NLS^{1,2,3m} and were incubated with RO-3306 to achieve late G2 arrest. Cells were lysed and immunoblotted anti-RIN1 and anti-tubulin to evaluate RIN1 expression. (B) HeLa cells were cultured with doxycycline to induce overexpression of RIN1 or RIN1-NLS^{1,2,3m}. Cells were lysed and immunoprecipitated with anti-RIN1 or IgG. Whole cell lysates and IP samples were immunoblotted for RIN1, RAS and 14-3-3. The immunoblots shown are representative of two independent experiments.

Figure 3-S4. Effect of NLS1 mutation on RIN1 subcellular localization. (A) Asynchronous HeLa cells expressing RIN1 or RIN1^{NLS1m} (mutations in ^{237}KREK) were fixed and stained with anti-RIN1 and DAPI. Cells were scored for RIN1 signal intensity in the cytoplasm (C) vs. nucleus (N). >200 cells were counted blindly per condition, and the results are averaged from 2 independent 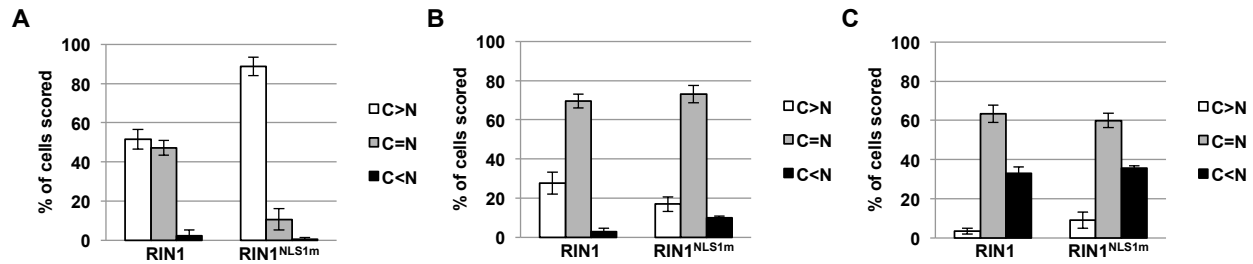experiments. Error bars = standard deviation. (B) Cells were synchronized in S phase using double thymidine followed by release for three hours, then fixed and analyzed as in (A). (C) Cells were arrested in late G2 phase using RO-3306, then fixed and analyzed as in (A).
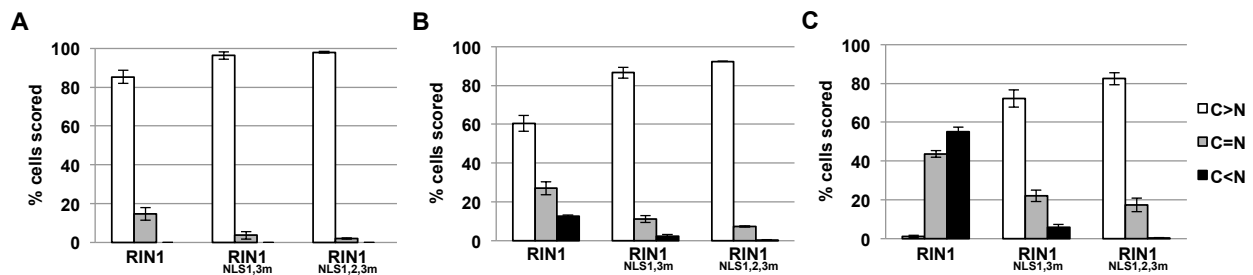
Figure 3-S5. Comparison of effects of NLS1,3 and NLS1,2,3 mutations on RIN1 subcellular localization. (A) Serum-starved HeLa cells expressing RIN1, RIN1^{NLS1,3m} (mutations in ^{237}KREK and ^{451}RLRRR) or RIN1^{NLS1,2,3m} (mutations in ^{237}KREK, ^{342}RRR and ^{451}RLRRR) were fixed and stained with anti-RIN1 and DAPI. Cells were scored for RIN1 signal intensity in the cytoplasm (C) vs. nucleus (N). >200 cells were counted blindly per condition, and the results are averaged from 2 independent experiments. Error bars = standard deviation. (B) Cells were synchronized in S phase using double thymidine followed by release for three hours, then fixed and analyzed as in (A). (C) Cells were arrested in late G2 phase using RO-3306, then fixed and analyzed as in (A).

54

RIN1 knockdown has no effect on cell cycle progression

We next sought to define the nuclear function of RIN1. Because RIN1 is translocated into the nucleus in a cell-cycle dependent manner, we focused our experiments on cell cycle progression in the context of RIN1 knockdown. RIN1 knockdown in HeLa cells was achieved using one of three RIN1-targeted shRNAs (Figure 3-S6A) and had no significant effect on short-term cell growth as measured by MTS assay (Figure 3-S6B). DNA profiles of asynchronously proliferating control and RIN1-shRNA cells were also similar (Figure 3-S7), suggesting that RIN1 is dispensable for passage through the cell cycle. Control and RIN1-shRNA cells that were arrested at G1/S and released also proceeded similarly through S, G2 and M (Figure 3-S8).
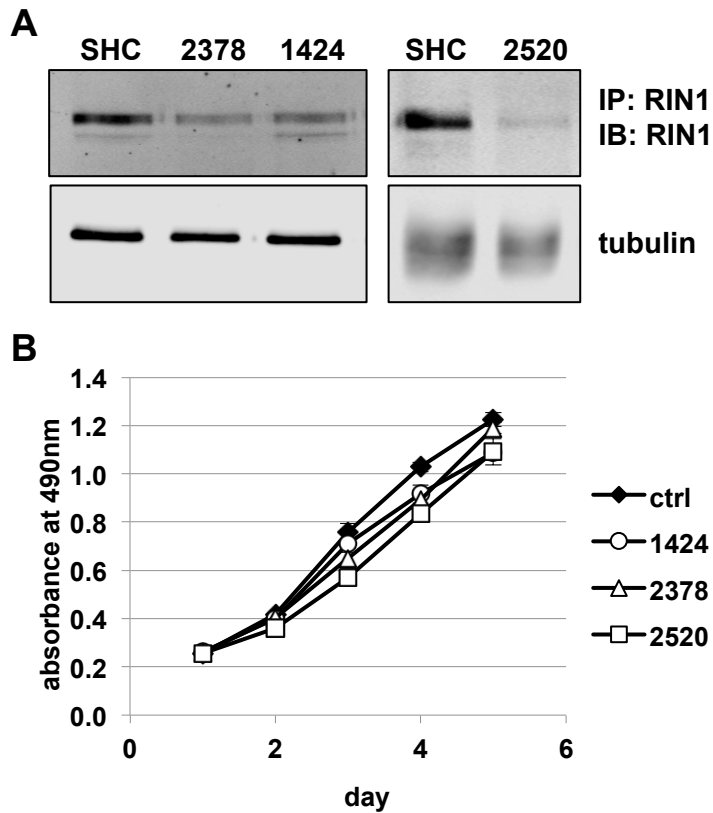
Figure 3-S6. RIN1 knockdown has no significant effect on short-term cell growth. (A) HeLa cells were transduced with a lentivirus encoding a control shRNA or one of three RIN1 shRNAs targeting either the coding sequence (1424 and 2378) or the 3'UTR (2520). Cells were lysed and endogenous RIN1 was detected by immunoprecipitation followed by immunoblotting. Tubulin was probed as a loading control. The immunoblots shown are representative of two independent experiments. (B) Growth of HeLa cells stably expressing a control (ctrl) or RIN1-targeted (1424, 2378, 2520) shRNA was assessed by MTS assay over a five-day period. Experiments were performed in quadruplicate. Error bars = standard deviation.

55
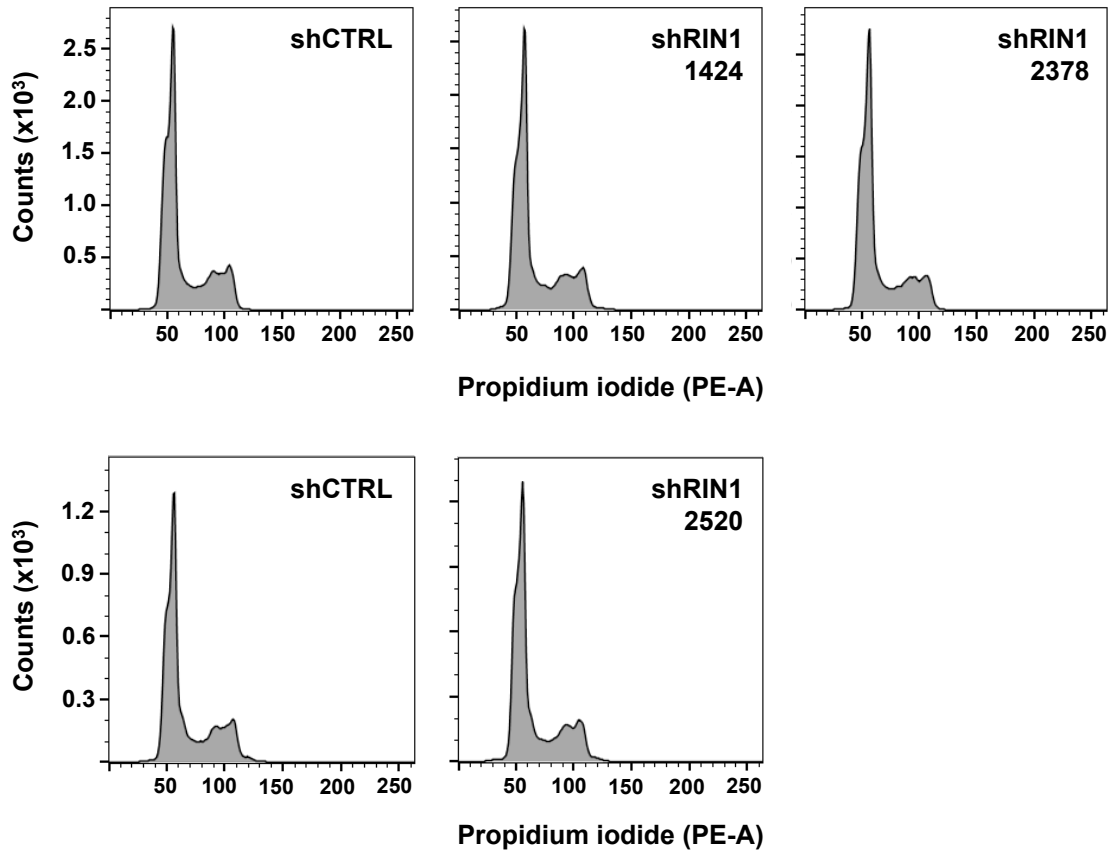
Figure 3-S7. RIN1 knockdown has no significant effect on distribution of asynchronous HeLa cells across cell cycle phases. Asynchronously growing HeLa cells stably expressing a control (ctrl) or RIN1-targeted (1424, 2378, 2520) shRNA were harvested and fixed, stained with propidium iodide, then analyzed by flow cytometry for DNA content. The plots shown are representative of two independent experiments.

56

Figure 3-S8. RIN1 knockdown has no significant effect on cell cycle progression. Hela cells stably expressing a control (ctrl) or RIN1-targeted (2378, 2520) shRNA were synchronized at G1/S using double aphidicolin. Samples were harvested and fixed at the indicated hours post-release, stained with propidium iodide, and analyzed by flow cytometry for DNA content. The plots shown are representative of two independent experiments.

Because peak nuclear localization of RIN1 coincided with G2 phase, we also sought to examine the integrity of the G2 checkpoints and decision points in RIN1-depleted cells. The G2-M DNA damage checkpoint ensures that cells repair damaged DNA after replication and before mitosis (reviewed in (224)). When treated with the topoisomerase inhibitor SN-38, which induces double-stranded DNA breaks (225), both control and RIN1-shRNA cells arrested (Figure 3-S9), suggesting an intact checkpoint. We also tested the ability of the cells to arrest proliferation, as recent evidence suggests that the decision to enter quiescence occurs during G2 phase (226). When serum-starved, both control and RIN1-shRNA MCF10A cells stopped incorporating BrdU (Figure 3-S10), suggesting that RIN1 is dispensable for entry into quiescence.

Figure 3-S9. RIN1 knockdown has no significant effect on cell cycle response to SN-38-induced DNA damage. Hela cells stably expressing a control (ctrl) or RIN1-targeted (2378, 2520) shRNA were treated with 1.5 or 8 nM SN-38 for 24 hours. Cells were then harvested, fixed, stained with propidium iodide, and analyzed by flow cytometry for DNA content. The plots shown are representative of two independent experiments.
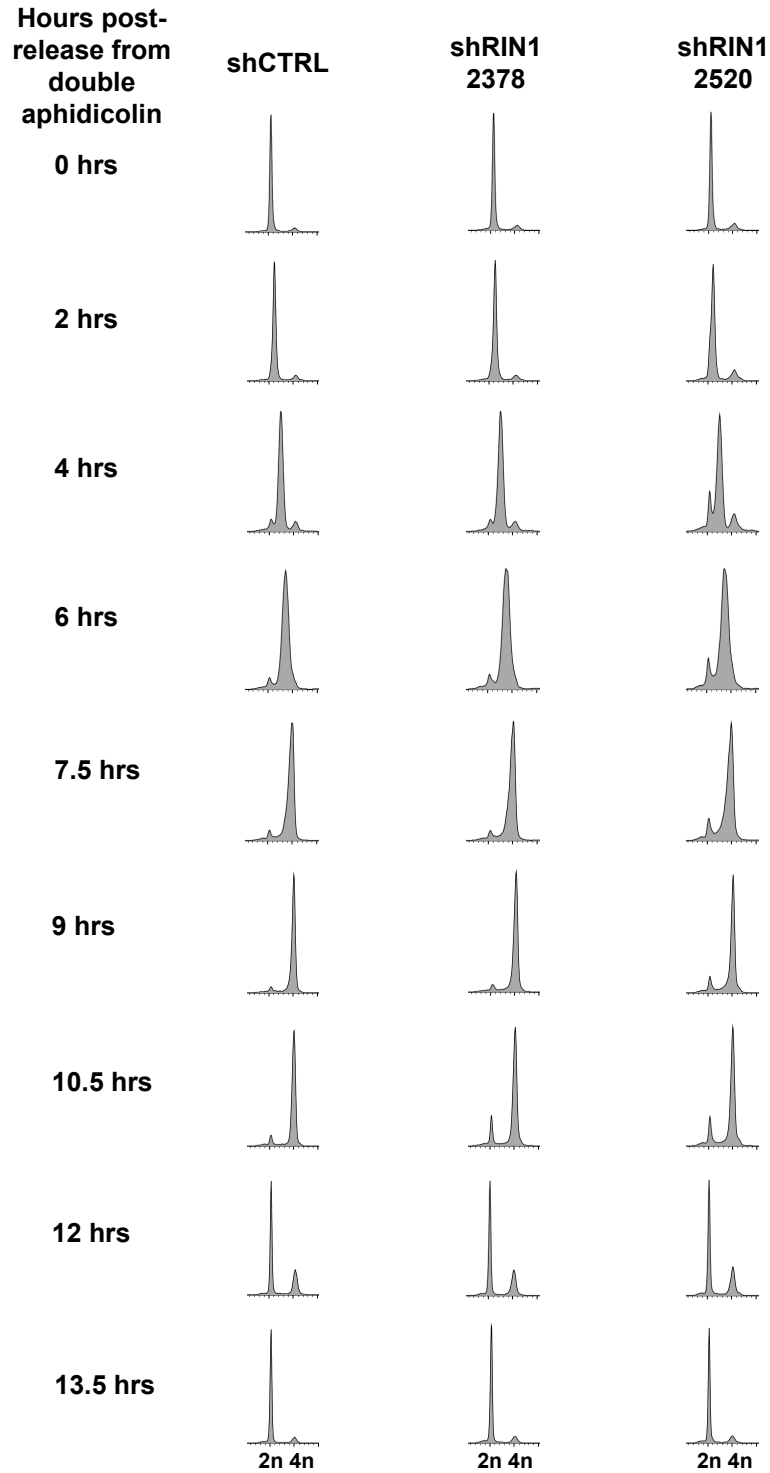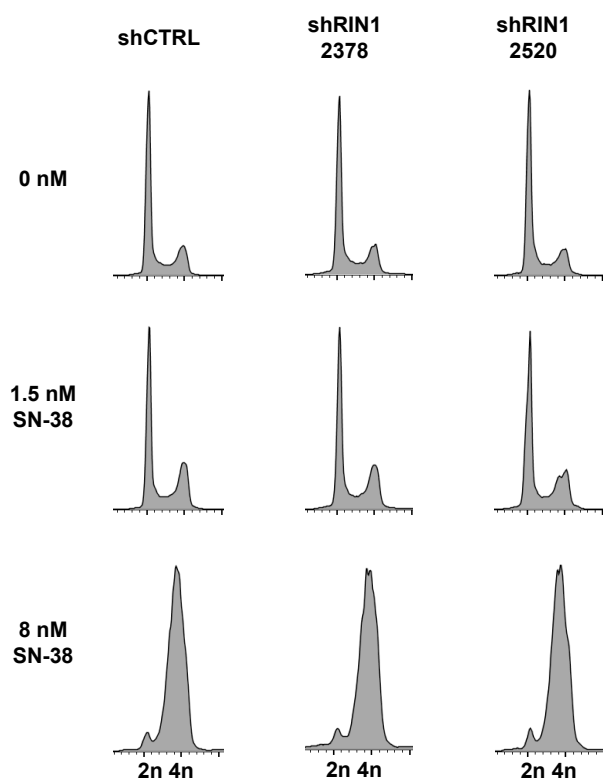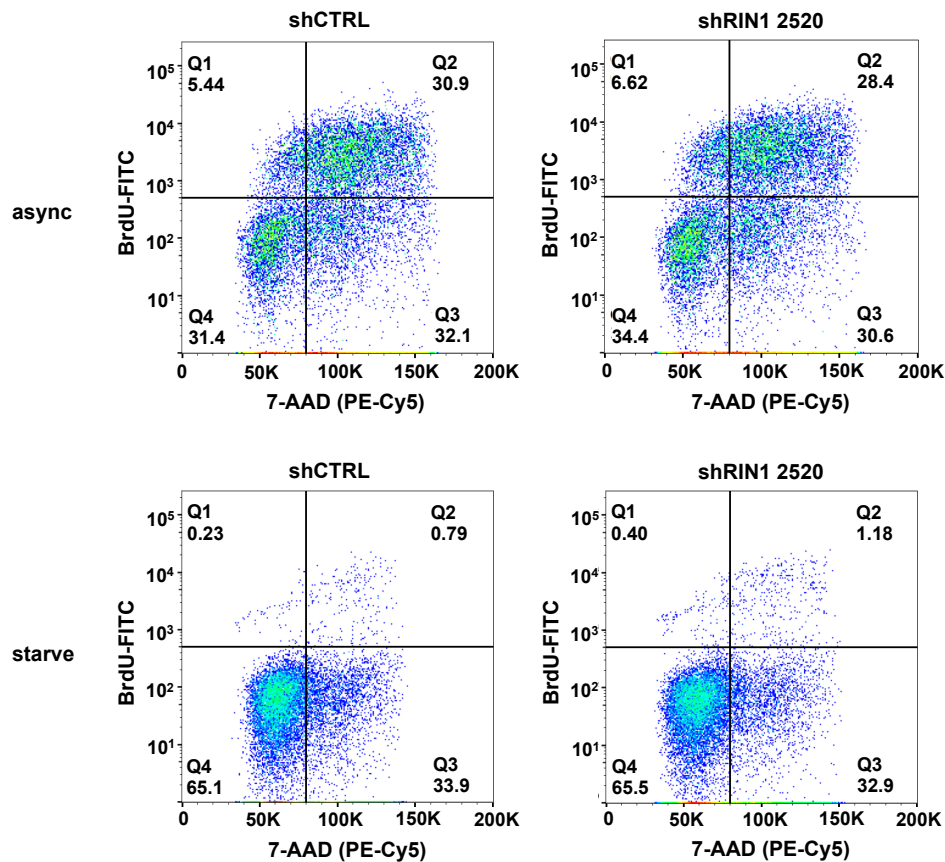
Figure 3-S10. RIN1 knockdown has no significant effect on cell cycle response to serum-starvation. MCF10A cells stably expressing a control (ctrl) or RIN1-targeted (2520) shRNA were allowed to grow asynchronously or serum-starved for 72 hours. BrdU was then added to the medium, and cells were incubated for 3 hours to allow BrdU incorporation. Cells were then harvested, fixed and permeabilized, stained with anti-BrdU-FITC and 7-AAD and analyzed by flow cytometry.

Nuclear RIN1 binds chaperones, nucleic acid binding proteins and ribonucleoproteins during G2 phase

As a complementary approach to understanding the functional implications of RIN1 nuclear localization, we used multidimensional protein identification technology (MudPIT) to identify nuclear interaction partners. By comparing RIN1 and RIN1^{NLS1,2,3m}-coimmunoprecipitating proteins from cells arrested in G2 phase, we identified G2-specific, nuclear protein interactors. As an additional control, we also examined RIN1-coimmunoprecipitating proteins from asynchronous cells. In total, we identified 73 RIN1 and/or RIN1^{NLS1,2,3m}-binding proteins, including known interactors such as members of the ABL, RAS and 14-3-3 protein families (Table 3-S1).

	HeLa - RIN1 (G2 phase)			HeLa - RIN1 NLSm (G2 phase)			HeLa - RIN1 NLSm (async)		
Protein	NSAF	spectra	coverage	NSAF	spectra	coverage	NSAF	spectra	coverage
RIN1	1096.018	85	55.0%	721.424	60	47.9%	1076.530	78	46.9%
PPHLN1	66.133	3	3.3%	41.112	2	4.1%	47.191	2	3.5%

	HeLa - RIN1 (G2 phase)			HeLa - RIN1 NLSm (G2 phase)			HeLa - RIN1 NLSm (async)		
Protein	NSAF	spectra	coverage	NSAF	spectra	coverage	NSAF	spectra	coverage
YWHAB	1641.668	40	38.6%	0.000			0.000		
YWHAH	1108.126	27	40.2%	0.000			0.000		
YWHAG	572.258	14	43.3%	0.000			0.000		
YWHAZ	535.720	13	38.4%	0.000			0.000		
YWHAQ	370.883	9	30.6%	0.000			0.000		
ABL1	125.086	14	6.1%	0.000			0.000		
ABL2	93.958	11	1.9%	0.000			0.000		
MRPS7	83.440	2	10.3%	0.000			0.000		
TAF15	68.218	4	5.2%	0.000			0.000		
TFPI	66.423	2	11.5%	0.000			0.000		
ZNF771	63.699	2	6.6%	0.000			0.000		
ELAVL1	61.940	2	7.4%	0.000			0.000		
HNRNPA3	53.419	2	10.1%	0.000			0.000		
DKC1	39.285	2	6.4%	0.000			0.000		
EPHB6	29.666	3	2.4%	0.000			0.000		
DDX1	27.287	2	4.7	0.000			0.000		
CEP170	19.122	3	2.7%	0.000			0.000		
EHBP1L1	13.258	2	1.7%	0.000			0.000		

	HeLa - RIN1 (G2 phase)			HeLa - RIN1 NLSm (G2 phase)			HeLa - RIN1 NLSm (async)		
Protein	NSAF	spectra	coverage	NSAF	spectra	coverage	NSAF	spectra	coverage
TUBA1A	0.000			688.872	33	57.9%	0.000		
TUBA3C	0.000			648.560	31	48.9%	0.000		
ACTBL2	0.000			450.698	18	16.5%	0.000		
TUBA8	0.000			398.390	19	28.1%	0.000		
POTEE	0.000			332.795	38	9.6%	0.000		
HRAS	0.000			298.876	6	34.9%	0.000		
KRAS	0.000			298.876	6	33.9%	0.000		
S100A4	0.000			186.427	2	17.8%	0.000		
RPS15	0.000			129.856	2	18.6%	0.000		
CAPZA2	0.000			98.754	3	12.2%	0.000		
SLC25A4	0.000			94.778	3	9.7%	0.000		
KRT4	0.000			88.152	5	6.4%	0.000		
BASP1	0.000			82.948	2	19.8%	0.000		
RPL5	0.000			63.398	2	6.1%	0.000		
ATP2A1	0.000			56.431	6	4.5%	0.000		
RBM39	0.000			53.290	3	8.1%	0.000		
ARL6IP4	0.000			52.303	2	7.2%	0.000		

Protein									
KRT3	0.000			44.903	3	4.8%	0.000		
ATP2A3	0.000			36.106	4	4.0%	0.000		
BAG3	0.000			32.746	2	5.0%	0.000		
FIP1L1	0.000			31.699	2	5.9%	0.000		
TKT	0.000			30.223	2	2.9%	0.000		
MYO1C	0.000			26.570	3	4.4%	0.000		
DDB1	0.000			24.775	3	3.0%	0.000		
MYH7B	0.000			24.252	5	1.0%	0.000		
MAP7D1	0.000			22.389	2	3.6%	0.000		
ACTN3	0.000			20.898	2	2.1%	0.000		
DSG1	0.000			17.950	2	3.5%	0.000		

	HeLa - RIN1 (G2 phase)			HeLa - RIN1 NLSm (G2 phase)			HeLa - RIN1 NLSm (async)		
Protein	NSAF	spectra	coverage	NSAF	spectra	coverage	NSAF	spectra	coverage
LGALS1	0.000			0.000			160.099	2	17.0%
RPL12	0.000			0.000			130.990	2	19.4%
C1QBP	0.000			0.000			114.965	3	23.8%
ZBED5	0.000			0.000			93.565	6	3.8%
MVP	0.000			0.000			36.305	3	2.5%
TAF4	0.000			0.000			29.880	3	5.0%
OGT	0.000			0.000			20.663	2	3.3%

	HeLa - RIN1 (G2 phase)			HeLa - RIN1 NLSm (G2 phase)			HeLa - RIN1 NLSm (async)		
Protein	NSAF	spectra	coverage	NSAF	spectra	coverage	NSAF	spectra	coverage
YWHAE	1821.286	46	47.1%	110.760	3	7.5%	0.000		
RPS17	149.574	2	8.9%	209.213	3	23.0%	0.000		
RBMX	258.216	10	5.4%	96.313	4	13.0%	0.000		
PRDX4	111.767	3	12.2%	138.961	4	14.0%	0.000		
LEMD3	33.248	3	3.8%	31.003	3	3.8%	0.000		

	HeLa - RIN1 (G2 phase)			HeLa - RIN1 NLSm (G2 phase)			HeLa - RIN1 NLSm (async)		
Protein	NSAF	spectra	coverage	NSAF	spectra	coverage	NSAF	spectra	coverage
RPS27	1562.516	13	25.0%	0.000			385.954	3	23.8%
CFL1	121.642	2	15.1%	0.000			130.201	2	25.9%
APEX2	58.473	3	10.2%	0.000			41.725	2	8.5%

	HeLa - RIN1 (G2 phase)			HeLa - RIN1 NLSm (G2 phase)			HeLa - RIN1 NLSm (async)		
Protein	NSAF	spectra	coverage	NSAF	spectra	coverage	NSAF	spectra	coverage
NRAS	0.000			348.688	7	38.1%	800.497	14	46.0%
HSPA2	0.000			471.466	32	15.6%	456.622	27	15.5%
ATP5A1	0.000			136.197	8	13.0%	39.084	2	4.9%
JUP	0.000			63.185	5	8.1%	29.011	2	3.6%
HRNR	0.000			59.461	18	6.7%	7.584	2	1.0%
KANK2	0.000			33.189	3	4.3%	25.398	2	4.3%

Table 3-1. G2 and nuclear-specific binding partners identified by MudPIT. RIN1 or RIN1-NLS[1,2,3m] were expressed in HeLa cells, which were grown asynchronously or synchronized at late G2 phase using RO-3306. RIN1 was immunoprecipitated and interacton partners were identified by multidimensional protein identification technology.

Functional category enrichment in the samples was evaluated against the entire human genome using The Database for Annotation, Visualization and Integrated Discovery (DAVID). A *p*-value of <0.05 was considered an enriched gene ontology (GO) category. The most significantly enriched GO categories under molecular function and biological process are indicated in Figure 4. In the molecular function category, GO terms related to chaperones, nucleic acid binding and ribonucleoproteins were overrepresented as G2-specific nuclear RIN1-binding partners. In contrast, G2-specific cytoplasmic RIN1-binding partners were enriched for cytoskeletal proteins, tubulin, actin binding cytoskeletal proteins and microtubule family cytoskeletal proteins (Figure 3-4A). In the biological process category, GO terms related to protein localization and cell cycle were overrepresented among G2-specific nuclear RIN1-binding partners, while G2-specific cytoplasmic RIN1-binding partners were enriched for cell structure, motility, mitosis, oncogene and chromosome segregation (Figure 3-4B).
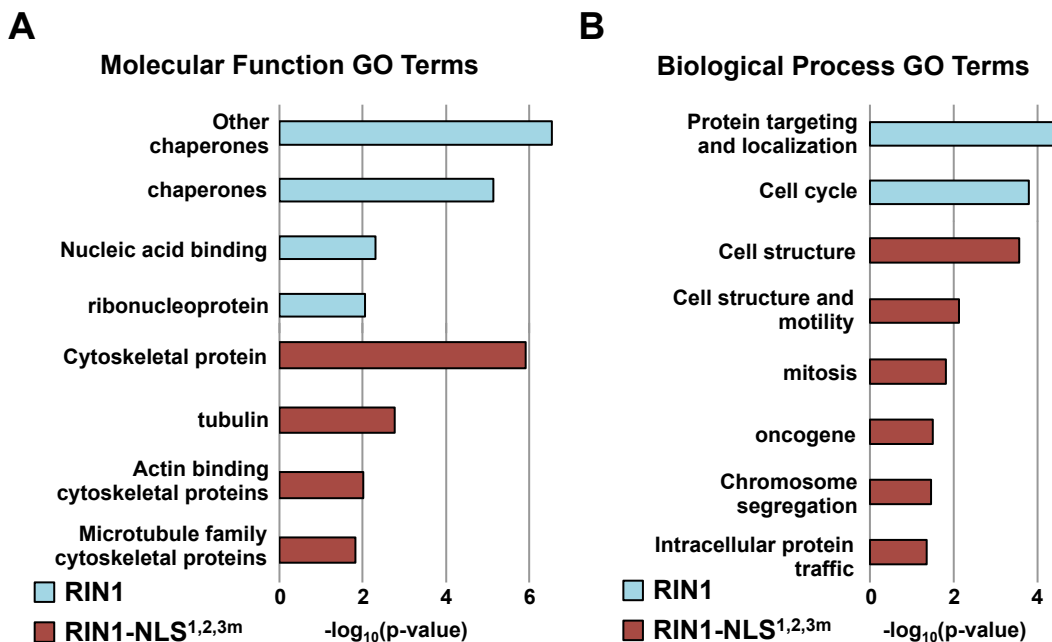

Figure 3-4. GO term enrichment of RIN1-binding proteins during late G2 phase. (A) Enriched GO molecular function terms. Blue bars represent terms enriched among RIN1-binding proteins during late G2 phase. Red bars represent terms enriched among RIN1-NLS[1,2,3m]-binding proteins during late G2 phase. (B) Enriched GO biological process terms.

3.4 DISCUSSION

Here, we report the nuclear localization of RIN1 and provide evidence that RIN1 undergoes a regulated subcellular translocation that places maximum levels of this signaling protein in the nucleus during G2 phase of the cell cycle. Mutation of three putative nuclear localization sequences blocked nuclear translocation. Sequence analysis also uncovered two putative nuclear export sequences, [462]LGRLAEGLRL and [579]LTSLSASLAL, that conform to the canonical sequence $L\text{-}x_{2\text{-}3}\text{-}L\text{-}x_{2\text{-}3}\text{-}L\text{-}x\text{-}L$ (227). We also sporadically observed nucleolar localization of RIN1 (data not shown), although this did not appear to be cell-cycle dependent. Sequence analysis of RIN1 using Nucleolar Localization sequence Detector (NoD) (228) suggested one putative nucleolar localization sequence [233]LGPTKREKFKRSFKVRVSTE.

RIN1 nuclear localization was regulated by three serine residues (S^{291}, S^{292} and S^{351}), which also mediated binding to 14-3-3. 14-3-3 binding is primarily phosphorylation-dependent (229), suggesting that RIN1 subcellular localization may be regulated by the activity of kinases and phosphatases. S^{292} is reported to be a PKD substrate, and its phosphorylation controls RIN1-mediated inhibition of cell migration (119), although it is unclear how this might collaborate with or influence 14-3-3 binding and/or nuclear localization. While serine phosphorylation and 14-3-3 binding control the subcellular localization of many proteins, including cell cycle regulators, we cannot exclude alternative factors that may also regulate subcellular localization. For example, serine resides can also be modified by O-GlcNAcylation, and this may compete with phosphorylation for occupancy of the same sites (reviewed in (230)). O-GlcNAcylation regulates the nuclear localization of beta-catenin (231) and SP1 (232). Alternatively, the serine resides themselves may be structurally important for conformation.

Previous studies of RIN1 have focused primarily on its role in modulating endocytosis (91,94,95,98,115,116,215) and cytoskeleton remodeling (112,119,233), functions consistent with its cytoplasmic localization. However, the cell cycle-dependent nuclear localization of RIN1 suggests a novel function for this endocytic protein. This is consistent with new findings in the past decade that describe nuclear translocation of several endocytic proteins, although their nuclear functions are generally still unknown. Clathrin CHC17 has been reported in the nucleus, where it binds to p53 and contributes to p53-mediated transcription (234). In response to extracellular stimuli, the RAB5 effectors APPL1 and APPL2 translocate from endosomes to the nucleus where they interact with the nucleosome remodeling and histone deacetylase complex NuRD/MeCP1 (235). Other nucleocytoplasmically shuttled endocytic proteins include eps15, CALM (236), epsin (237), HIP1 (238) and NUMB (239). Although RIN1's nuclear function remains to be elucidated, its cell-cycle dependent nuclear localization suggests a novel pathway by which this RAS effector links signal transduction from the plasma membrane to the nucleus.

3.5 METHODS

Expression constructs

pLVX-tight-puro^R-RIN1 and RIN1^{S351A} were constructed by PCR amplifying RIN1 from pM4-blast^R-RIN1 (102) and pM4-blast^R-RIN1^{S351A} (95), respectively. For site-directed mutagenesis to create the additional serine and NLS mutants, RIN1 was subcloned into pBluescript KS using XbaI and EcoRI sites. The S291A/S292A mutations were made using forward primer encoding 5'- GCTACGGAGGGAGGCCGCAGTGGGGTACCG – 3'. Mutation of the canonical nuclear localization sequence, ^{237}KREK, was made by the following mutations: K237A, R238G, K240A, using the forward primer 5' – GGGACCTAGGGCCCACCGCGGGGGAGGCATTCAAGAGAAGC – 3'. The arginine rich

sequence ^{342}RRR was mutated to ^{342}AAA using the forward primer 5' – CCTCACCCCACCTGGGCGCCGCAGCACCTCTGCTTCGGTCC – 3'. The arginine rich sequence ^{451}RLRRR was mutated to ^{451}RLAAA using the forward primer 5' – CCTGGCAGCCCGCCTGGCCGCCGCCCTTGCCGCAGACGGC – 3'. 3xHA-3xFLAG-tagged constructs were made by PCR amplifying the tag from pcDNA5 FRT/TO 3HA-3FLAG

All shRNAs against RIN1 were from Sigma-Aldrich and in the pLKO.1-puro^R vector. One shRIN1 targeted the 3'UTR (Clone ID: NM_004292.1-2520s1c1) and two shRIN1s targeted the CDS (Clone IDs: NM_004292.1-1424s1c1 and NM_004292.1-2378s1c1).

Cell culture and reagents

HeLa cells were maintained in DMEM (Media Tech) with 10% Fetal Bovine Serum (Hyclone) and 1% penicillin streptomycin (Invitrogen). HeLa cells with stable silencing of RIN1 were established by infection with pLKO.1-shRIN1-puro^R and selection with 1 μg/mL puromycin (Invivogen).

The M296 cell line was a generous gift of Dr. Antoni Ribas (UCLA, Los Angeles, CA). M296 is a human melanoma cell line with an NRAS^{Q61L} mutation and has previously been described (240). M296 cells were cultured in RPMI-1640 (Media Tech) with 10% Fetal Bovine Serum (Hyclone) and 1% penicillin streptomycin (Invitrogen).

MCF10A cells were grown in medium composed of DMEM/F12 supplemented with 5% horse serum, 20 ng/mL epidermal growth factor, 10 μg/mL insulin, 0.5 μg/mL hydrocortisone, 100 ng/mL cholera toxin and 1% penicillin streptomycin.

HeLa, M296 and MCF10A cells with tetracycline-inducible expression of RIN1 were established by lentivirus infection with pLVX-Tet-ON Advanced (Clontech) and selection with G418 (Life Technologies), followed by lentivirus infection with pLVX-tight-puro^R-RIN1 and

puromycin selection. HeLa and MCF10A cells were selected with 400 μg/mL G418 and 1 μg/mL puromycin. M296 were selected with 500 μg/mL G148 and 0.5 μg/mL puromycin.

Early G1 synchronization was achieved by treatment with 20μM lovastatin (Sigma-Aldrich) for 24 hours followed by 1-2 hours release with 1mM mevalonate. Late G2 arrest was performed with 2 mM thymidine for 24 hours, followed by washout and release for 2 hours, then addition of 10μM RO-3306 (Sigma-Aldrich) and incubation for 22 hours. Serum starved cells were starved for 48-72 hours. Double aphidicolin was performed with 2μg/mL aphidicolin and incubating for 20 hours. Cells were washed and released for 12 hours, then 2μg/mL aphidicolin added and incubated for 20 hours. Double thymidine block was performed with 2mM thymidine for 19 hours, washed and released for 9 hours, followed by incubation with 2.5mM thymidine for 24 hours.

Immunofluorescence, Immunoblotting and Immunoprecipitation

Antibodies used for immunoblotting were as follows: tubulin (Sigma Aldrich, T6074), RIN1 (mouse mAb, clone #C9E11, Colicelli lab, AbPro), histone H3 (Cell Signaling Technology, 9715), pan 14-3-3 (Santa Cruz Biotechnology, sc-1657), goat-anti-rabbit IRDye 800 (Li-Cor Biosciences, 926-32211) and goat-anti-mouse-IRDye 680 (Li-Cor Biosciences, 926-32220). For immunoblotting, proteins were transferred to nitrocellulose membranes overnight, followed by blocking in 5% milk in Tris-buffered saline with 0.1% Tween-20 and incubation with primary and secondary antibodies. Membranes were imaged on a Li-Cor Odyssey scanner. For immunoprecipitation, cells were lysed in NP-40 lysis buffer containing 1mM DTT and protease inhibitors. Lysates were incubated with 2 μg goat-anti-RIN1 (Santa Cruz, N-19, sc-1971) and protein A/G agarose beads. Following incubation, beads were washed in NP-40 lysis buffer, boiled in SDS sample buffer and run on SDS-PAGE followed by immunoblotting.

For immunofluorescence, glass coverslips were coated with 10µg/mL fibronectin (Sigma-Aldrich) in PBS. After 1 hour incubation at 37°C, the fibronectin was aspirated and coverslips were washed twice with PBS and cells were plated on top. Prior to staining, cells were fixed in 4% paraformaldehyde (Santa Cruz Biotechnology) for 15 minutes at room temperature. They were then washed three times with PBS, followed by incubation in blocking buffer (1x PBS, 5% normal goat serum, 0.3% Triton X-100) for 1 hour at room temperature. Antibody staining was performed in antibody dilution buffer (1x PBS, 1% BSA, 0.3% Triton X-100). Following secondary antibody incubation, DAPI staining was performed for 5 minutes. Coverslips were mounted onto slides using Aqua-Poly/Mount (Polysciences). The following antibodies were used for immunofluorescence: RIN1 (mouse mAb, clone #C9E11, Colicelli lab, AbPro) and goat-anti-mouse Alexa Fluor 488 (Invitrogen, A11001).

Microscopy

For immunofluorescence, cells were examined on a laser scanning confocal microscope (Axiovert 200M, Carl Zeiss LSM 5 Pascal) or spinning disc confocal microscope (Yokagawa CSU-22 spinning disc, Hamamatsu C9100-13 EMCCD camera, Zeiss Axiovert 200M). Cells were imaged with a plan/neofluar 100× oil lens, NA 1.3 (Carl Zeiss) or a 40x air objective, and 8-bit digital images were captured using a cooled charge-coupled device (transmitted light channel for lsm5 camera, Zeiss). Images were processed using LSM 5 PASCAL software (release version 4.2 sp1). Subcellular localization was assessed and quantified blindly, and all statistical analyses were performed using Student's *t*-test.

Cell fractionation

Asynchronous and synchronized cells were trypsinized and washed once with PBS + 1mM EDTA. Pellets were gently resuspended in 50µL of lysis buffer (10 mM Tris-HCl pH 7.5,

150 mM NaCl, 0.1% NP-40) and incubated on ice for 5 minutes. Half of the sample was reserved as whole cell lysate, while the other half was carefully layered onto 125 µL sucrose (24% sucrose in lysis buffer). Cells were centrifuged at 4°C, 10,000 rpm for 10 minutes. The supernatant (cytoplasmic fraction) was transferred to a new tube. The nuclei pellet was gently washed by adding 100 µL PBS + 1mM EDTA and pipetting off excess liquid. The pellet was resuspended in 400 µL of lysis buffer and sonicated.

The volume of the whole cell lysate and cytoplasmic fractions was brought up to 400 µL with lysis buffer. To immunoprecipitate endogenous RIN1, 2 µg of goat-anti-RIN1 antibody (Santa Cruz Biotechnologies, N-19) was added and pulled down over protein A/G beads.

MTS assay

HeLa cells stably expressing control or RIN1 shRNAs were plated in quadruplicate in a 96-well plate at 1.25×10^3 cells/well and incubated at 37°C for 1-5 days. MTS assay was performed by adding 20 µL of CellTiter 96® AQ$_{ueous}$ One Solution Reagent (Promega) to each well and incubating at 37°C for 35 minutes. Absorbance at 490nm was measured using a PerkinElmer Victor3 plate reader.

MudPIT analysis to identify RIN1 associated proteins

HeLa cells with tetracycline-inducible RIN1-3xHA-3xFLAG or RIN1-NLS^m-3xHA-3xFLAG were allowed to grow asynchronously, or arrested at late G2 phase. Late G2 arrest was accomplished by combining a double thymidine protocol with RO-3306 as follows: cells were incubated with 2mM thymidine for 21 hours, washed and released for 10 hours, incubated with 2mM thymidine for 16 hours, washed and released for 2 hours and incubated with 10 µM RO-3306 for 10 hours. All conditions were induced with 1 µg/mL doxycycline for 60 hours.

Cells were harvested by trypsinization and lysed in FLAG buffer (100 mM Tris-HCl 8.0, 150 mM NaCl, 5 mM EDTA, 5% glycerol, 0.2% NP-40, 1 mM DTT, PMSF, pepstatin, leupeptin, sodium fluoride, sodium orthovanadate) while rotating at 4°C for 45 minutes. Clarified lysate was incubated with EZview Red Anti-FLAG M2 Affinity gel (Sigma-Aldrich) at 4°C for 2 hours. Beads were then washed 4x with FLAG buffer and 2x with detergent-free FLAG buffer. Proteins were eluted sequentially using urea elution buffer (8M urea in 100 mM Tris pH 8.5).

Immunopurified protein complexes were reduced, alkylated and digested by the sequential addition of lys-C and trypsin proteases as described earlier (208). The digested peptide mixture was fractionated online using strong-cation exchange and reverse phase chromatography and eluted directly into a LTQ-Orbitrap mass spectrometer (Thermofisher) (208,209). MS/MS spectra were collected and subsequently analyzed using the ProLuCID and DTASelect algorithms (210,211) . Protein and peptide identifications were further filtered with a false positive rate of less than 5% as estimated by a decoy database strategy (212). Normalized spectral abundance factor (NSAF) values were calculated as described and multiplied by 10^5 to improve the readability (213).

Flow cytometry

For asynchronous profiles, cells were trypsinized and washed in PBS before being resuspended in 70% (v/v) ethanol (at -20°C) per 1×10^6 cells while vortexing gently. Cells were stored at -20°C indefinitely. For staining, cells were pelleted at 400x*g* for 10 minutes and the ethanol aspirated. Cells were then resuspended in 1 mL staining solution (40 μg/mL propidium iodide, 400 μg/mL RNAse) per 1×10^6 cells and incubated at 37°C for 30 min. After staining, the cells were passed through a 35 μm strainer and run on FACS (BD FSRII) using BD FACS Diva

software. Results were analyzed using FlowJo. FACS graphs were gated first on the viable cell population, then on singlets by plotting PE-height vs. PE-area.

For cell cycle progression, 5×10^5 HeLa cells were plated/6cm plate with 2 µg/mL aphidicolin and incubated for 16 hours. Cells were then washed and released for 12 hours. After 12 hours, 2 µg/mL aphidicolin was added to the media and cells were incubated for 16 hours. Cells were then washed and released synchronously into S phase. One plate was harvested at each indicated time point and fixed as above. Cells were then stained together and evaluated as above.

For DNA damage experiments, 2×10^5 HeLa cells were plated/6cm plate and allowed to adhere overnight. Cells were then treated with 0, 1.5 or 8 nM SN-38 for 24 hours. Cells were trypsinized and washed with PBS and then fixed and stained as above.

For quiescence experiments, 1×10^6 MCF10A cells were plated/10cm plate and allowed to adhere overnight. Cells were then washed with PBS and media replaced with DMEM F12 + 1% P/S for 72 hours to starve the cells. Asynchronous cells were plated 1×10^6 MCF10A were plated/10cm plate and allowed to grow for 24 hours. BrdU was added to the plate for 3 hours prior to harvest by trypsinization. Cells were then stained with anti-BrdU-FITC and 7-AAD using the BD Pharmingen FITC BrdU Flow Kit, according to manufacturer's protocol. After staining, the cells were passed through a 35 µm strainer and run on FACS (BD FSRII) using BD FACS Diva software. Results were analyzed using FlowJo. FACS graphs were gated first on the viable cell population, then on singlets by plotting PE-height vs. PE-area.

CHAPTER 4. ABL FUSION ONCOGENE TRANSFORMATION AND INHIBITOR SENSITIVITY ARE MEDIATED BY THE CELLULAR REGULATOR RIN1

4.1 ABSTRACT

ABL gene translocations create constitutively active tyrosine kinases that are causative in chronic myeloid leukemia (CML), acute lymphocytic leukemia (ALL) and other hematopoietic malignancies. Consistent retention of ABL SH3/SH2 autoinhibitory domains, however, suggests that these leukemogenic tyrosine kinase fusion proteins remain subject to regulation. We resolve this paradox, demonstrating that BCR-ABL1 kinase activity is regulated by RIN1, an ABL SH3/SH2 binding protein. BCR-ABL1 activity was increased by RIN1 over-expression and decreased by RIN1 silencing. Moreover, $Rin1^{-/-}$ bone marrow cells were not transformed by BCR-ABL1, ETV6-ABL1 or BCR-ABL1^{T315I}, a patient-derived drug resistant mutant. Rescue by ectopic RIN1 verified a cell autonomous mechanism of collaboration with BCR-ABL1 during transformation. Sensitivity to the ABL kinase inhibitor imatinib was increased by RIN1 silencing, consistent with RIN1 stabilization of an activated BCR-ABL1 conformation having reduced drug affinity. The dependence on activation by RIN1 to unleash full catalytic and cell transformation potential reveals a previously unknown vulnerability that could be exploited for treatment of leukemias driven by ABL translocations. The findings suggest that RIN1 targeting could be efficacious for imatinib resistant disease, and might complement ABL kinase inhibitors in first line therapy.

4.2 INTRODUCTION

Chromosome translocations that join the *BCR* and *ABL1* (a.k.a. c-*Abl*) genes give rise to BCR-ABL1 fusion proteins causative in virtually all cases of chronic myeloid leukemia (CML), many cases of acute lymphocytic leukemia (ALL) and occasionally other myeloproliferative disorders (reviewed in(161)). In addition, *ETV6* (a.k.a. *TEL*) forms fusion oncogenes with *ABL1*(241) and the closely related *ABL2* (a.k.a. Arg)(242) in some leukemias. ABL proteins are non-receptor tyrosine kinases normally under tight regulation, but BCR-ABL1 fusions are constitutively active. The ABL kinase inhibitor imatinib mesylate (a.k.a. STI571 or Gleevec) is a highly effective treatment for CML (reviewed in(243)), providing a demonstration that drugs directly targeted to oncoproteins can be used to manage cancer and perhaps eventually be part of a curative therapy.

Unfortunately, some leukemias with activated ABL oncoproteins do not respond to imatinib. For CML patients who do respond, there is a significant risk of developing resistance due to strong selective pressure for BCR-ABL1 kinase domain mutations that block inhibitor action but retain the catalytic function of the oncoprotein(168). Second-generation kinase inhibitors offer hope for combating imatinib resistance, with some drugs successfully targeting the highly refractory BCR-ABL1^{T315I} mutant (244). But even these new catalytic site inhibitors have limitations in their effectiveness during accelerated and blast phase CML, as well as in the treatment of other ABL fusion leukemias including ALL. In addition, compound mutations following sequential treatment of CML patients with multiple kinase inhibitors (245) provide a path to broad resistance. Some attempts have been made to circumvent resistance by reducing BCR-ABL1 expression (246,247) or stability (248,249) or by targeting collaborative signaling

pathways (250-253). A more direct approach for improving treatment would be to maintain focus on reducing tyrosine kinase activity by targeting oncogenic ABL outside the catalytic site.

ABL tyrosine kinases act in the cytoplasm to coordinate actin remodeling, a function mediated by carboxy terminal filamentous actin binding and bundling domains and by the tyrosine phosphorylation of multiple actin remodeling regulator proteins. ABL1 also has nuclear DNA damage response functions mediated by a DNA binding domain and targeted tyrosine phosphorylation. ABL activity is normally regulated at multiple levels. An amino terminal myristoyl group can attach to a surface pocket in the kinase domain, contributing to an auto-inhibitory fold (137,139), while a short amino terminal "cap" peptide further stabilizes an inactive conformation through additional surface interactions. Downstream of this peptide are SH3 and SH2 domains that cradle the kinase domain and contribute to the adoption of a less active enzyme conformation (254). In addition, several tyrosines in and around the ABL kinase domain can be phosphorylated in trans (by ABL itself and by SRC family kinases) leading to increased catalytic activity (141-143,255). It appears that each form of regulation is conserved between ABL1 and ABL2, which are more than 90% identical throughout their SH3, SH2 and kinase domains.

Chromosome translocations that give rise to *BCR-ABL1* and other *ABL1* fusion oncogenes remove the first coding exon of *ABL1*. This eliminates both the myristoylation site and the amino terminal "cap" that participate in stabilizing the inactive conformation, explaining in part the elevated and constitutive kinase activity of the fusion protein. The same ABL breakpoint is seen regardless of the BCR breakpoint, which is variable. Even with fusion partners other than BCR, the ABL1 breakpoint resides between the alternate first exon (1b) and the second exon (2a) (256). Moreover, oncogenic translocations involving ABL2, though less

common, show the same arrangement (242). In summary, except for extremely rare variants (reviewed in (257)), human ABL fusion oncoproteins are devoid of the autoinhibitory cap peptide but consistently retain ABL SH3 and SH2 domains that provide a separate autoinhibitory function likely to limit kinase activity (258). In the murine retroviral v-Abl oncoprotein, by contrast, the Abl1 SH3 domain is disrupted by fusion with viral Gag sequences. As a result, v-Abl is a highly active kinase and *v-Abl* is a more potent transforming gene than *BCR-ABL1* (259).

RIN1 is a RAS effector protein that binds to and activates ABL tyrosine kinases (112,144). Signaling is initiated by low affinity binding of a proline rich sequence on RIN1 to the SH3 domain of ABL. This interaction leads to phosphorylation of RIN1 on tyrosine 36, which subsequently associates with the ABL SH2 domain. The resulting stable divalent interaction (RIN1 proline-rich motif and phospho-Tyr^{36} bound to ABL SH3 and SH2 domains, respectively) relieves the ABL autoinhibitory fold and leads to activation of the ABL kinase through enhanced catalytic efficiency (144). Both ABL1 and ABL2 are activated by RIN1, and this requires only the ABL SH3, SH2 and kinase domains. Activation by RIN1 is independent of ABL trans-phosphorylation and is unaffected by an imatinib-resistance mutation (144). Silencing of RIN1 results in less tyrosine phosphorylation on CRKL, one of the best characterized ABL substrates, and deletion of the mouse *Rin1* gene causes reduction in basal levels of phospho-CRKL (112). These observations demonstrate that RIN1 directly stimulates the tyrosine kinase activity of ABL proteins and is required for maintaining normal ABL kinase activity *in vivo*.

We showed previously that RIN1 interacts with BCR-ABL1 and that over-expression of RIN1 promotes the transforming ability of BCR-ABL1 in hematopoietic cells and can rescue low transformation efficiency BCR-ABL1 mutants (111). Moreover, RIN1 significantly enhanced

the leukemogenic properties of BCR-ABL1 in a murine model system (111). These findings

suggested that the "constitutively active" BCR-ABL1 oncoprotein remains responsive to positive

regulation by RIN1. Here we show that BCR-ABL1 positive leukemia cell phosphotyrosine

levels are increased by RIN1 over-expression, providing an explanation for leukemogenic

enhancement by RIN1. Deletion of RIN1 blocked transformation of bone marrow cells by

multiple ABL fusion oncogenes including the kinase inhibitor-resistant mutant BCR-ABL1^{T315I},

demonstrating the cell-autonomous dependence of ABL oncoproteins on RIN1. Silencing of

RIN1 in a BCR-ABL1 positive leukemia cell line and primary ALL cells decreased levels of

cellular phosphotyrosine and at the same time increased sensitivity to imatinib. Our results

demonstrate a vital role for the physiological ABL regulator RIN1 in transformation by BCR-

ABL1, while uncovering a novel point of vulnerability that could be exploited for treatment of

leukemias driven by ABL tyrosine kinase oncoproteins.

4.3 RESULTS

BCR-ABL1 activity is increased by RIN1

Because RIN1 stimulates tyrosine kinase activity by binding to the ABL SH3 and SH2

autoinhibitory domains (112,144), and these domains are consistently present in human

leukemogenic ABL fusion proteins (Fig. 4-1A), we asked whether over-expression of RIN1

could enhance BCR-ABL1 kinase activity. K562 cells, which are derived from a BCR-ABL1

positive CML patient sample, were transduced with a RIN1 lentivirus or a control vector. The

RIN1 over-expressing K562 cells had elevated levels of total cellular tyrosine phosphorylation,

consistent with higher BCR-ABL1 kinase activity, when compared to vector control cells (Fig.

4-1B, left two lanes). Note that RIN1, itself an ABL substrate, appears on the phospho-tyrosine

immunoblot near the 95 kDa marker. There was no change in the level of BCR-ABL1 protein in

K562 cells over-expressing RIN1 (Fig. 4-1C), indicating that activation of existing BCR-ABL1 was responsible for the observed increase in cellular tyrosine phosphorylation.

We next examined tyrosine phosphorylation of a specific BCR-ABL1 substrate. CRKL is a well-characterized target of ABL1, ABL2 and BCR-ABL1. Indeed, CRKL phosphorylation is used as an indicator of BCR-ABL1 activity in patient-derived CML cells (168). We observed an elevation of CRKL tyrosine phosphorylation levels in RIN1 transduced K562 cells compared to vector control cells (Fig. 4-1D). These results make clear that, while it is constitutively active relative to ABL1, the BCR-ABL1 oncogene is still responsive to the physiological regulator RIN1. Elevated kinase activity likely accounts, at least in part, for the enhancement of *BCR-ABL1* mediated transformation and leukemogenesis by RIN1.
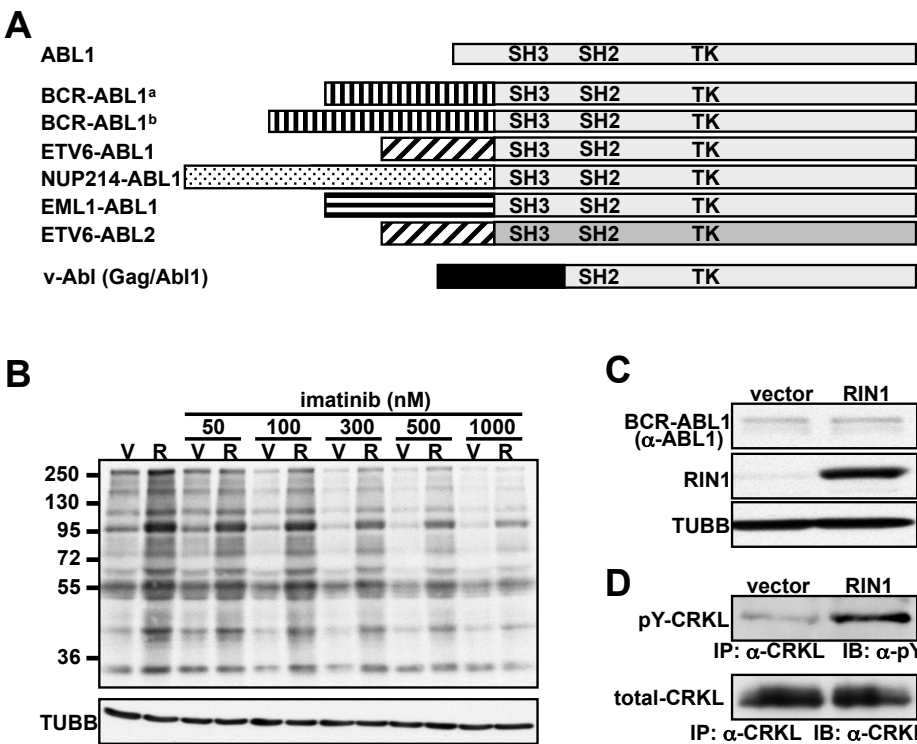
Figure 4-1. BCR-ABL1 kinase activity in K562 cells is increased by RIN1. A. Linear representation of ABL1 (top), translocation-derived human ABL1 and ABL2 fusion oncoproteins (middle six entries) and murine retroviral v-Abl (bottom). Src homology domains (SH2 and SH3) and tyrosine kinase (TK) domains are indicated. BCR-ABL1[a] represents the p190 isoform associated predominantly with ALL; BCR-ABL1[b] represents the p210 isoform associated predominantly with CML. **B.** K562 cells transduced with vector (V) or RIN1 expression lentivirus (R) were treated with imatinib for 30 minutes at the indicated concentration and analyzed by immunoblot with anti-phosphotyrosine (MW markers in kDa at left). The ~95 kDa band that intensifies in the R sample is most likely RIN1. β-tubulin (TUBB) immunoblot was used for normalization. **C.** Levels of BCR-ABL1 (210 kDa) expression were evaluated by anti-ABL1 immunoblot of control (vector) and RIN1 over-expression (RIN1) K562 cells (ABL1

76

migrates below this region). RIN1 immunoblot showed approximately 8-10 fold over-expression above endogenous levels. TUBB immunoblot was used to normalize extracts. **D.** Tyrosine phosphorylated endogenous CRKL (pY-CRKL) evaluated by immunoprecipitation with anti-CRKL and immunoblot with anti-phosphotyrosine (top) or anti-CRKL (bottom).

The ABL inhibitor imatinib works by binding to and stabilizing an inactive conformation of the kinase domain (260). We therefore tested whether RIN1, which our model predicts should induce an active conformation, might enhance catalytic activity even in the presence of this kinase inhibitor drug. The levels of total cellular phosphotyrosine remained elevated in RIN1 over-expression cells compared to control cells across a wide range of imatinib concentrations (Fig. 4-1B), suggesting that enhancement of endogenous BCR-ABL1 kinase activity by RIN1 continues in the presence of imatinib. The persistence of higher tyrosine phosphorylation levels in the RIN1 over-expression K562 cells also correlated with resistance to long term culture in imatinib (Fig. 4-S1). This modest effect may reflect other changes, however, and its relevance to in vivo resistance has not been validated.
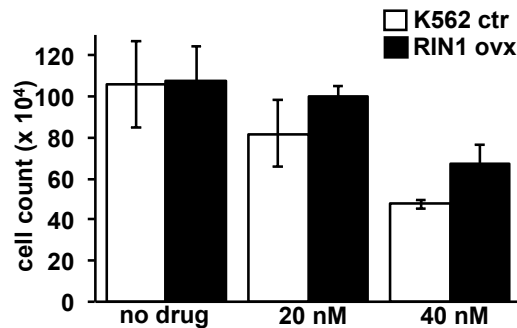
Figure 4-S1. RIN1 overexpression promotes K562 cell survival in imatinib. K562 cells ($1x10^5$/ml) transduced with vector (ctr) or RIN1 virus (ovx) were grown without or with imatinib (20 nM or 40 nM) for 4 days and then trypan blue negative cells were counted. Standard deviations were derived from duplicate samples counted in triplicate.

RIN1 is expressed in hematopoietic cells but is not needed for lineage development or engraftment

The mouse Rin1 gene is expressed most highly in brain but also in other tissues (113). We detected Rin1 in the murine hematopoietic cell lines 32D (myeloid) and BaF3 (lymphoid; pro-B) (Fig. 4-2A) as well as in spleen and thymus, tissues rich in lymphoid cells (Fig. 4-2B). Examination of thymus tissue showed Rin1 expression throughout the T cell-rich medullary and
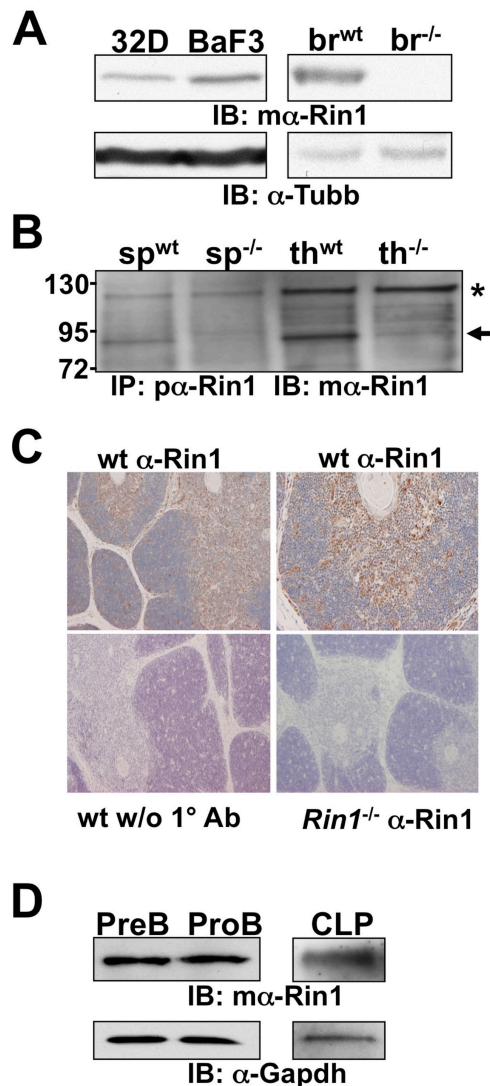
Figure 4-2. Endogenous mouse Rin1 expression. A. Left: Immunoblot (IB) of Rin1 in 32D and BaF3 cells. Right: IB of wild type (wt) and $Rin1^{-/-}$ (-/-) brain (br) tissue confirming antibody specificity. **B.** IB of immunoprecipitated (IP) material from spleen (sp) and thymus (th) tissue of wt and $Rin1^{-/-}$ mice. Arrow indicates Rin1. Asterisk marks background band. **C.** Immuno-histochemical stain of Rin1 in mouse thymus. Top two panels are wild type thymus probed with anti-Rin1 and counter stained with hematoxylin (left = 4X mag; right = 10X mag). Bottom left is wild type control without anti-Rin1. Bottom right is $Rin1^{-/-}$ thymus control. **D.** IB of Rin1 in PreB, ProB and common lymphoid progenitor (CLP) cells.

cortical regions (Fig. 4-2C). Rin1 was also observed in sorted populations of common lymphoid progenitor cells as well as pro- and

pre-B cells (Fig. 4-2D). $Rin1^{-/-}$ mutant mice develop normally, however, with cell types and tissues that would otherwise express Rin1 appearing unchanged (110). When bone marrow cells from wild type and matched $Rin1^{-/-}$ mice were examined in more detail using multi-marker FACS analysis, no significant changes in lineage composition were uncovered (data not shown). This result suggests that while some aspects of Ras signaling contribute to hematopoietic differentiation (261), the Ras effector Rin1 is not required for normal development in these lineages. Cultured $Rin1^{-/-}$ bone marrow cells also proliferated at the same rate as wild type cells in response to IL7 and M-CSF (data not shown), demonstrating that $Rin1^{-/-}$ bone marrow cells remain responsive to these physiological factors.

The surface marker and growth factor response analyses suggested that Rin1 is unnecessary for lineage development. Alterations in hematopoietic stem or progenitor cells may have been

undetectable with these methods, however. We next engrafted bone marrow from wild type or

Rin1^{-/-} donors (CD45.2) into lethally irradiated recipients (CD45.1). At 34 and 105 days post-transplantation, hematopoietic compartments (bone marrow, spleen and thymus) were isolated from recipient mice and examined for lineage composition. Similar profiles were observed for both genotypes at both time points (Table 4-1), suggesting that Rin1 is dispensable for the regeneration of a complete hematopoietic system.

	Day 34		**Day 105**	
Antibody (lineage)	**wild type**	***Rin1*^{-/-}**	**wild type**	**Rin1^{-/-}**
Bone Marrow				
CD19 (B cell)	18%	15%	26%	25%
CD11b (mac/gran)	26%	25%	42%	41%
Ter119 (erythroid)	14%	16%	22%	27%
Spleen				
CD19 (B cell)	50%	52%	73%	72%
CD11b (macro/granulo)	4%	4%	5%	4%
CD3e CD4 (helper T)	6%	4%	7%	15%
CD3e CD8 (cytotoxic T)	3%	2%	8%	6%
Thymus				
CD4$^+$ CD8$^-$ (mature T)	9%	9%	6%	10%
CD4$^-$ CD8$^+$ (mature T)	3%	3%	7%	6%
CD4$^+$ CD8$^+$ (immature T)	80%	81%	82%	82%
CD4$^-$ CD8$^-$ (immature T)	2%	2%	5%	3%

Table 4-1. Engraftment of *Rin1*^{-/-} bone marrow cells. CD45.2 wild type or Rin1-/- bone marrow samples were transplanted into lethally irradiated CD45.1 mice. After 34 or 105 days, flow cytometric analysis was performed on BM, spleen and thymus cell suspensions. Data are presented as the percentage of single live donor cells (CD45.2+ and 7AAD excluded).

Previous studies showed that *Rin1*^{-/-} neurons and epithelial cells exhibit conditional (e.g. stimulation- and stress-dependent) phenotypes (110,112). We therefore considered whether *Rin1*^{-/-} bone marrow cells might be compromised in their response to oncogenic forms of ABL1.

RIN1 is required for transformation by BCR-ABL1 and ETV6-ABL1

BCR-ABL1 transforms primary bone marrow cells, and this leads to measurable growth factor independent proliferation *in vitro* (262). To test whether RIN1 is required for transformation, the p210 isoform of BCR-ABL1, which is common in CML, was introduced by retroviral transduction into primary bone marrow cells from wild type or *Rin1*$^{-/-}$ mutant mice. Cells were then cultured in the absence of growth factors and periodically counted. *Rin1*$^{-/-}$ cells showed much less expansion than wild type cells in these assays (Fig. 4-3A), but grew equally well in the presence of growth factors (data not shown). This suggested that the growth factor independence normally conferred by BCR-ABL1 (262) is to a large degree dependent on the presence of RIN1. Similar results were seen when using the ETV6-ABL1 oncogene (Fig. 4-3B), indicating that the need for RIN1 is associated with the ABL tyrosine kinase rather than the upstream fusion partner.

To determine whether RIN1 is required cell autonomously for ABL-mediated transformation, we transduced bone marrow cells with BCR-ABL1 and RIN1. For these experiments we used the ABL-binding domain of RIN1 (RIN1^{ABD}). This fragment, like full length RIN1, can enhance cell transformation by BCR-ABL1 (111). Reconstitution of RIN1 expression restored BCR-ABL1-mediated transformation of *Rin1*$^{-/-}$ cells (Fig. 4-3C). RIN1 and RIN1^{ABD} have no transforming activity on their own in this assay (111), so the recovery of transforming potential can be attributed to the restored collaboration of RIN1 and BCR-ABL1. As a further control, we employed a RIN1 mutant with multiple tyrosine-to-phenylalanine substitutions that severely compromise ABL binding and activation (112,183). The mutant was unable to rescue *Rin1*$^{-/-}$ bone marrow cells for transformation by BCR-ABL1 (Fig. 4-3D). Taken together, these results support a direct and obligate role for RIN1 in the transformation of primary bone marrow cells by BCR-ABL1.
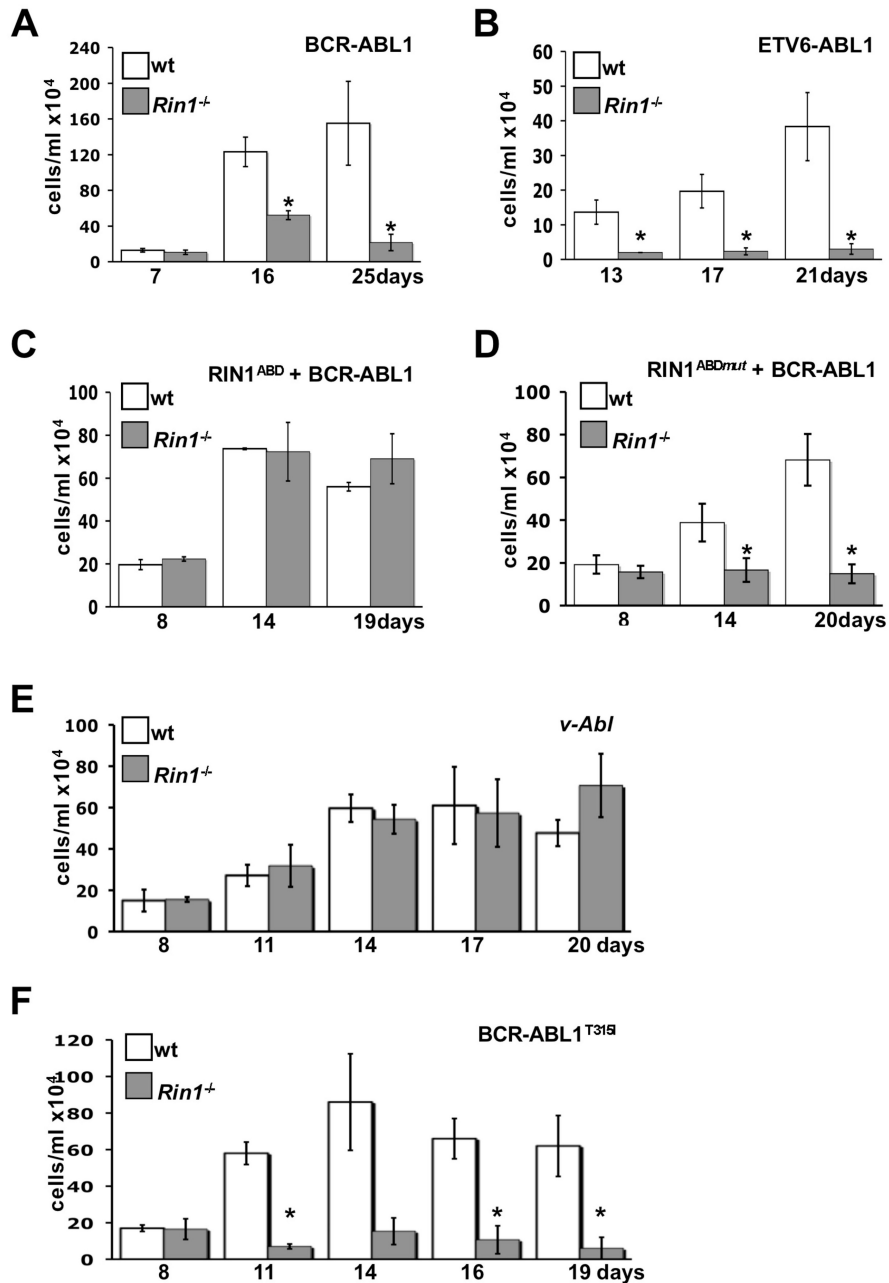
Figure 4-3. Rin1 is required for transformation of primary bone marrow (BM) cells to growth factor independence. A. BM cells from wild type or $Rin1^{-/-}$ mice were infected with a BCR-ABL1 (p210) retrovirus, cultured without growth factors and counted at indicated times. **B.** BM cell transformation as in "A", except using ETV6-ABL1 (a.k.a. TEL-ABL) retrovirus. **C.** BM cell transformation as in "A", except using virus expressing both BCR-ABL1 and RIN1[ABD]. **D.** BM cell transformation as in "C", except using a mutant (RIN1[ABDmut]) that does not bind ABL1. **E.** BM cell transformation as in "A", except using v-*Abl* retrovirus. **F.** BM cell transformation as in "A" except using the multi-drug-resistant mutant BCR-ABL1[T315I]. All results are for duplicate samples counted in triplicate. Bars show standard deviation; * indicates P < 0.05 between wt and $Rin1^{-/-}$. In panel F, 14 day sample P = 0.06 between wt and $Rin1^{-/-}$.

BCR-ABL1 transduced bone marrow cells from wild type and *Rin1⁻/⁻* donors were also examined in transplantation experiments. We observed no striking differences in the penetrance or intensity of disease in models of lymphoid (111) or myeloid (263) leukemia (Fig. 4-S2). The absence of a dramatic reduction in leukemogenesis comparable to that seen in growth factor independence assays of cultured bone marrow cells may reflect a richer growth environment and longer time frame for the *in vivo* experiments.
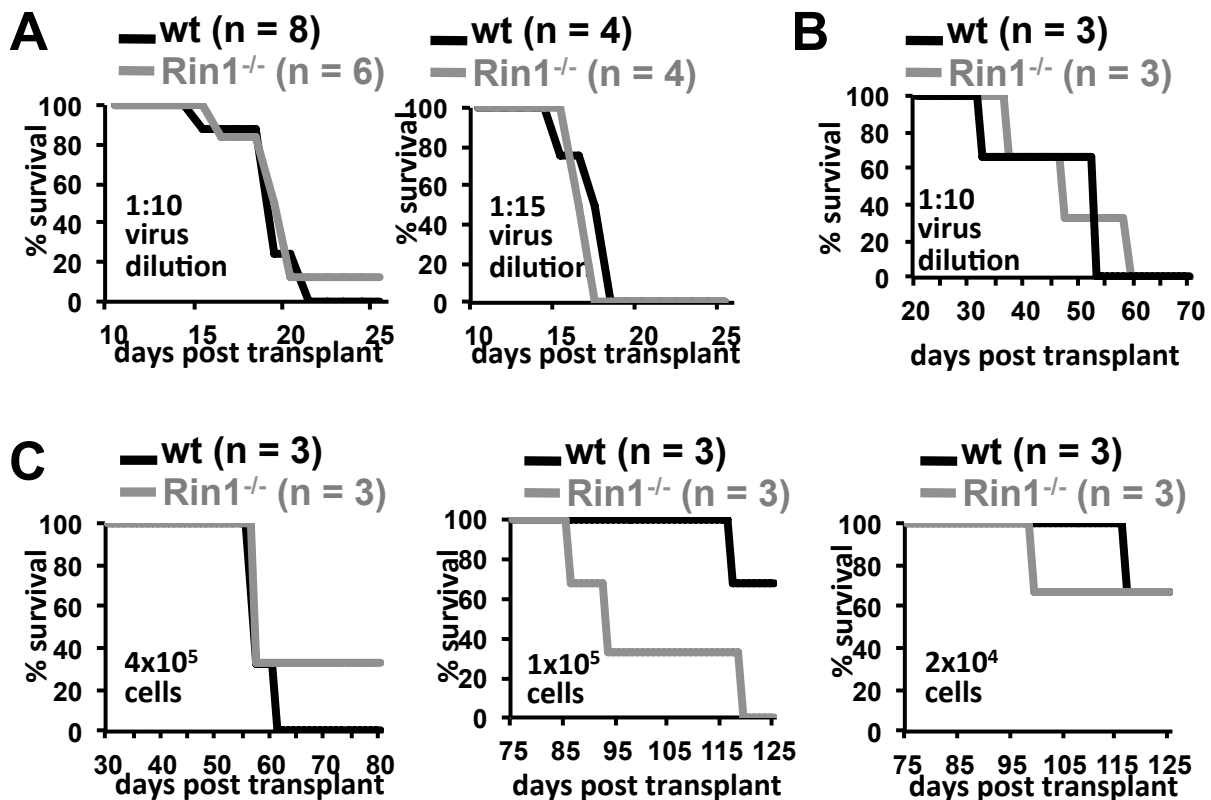
Figure 4-S2. Bone marrow transplant leukemia model system. A. Bone marrow cells from 5FU-treated wild type (wt) and *Rin1⁻/⁻* mice were infected with a BCR-ABL1 (p210) retrovirus at the indicated dilution and transplanted in lethally irradiated recipient mice that were monitored for myeloid disease over the indicated time course. **B.** Bone marrow infection and transplantation as in "A" except donor mice were not treated with 5-FU, and recipient mice were monitored for lymphoid disease. **C.** Secondary transplant experiments were performed by injection of transformed myeloid cells from recipients of p210 infected bone marrow cells (as in "A" except that sub-lethal irradiation was used). The number of injected cells is indicated.

v-Abl does not require de-repression by RIN1 for cell transformation

The murine *v-Abl* oncogene arises from the fusion of a retroviral *Gag* gene and cellular *Abl1* sequences. Unlike human ABL fusion oncoproteins, v-Abl does ***not*** include the autoinhibitory SH3 domain (Fig. 4-1A). As a consequence, *v-Abl* is a more active tyrosine kinase and a more potent transforming gene than *BCR-ABL1*(259). *Rin1*$^{-/-}$ bone marrow cells were transformed to growth factor independence by *v-Abl* as efficiently as wild type bone marrow cells (Fig. 4-3E), indicating that an ABL oncoprotein unhindered by SH3 domain autoinhibition does not require RIN1 binding. Although v-Abl differs from BCR-ABL1 in other ways, this result is consistent with RIN1 acting through de-repression of the ABL SH3 domain to promote transformation.

The kinase inhibitor-resistant BCR-ABL1*^{T315I} *mutant still requires RIN1

We next asked whether RIN1 was required by a multi-drug-resistant BCR-ABL1 mutation observed in CML patients. An otherwise normal (non-fusion) ABL1 kinase with the T315I kinase domain "gatekeeper" mutation is still responsive to RIN1 (144), suggesting that this mutation does not alter RIN1 binding and subsequent kinase derepression. Indeed, although wild type bone marrow cells transduced with BCR-ABL1^{T315I} proliferated well, equivalent *Rin1*$^{-/-}$ bone marrow cells transduced with the same BCR-ABL1^{T315I} virus were not transformed (Fig. 4-3F). This provides further evidence that BCR-ABL1 is reliant on RIN1 for relief of autoinhibition and perhaps for additional contributions to signal transduction pathways required for transformation. This result also demonstrates that regulation by RIN1 is independent of ABL active site alterations conferring resistance to kinase inhibitors, and strongly suggests that drug-resistant BCR-ABL1 mutants may be susceptible to blockade of RIN1 association.

RIN1 directly regulates drug response in human leukemia cells

A

KU812

no drug ☐
10 nM ☐
20 nM ☐
40 nM ☐
80 nM ☐
160 nM ■

% viability

2 days   4 days   6 days

B

KY01

% viability

2 days   4 days

C

LAMA84

% viability

2 days   4 days   6 days

D

K562

% viability

3 days   5 days   7 days

E

JURL-MK1

no drug ☐
125 nM ☐
250 nM ☐
500 nM ☐
1000 nM ☐
1500 nM ■

% viability

2 days   4 days   6 days

F

BV173

% viability

2 days   4 days

G

KCL22

% viability

2 days   4 days   6 days

H

Cell Line	EC50 range
KU812	20-40 nM
KY01	20-40 nM
LAMA84	10-20 nM
K562	20-40 nM*
JURL-MK1	125-250 nM
BV173	125-250 nM
KCL22	125-250 nM

Figure 4-S3. Imatinib response of human leukemia cell lines. Cells were cultured for 2, 4 or 6 days in the indicated concentration of imatinib and the percent of viable cells (trypan blue negative versus total) was plotted for **A.** KU812; **B.** KY01; **C.** LAMA84; **D.** K562; **E.** JURL-MK1; **F.** BV173; **G.** KCL22. Initial culture densities were 1 x 10^4 cells/ml. **H.** shows approximate EC50 range for cell viability of each line at 4 days (*5 days for K562).

We next turned to cell lines originating from human leukemias with *BCR-ABL1* oncogenes for additional insight into the role of RIN1. RIN1 was detected in multiple BCR-ABL1 positive myeloid leukemia lines (KCL22, JURL-MK1 and K562) and B cell lineage leukemia cell lines (BV173, TOM-1 and SUP-B15) (Fig. 4-4A). RIN1 was not detected by immunoblot in three other CML lines (LAMA-84, KU-812 and KY01). We found a suggestive association between RIN1 expression and imatinib sensitivity (Fig. 4-S3); the three lines with undetectable RIN1 were the most sensitive to imatinib (Fig. 4-S3A-C & H), while KCL22 had the highest RIN1 level and was least sensitive (Fig. 4-S3G & H). Further analysis with more leukemia cell samples and more precise drug response data will be needed to validate the significance of this correlation, which does not account for factors such as drug efflux rates.
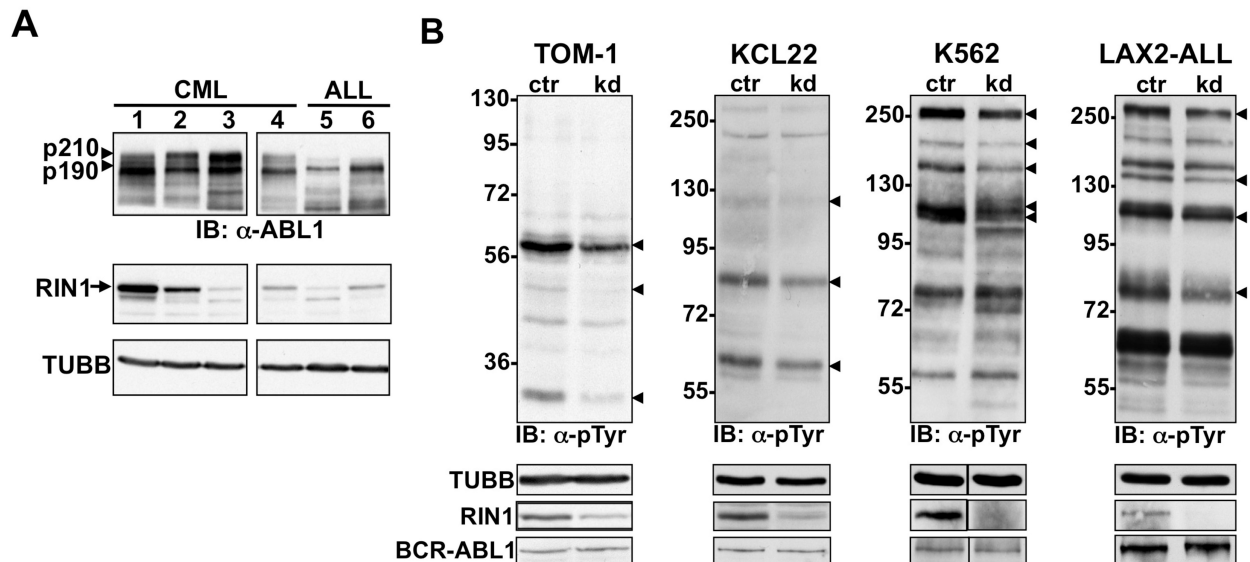
Figure 4-4. Analysis of human leukemia cells. A. Panel of CML and ALL cell lines immunoblotted with anti-ABL1 (top), anti-RIN1 (middle) or anti-TUBB (bottom). CML cells (1=KCL22; 2=JURL-MK1; 3=K562) and a B lymphoid CML blast crisis cell line (4=BV173) express the p210 form of BCR-ABL, while ALL-derived cells (5=TOM-1; 6=SUP-B15) express the p190 form (arrowheads). Full length RIN1 is marked with an arrow (faster migrating bands may be alternately spliced isoforms). **B.** TOM-1, KCL22, K562 and primary pre-B-ALL cells infected with control (ctr) or RIN1-directed (kd) shRNA were analyzed by immunoblot with anti-phosphotyrosine. MW (kDa) markers are at left, arrowheads mark bands most clearly reduced by RIN1 silencing. Lower panels show immunoblots for TUBB, RIN1 and BCR-ABL1.

Given the unique nature of each established leukemia cell line, we chose to directly evaluate the contribution of RIN1 to BCR-ABL1 function in several lines. Constitutive knock down of RIN1 expression using shRNA altered the total phosphotyrosine patterns in TOM-1, KCL22 and K562 cells (Fig. 4-4B). Although many phospho-proteins appeared unaffected, numerous bands were weaker in the RIN1 knock down cell lines. No change was detected in the amount of BCR-ABL1, consistent with a reduction in enzyme activity as an explanation for the primarily diminished cellular phosphotyrosine profile. The few band intensity increases in K562 cells may reflect enhanced kinases or repressed phosphatases downstream of BCR-ABL1.

We reasoned that the loss of RIN1 might reduce the stability of the active BCR-ABL1 kinase conformation, and render these leukemia cells more susceptible to an ABL kinase inhibitor that preferentially binds the inactive conformation. Silencing RIN1 expression in TOM-1 (264) cells markedly increased sensitivity to 8µM imatinib (Fig. 4-5A), a concentration selected as moderately cytotoxic to this ALL line. This result suggested that the loss of RIN1 can synergize with standard kinase inhibitors to block oncogenic ABL kinases. The viability and proliferation rate of TOM-1 cells with the RIN1-targeted shRNA showed no significant difference from TOM-1 cells with the scrambled shRNA control (Fig. 4-S4A), perhaps because silencing was less than complete or because these established leukemia cell lines have been selected for additional mutations that promote vigorous growth in culture. To rule out off-target effects, the stable RIN1 knock-down TOM-1 cell line was transduced with a murine *Rin1* cDNA that is resistant to the human RIN1-targeted shRNA (data not shown). Ectopic Rin1 rescued imatinib resistance (Fig. 4-5B). Consistent with restored BCR-ABL1 activity, expression of murine Rin1 also reversed most of the phosphotyrosine signal suppression in RIN1 kd TOM-1 cells (Fig. 4-5C).
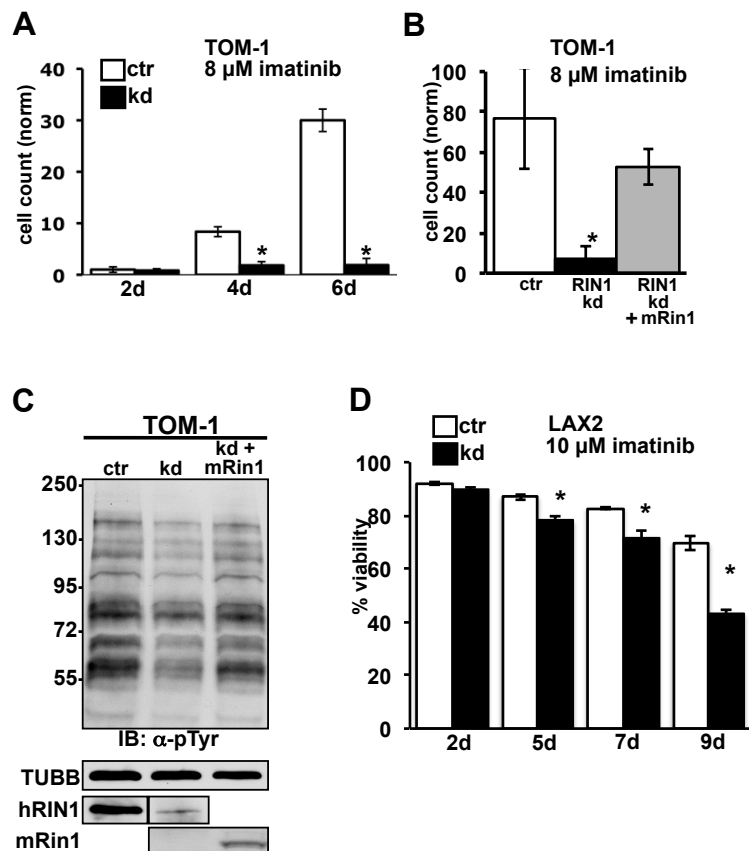
Figure 4-5. RIN1 silencing sensitizes ALL cells to imatinib. A. Control (ctr) and RIN1 silenced (kd) TOM-1 cells (1×10^4/ml) were cultured in 8 μM imatinib for the indicated time. Cell counts normalized to 2d-ctr. **B.** Control (shCTR), RIN1 knockdown (shRIN1) and knockdown rescued with mouse Rin1 (shRIN1 + mRin1) TOM-1 cells were cultured in 8 μM imatinib for 9 days. **C.** Control, RIN1 kd and RIN1 kd + mRin1 TOM-1 cells were immunoblotted with anti-phospho-tyrosine. TUBB and RIN1 immunoblots are shown below. Murine Rin1 and human RIN1 were detected using different antibodies. Note: the hRIN1 bands are from the *same* exposure of a single immunoblot. **D.** Control (ctr) and RIN1 silenced (kd) B-ALL cells were cultured in 10 μM imatinib for the indicated time. Cell viability was determined by propidium iodide stain and flow cytometry. Panels **A**, **B** and **D**: standard deviations from triplicate samples counted in duplicate; * indicates P < 0.05 between control and knockdown.

Primary pre-B ALL cells from the bone marrow biopsy of a 38 year-old male patient were used next to evaluate the translational relevance of RIN1-targeted silencing. These cells were collected from a relapse leukemia and carry the p210 form of BCR-ABL1 with a T315I mutation, which confers imatinib-resistance. RIN1 knock down reduced the intensity of the cellular phosphotyrosine signal (Fig. 4-4B) and enhanced imatinib sensitivity (Fig. 4-5D), without altering baseline proliferation rate of the cells (Fig. 4-S4C). These findings support and extend the conclusion that a direct ABL activator, RIN1, controls the set point for imatinib sensitivity, even in cells expressing the normally refractory BCR-ABL1^{T315I} allele. They also imply that RIN1 silencing or inhibition might collaborate with a direct kinase inhibitor to overcome the leukemogenic properties of ABL fusion proteins.

A

TOM-1

B

TOM-1 (09/08)   TOM-1 (01/09)

RIN1

TUBB

C

LAX2 (preB-ALL)
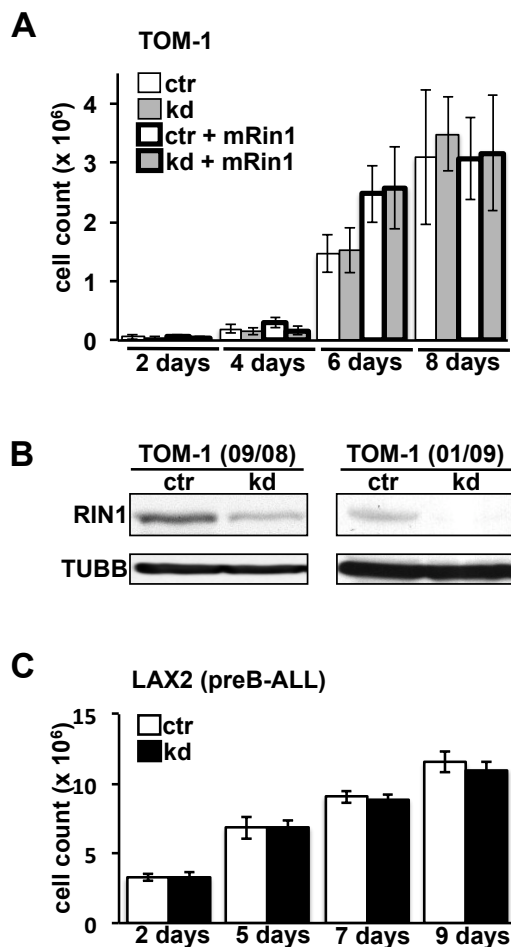
Figure 4-S4. Proliferation of leukemia cells with silenced RIN1. A. Control (ctr) and RIN1 knockdown (kd) TOM-1 cells (1×10^4/ml), were grown over the indicated time course and the number of live cells (trypan blue negative) determined. **B.** RIN1 expression in TOM1 cells transduced with control or RIN1 shRNA. Cells were frozen and thawed between the first and second immunoblot. **C.** Control (ctr) and RIN1 knockdown (kd) LAX2 cells (2.5×10^6/well) were cultured and the viable cell number determined as in "A". Standard deviations were derived from triplicate samples counted in duplicate.

4.4 DISCUSSION

Translocations that create BCR-ABL1 and other human leukemogenic ABL gene fusions consistently retain the ABL SH3 and SH2 domains, despite the fact that biochemical and structure data have established that these domains restrain kinase activity. Our data suggest that RIN1 binding to ABL SH3 and SH2 domains stabilizes the active conformation of the kinase, enhancing the already constitutive activity of the fusion protein (Fig. 4-6). The result is increased cellular tyrosine phosphorylation and transforming activity in the presence of RIN1, which comports with the observed over-expression of RIN1 in some leukemias and lymphomas (265). RIN1 loss greatly reduced the ability of ABL1 fusions to establish a transformed phenotype in bone marrow cells, consistent with a cell autonomous requirement for RIN1 to unleash the full potential of ABL tyrosine kinases. Even BCR-ABL[T315I], a drug-resistant mutant with increased transformation potency (266), was dependent on RIN1 for bone marrow cell transformation. However, we did not detect any significant effects of Rin1 deletion on leukemogenesis by BCR-ABL1 transduced bone marrow cells in mouse transplantation model systems. These data

suggest an important supporting role for RIN1 in BCR-ABL1 mediated transformation, but do not fully resolve the contribution of RIN1 in spontaneous leukemias.
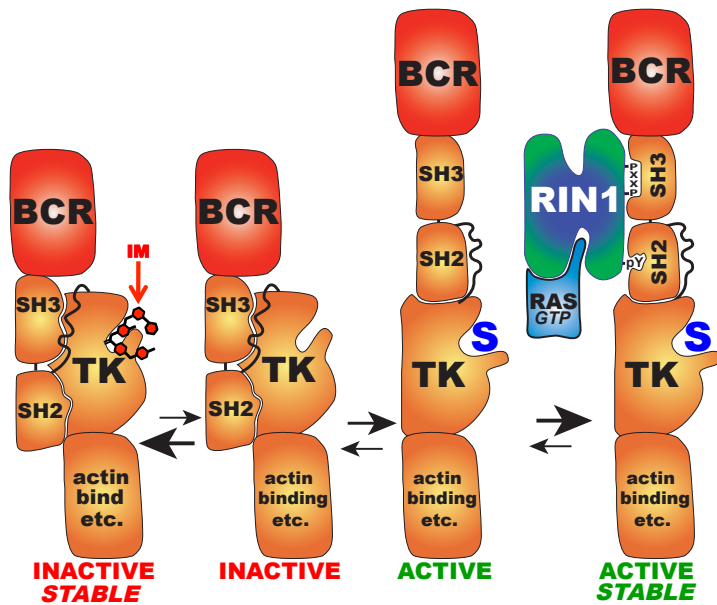
Figure 4-6. Model of RIN1 effect on BCR-ABL1 activity and imatinib sensitivity. BCR-ABL1 equilibrates between active and inactive conformations, favoring the active form (open to substrate (S)) relative to ABL1. **Right:** RIN1 binds to ABL1 SH3 and SH2 domains, alleviating residual autoinhibition and stabilizing a high activity conformation. RIN1 is also a RAS effector (79,112). **Left:** Imatinib (IM) preferentially binds and stabilizes the inactive conformation of the ABL1 catalytic site (260). RIN1 over-expression shifts equilibrium to right; RIN1 silencing shifts equilibrium to left.

The absence of an SH3 domain in murine v-Abl (Gag-Abl1) increases its constitutive kinase activity and makes it a highly potent oncogene. Deletion of the autoinhibitory SH3 domain is likely to be more strongly activating than derepression by binding to endogenous RIN1. But while an SH3 deletion mutant of BCR-ABL1 does potently transform cells *in vitro* and produce myeloproliferative disorders in a xenograft model (267), it does not possess full leukemogenic potential (268). There are also significant differences in the types of leukemias induced by *v-Abl* versus *BCR-ABL1* (269). Together with the fact that oncogenic fusions disrupting the ABL1 SH3 domain are extremely rare in human leukemias (257), it seems likely that the ABL SH3 domain is retained through selective pressure because it contributes to leukemogenesis and/or leukemia progression *in vivo*. Additional evidence for this model comes from studies demonstrating that trans-phosphorylation of BCR-ABL1 SH3 and SH2 domain tyrosines modulates transforming activity (270). RIN1 likely functions, in part, to elevate ABL

tyrosine kinase activity above a transformation threshold level while allowing the SH3 domain to enhance leukemia progression through other mechanisms. RIN1 might additionally contribute to oncogenic ABL signaling by influencing substrate specificity, directing subcellular distribution of ABL fusion proteins or recruiting signaling partners that promote expansion of the leukemic cell population. An alternative explanation for consistent SH3 domain retention is strong preference for recombination in the first ABL1 intron. This is unlikely given the evidence cited and because all oncogenic ABL2 fusions show the same breakpoint (in this case between exons 2 and 3).

Because BCR-ABL1 is required to maintain cell transformation, a phenomenon described as "oncogene addiction", RIN1 silencing alone might be expected to impair tumor cell proliferation. Although reduced RIN1 expression did not arrest TOM-1 or LAX2 cells in our experiments, it did significantly heighten the sensitivity of these cells to imatinib. This enhanced drug responsiveness may result from a shift toward the inactive ABL1 kinase conformation that imatinib preferentially binds and stabilizes (260), and away from the active kinase conformation that RIN1 preferentially binds and stabilizes (144) (Fig. 4-6). Conformation stabilization does not imply protein stabilization, and we observed no indication that altered RIN1 levels affect BCR-ABL1 protein levels. The drug sensitizing effect of RIN1 silencing suggests that disruption of RIN1 binding might synergize with kinase inhibitors to significantly expand the range of leukemias that respond to these drugs. We note that some BCR-ABL1 positive leukemia cell lines had relatively low RIN1 levels. RIN1 may nevertheless be important in those cells for BCR-ABL1 activity and transformation. Alternatively, low RIN1 expression may indicate additional genetic alterations, occurring *in vivo* or in culture, that confer a degree of independence from RIN1.

In epithelial cells, RIN1 plays a role in plasma membrane receptor internalization and cell motility through the coordinated activation of RAB5 GTPases that regulate endocytosis and ABL tyrosine kinases that regulate actin remodeling (112,115). In solid tumors, RIN1 is a tumor suppressor in breast cancer (102), but a tumor enhancer in non-small cell lung cancer (98). In both cases, the main contribution of RIN1 appears to be through RAB5 activation and growth factor receptor trafficking. The rescue of $Rin1^{-/-}$ bone marrow cell transformation by a RIN1 amino terminal fragment with no RAB5-GEF domain, however, demonstrates that RAB5 activation is not required for collaboration with BCR-ABL1. The apparently contradictory roles for RIN1 as a myeloproliferative disorder enhancer and epithelial carcinoma suppressor (in breast cancer) is perhaps not surprising given the differences between these diseases and their cells of origin. Neither is it unprecedented; NOTCH1 gain of function is associated with T cell leukemias (271) while NOTCH1 silencing contributes to the progression of cervical cancers (272).

RIN1 silencing reduced BCR-ABL1 activity while enhancing imatinib sensitivity in established and primary leukemia cells, possibly the result of a shift toward the inactive ABL conformation. Mutations in the SH3-SH2 domains of BCR-ABL1 can also reduce imatinib sensitivity (273,274), perhaps by overriding the dependence on RIN1 binding. Importantly, the only such mutations validated to confer imatinib sensitivity in patient samples never occurred simultaneously with kinase domain mutations (274). This suggests the potential value of small molecule inhibitors that target the functional interaction of RIN1 and BCR-ABL1, through direct binding blockade or allosteric interference. Such drugs might be combined with kinase active site-directed inhibitors for a first line therapy that reduces relapse rates by requiring the simultaneous acquisition of independent resistance mutations.

4.5 MATERIALS AND METHODS

Expression constructs

The MSCV retrovirus constructs expressing BCR-ABL1, BCR-ABL1 + RIN1[ABD], ETV6-ABL1 and v-Abl have been previously described (111). The BCR-ABL1 + RIN1[ABDmut] was created by replacing the EcoRI flanked fragment of wild type RIN1[ABD] with the equivalent fragment from RIN1[ABDmut] (also called ABD[TM] (111,112)). Note that RIN1[ABD] was used instead of full length RIN1 to avoid the retrovirus size limit. The BCR-ABL1[T315I] mutant retrovirus was a generous gift of Charles Sawyers (Memorial Sloan Kettering Cancer Center). The RIN1 silencing shRNA lentivirus in the pLKO.1-puro vector and the scramble control lentivirus pLKO.1SCR-puro contain a puromycin resistance gene and were obtained from Sigma (Mission[TM] shRNAs SHGLY-NM_004292 and SHC002, respectively). The stability of RIN1 silencing in transduced TOM-1 cells was validated by immunoblot (Fig. 4B). Mouse Rin1 (mRin1) was expressed from an M4 lentivirus vector (183) containing a blasticidin resistance gene.

Cell culture reagents and conditions

Retroviruses and lentiviruses were produced in transfected HEK293T cells and concentrated stocks were created as previously described (112).

The myeloid BCR-ABL1 leukemia cell lines KU-812 and LAMA-84 (gifts of Brian Druker, Oregon Health and Science Univ.) and the B lymphoid BCR-ABL1 leukemia cell lines BV173 (gift of Brian Druker) and TOM-1 (gift of Kathleen Sakamoto, UCLA) were grown in RPMI 1640 medium with 10% FBS (Hyclone Defined) and 1% Penicillin Streptomycin (Gibco # 15140). LAX2 are primary BCR-ABL1 pre-B ALL cells from the bone marrow biopsy of a 38-year old patient with relapse leukemia. LAX2 cells were propagated in sub-lethally irradiated

NOD/SCID mice and kept on OP9 stromal cells in MEMa with 20% FBS. Lentivirus infections were carried out using 5×10^4 cells, or 1×10^7 cells for LAX2, and a 1:1 dilution of virus stock in 2X RPMI medium for 12-16 hours at 37°C. In some cases, infections were carried out in wells coated with retronectin (Takara Bio Inc.). Silencing shRNA infected cells were selected for with puromycin (1 µg/ml for LAX2; 1 µg/ml for TOM-1). mRin1 infected cells were selected with blasticidin (5 µg/ml).

Bone marrow cells were obtained from femurs and tibias of C57Bl/6 mice (6-8 weeks old) using a standard protocol (262). FACS analysis was performed, blindly, on wild type and $Rin1^{-/-}$ bone marrow cells using a selection of antibodies recognizing surface markers for B cells, T cells and granulocytes (B220, CD43, BP-1, CD24, IgM, CD19, Kit, CD4, CD8, Gr-1 and CD11b). Analysis of individual markers and Hardy fractions (275) showed no significant difference between wild type and mutant. Retrovirus infections were carried out as previously described (111) using a multiplicity of infection range from 0.1 to 10. Titers were based on transduction efficiency of NIH3T3 cells (all viruses encode a GFP marker). Each moi was based on minimum consistent transformation of bone marrow cells, to adjust for some variation among virus stock preparations. Infected cells were plated at a density of 5×10^6 cells/well in 6-well culture plates, with duplicate wells for each sample. On the indicated days, cells were resuspended and a sample removed for trypan blue staining and counting of viable cells. After each count, half of the culture from each well was discarded and replaced with fresh medium.

For phosphotyrosine analysis of K562 cells expressing vector control or RIN1 protein, cells were treated with the indicated concentrations of imatinib for a total of 30 minutes. Cells were incubated at 37°C for 15 minutes, followed by addition of 10 µM phenylarsine oxide

(PAO) and incubated for another 15 minutes. Cells were lysed in RIPA buffer prior to immunoblot analysis.

Cell proliferation assays were performed after first evaluating sensitivity of TOM-1 and LAX2 to a range of imatinib concentrations. For TOM-1, 1 x 10^5 cells were cultured in 4 mls RPMI + 10%FBS + PSG medium with or without 8 μM imatinib. We used 8 μM because it was the highest imatinib concentration that still allowed proliferation of control TOM-1 cells. For LAX2 cells we used 10 μM imatinib, which showed moderate cytotoxic effects on these primary ALL cells expressing BCR-ABL1^{T315I}. The BCR-ABL1 kinase domain of primary Ph+ ALL cells and cell lines was amplified and sequenced using PCR primers described (276). On the indicated days, the cells were resuspended and samples were removed for trypan blue staining and direct cell counting and for propidium iodide staining and flow cytometric analysis.

Immunoprecipitations, Immunoblots and Immunohistochemistry

Immunoprecipitations were performed, as indicated, with polyclonal anti-RIN1 (BD Transduction Laboratories - Discontinued) or polyclonal anti-CRKL (Santa Cruz Biotechnology #SS319). Immunoblots were done with polyclonal anti-RIN1 (BD Transduction Laboratories), monoclonal anti-phosphotyrosine 4G10 (Upstate #05-321), polyclonal anti-ABL1 K-12 (Santa Cruz Biotechnology), monoclonal anti-b-tubulin (Sigma#T6074). Expression analysis in mouse cell lines required the use of monoclonal and polyclonal antibodies specific for mouse Rin1 (112). Immunohistochemical staining was similarly performed with monoclonal antibody specific for mouse Rin1 (VECTASTAIN ABC System, VectorLabs). To reduce background from the mouse-derived anti-mouse Rin1, we used the Vector M.O.M. Basic Kit (BMK-2202) that contains a nonspecific blocking solution to block endogenous mouse immunoglobulin.

Bone Marrow Transplantation and Flow Cytometric Analysis and Sorting

For engraftment assays, 8-12 week old SJL mice (CD45.1) were lethally irradiated (1,100 rads) before receiving 1 x 10^6 bone marrow cells from 8-12 week old WT or Rin1$^{-/-}$ C57BL/6 mice (CD45.2). After 34 or 105 days, single cell suspensions were prepared from BM, spleen and thymus of euthanized recipient mice. Nucleated cells were identified using Turk's stain. Flow cytometric analysis was performed on a FACSCanto (BD Biosciences) using Diva v6.1.1 and 1x10^6 cells per sample. Surface marker staining was determined as a percentage of live cells (7AAD excluded). An isoform-specific antibody to CD45.2$^+$ was used to identify donor cells (277). Wild type mice were obtained from Jackson Labs (SJL) and Charles River (C57BL/6).

The markers used to sort and define bone marrow cell subpopulations for comparative Rin1 expression (Fig. 2) are as follows: Pre-B = surface IgM negative, CD19 positive, B220 positive, CD43 negative; Pro-B = IgM negative, CD19 positive, B220 positive, CD43 positive; CLP = Lineage negative, Kit dimly positive, Sca-1 dimly positive, IL7R alpha positive.

CHAPTER 5. IDENTIFICATION OF SMALL MOLECULES THAT DISRUPT SIGNALING BETWEEN ABL AND ITS POSITIVE REGULATOR RIN1

[Original Article: Ting PY, Damoiseaux R, Titz B, Bradley KA, Graeber TG, Fernandez-Vega V, Bannister TD, Chase P, Nair R, Scampavia L, Hodder P, Spicer TP, Colicelli J. *Identification of small molecules that disrupt ABL interaction with positive regulator RIN1 by high throuput screening.* **Revised and resubmitted]**

5.1 ABSTRACT

Constitutively active BCR-ABL kinase fusions are causative mutations in the pathogenesis of hematopoietic neoplasias including chronic myelogenous leukemia (CML). Although these fusions have been successfully targeted with kinase inhibitors, drug-resistance and relapse continue to limit long-term survival, highlighting the need for continued innovative drug discovery. We developed a time-resolved Förster resonance energy transfer (TR-FRET) -based assay to identify compounds that disrupt stimulation of the ABL kinase by blocking its ability to bind the positive regulator RIN1. This assay was used in a high throughput screen (HTS) of two small molecule libraries totaling 444,743 compounds. 708 confirmed hits were counter-screened to eliminate off-target inhibitors and reanalyzed to prioritize compounds with IC_{50} values below 10 μM. The CML cell line K562 was then used to identify five compounds that decrease MAPK1/3 phosphorylation, which we determined to be an indicator of RIN1-dependent ABL signaling. One of these compounds is a thiadiazole, and the other four are structurally related acyl piperidine amides. Notably, these five compounds lower cellular BCR-ABL kinase activity by blocking a positive regulatory interaction rather than directly inhibiting ABL catalytic function.

5.2 INTRODUCTION

Chromosome translocations that create ABL kinase fusion proteins are responsible for 95% of chronic myelogenous leukemia (CML), as well as some cases of acute lymphoblastic leukemia (ALL) and acute myelogenous leukemia (278). The most common translocation fuses BCR on chromosome 22 to ABL1 on chromosome 9 (151), creating a constitutively active BCR-ABL1 kinase that promotes hyperproliferation of progenitor hematopoietic cells. The selective kinase inhibitor imatinib has been successful in achieving what appear to be complete cytogenetic responses in most CML patients (167). Treatment is not curative, however, because dormant cancer cells can develop resistance to imatinib through mutations in BCR-ABL1 (168,279). The rate of patient relapse is 18% after a median of five years of kinase inhibitor therapy (280). The most refractory mutation, BCR-ABL1^{T315I}, is not responsive to the second generation kinase inhibitors nilotinib (281), dasatinib (169) and bosutinib (282). Although the third generation kinase inhibitor ponatinib is effective against BCR-ABL^{T315I} (283), compound mutations still lead to resistance in some patients (172,173).

The constitutive activity of BCR-ABL1 is attributed to loss of the ABL1 amino terminal autoinhibitory peptide, which is typically myristoylated (137,138), and its replacement by a BCR-encoded oligomerization domain (159). However, BCR-ABL1 retains the autoinhibitory ABL-SH2 and SH3 domains common in non-receptor tyrosine kinases (284). RIN1 stimulates ABL catalytic activity by directly binding these domains and relieving their autoinhibitory effect on the kinase domain (86,111,144). Retention of ABL-SH2 and SH3 sequences in BCR-ABL1 suggests that, although constitutively active relative to normal ABL kinases, BCR-ABL1 is still subject to positive regulation by RIN1. Indeed, altered RIN1 expression correlates directly with BCR-ABL1 activity (174).

RIN1 binding to ABL proteins is initiated by low affinity interaction between a proline rich motif on RIN1 and the SH3 domain of ABL (86). ABL subsequently phosphorylates RIN1 on Y^{36}, which then binds to the SH2 domain of ABL. This leads to a stable divalent interaction between the proteins and alleviation of ABL autoinhibition (111). RIN1 co-localizes with BCR-ABL1 when exogenously expressed in Cos-7 cells (285). In addition, RIN1 binds to and enhances the leukemogenic properties of BCR-ABL1 (111,174) and RIN1 is required for *ex vivo* BCR-ABL1 transformation of bone marrow cells to a state of growth factor independence. Moreover, RIN1 depletion in the ALL cell line TOM-1 increased imatinib sensitivity. This is consistent with RIN1 functioning as a BCR-ABL stimulator that works allosterically to promote catalytic activity. Notably, imatinib-resistant primary ALL cells from a BCR-ABL1^{T315I}-relapsed patient were re-sensitized to imatinib by RIN1 silencing (174).

To identify a novel class of drugs that exploits ABL's reliance on RIN1 for full kinase activity, we developed a time-resolved Förster resonance energy transfer (TR-FRET) high throughput screen (HTS) that provides an indirect measure of RIN1 binding to ABL. Compounds that block RIN1::ABL association might be effective as inhibitors of BCR-ABL1 mutants that are resistant to catalytic site inhibitors, as components in multi-domain targeting treatments, and as molecular probes to further study the mechanism of RIN1-induced ABL stimulation. We screened a combined 444,743 compounds at the UCLA Molecular Shared Screening Resource (MSSR) and The Scripps Research Institute, Florida (TSRI). The screen identified five compounds of interest that disrupt RIN1-stimulated BCR-ABL1 signaling in the CML cell line K562.

5.3 RESULTS

Assay development and validation

To measure binding between purified RIN1 and ABL proteins we designed a quantitative TR-FRET based assay. The first assay component is full-length human RIN1 fused at the carboxy terminus to a streptavidin binding peptide (RIN1-SBP), which binds stably to a streptavidin-terbium complex that serves as the TR-FRET donor. The second assay component is the amino terminal half of ABL1 (includes the SH3, SH2 and kinase domains and is fully activatable by RIN1) fused to eGFP (ABL1-eGFP), which serves as the TR-FRET acceptor (Figure 5-1A). Because the lanthanide ion donor, terbium, exhibits slowly decaying luminescence (286), FRET emission can be detected after excitation termination, reducing background relative to signal.
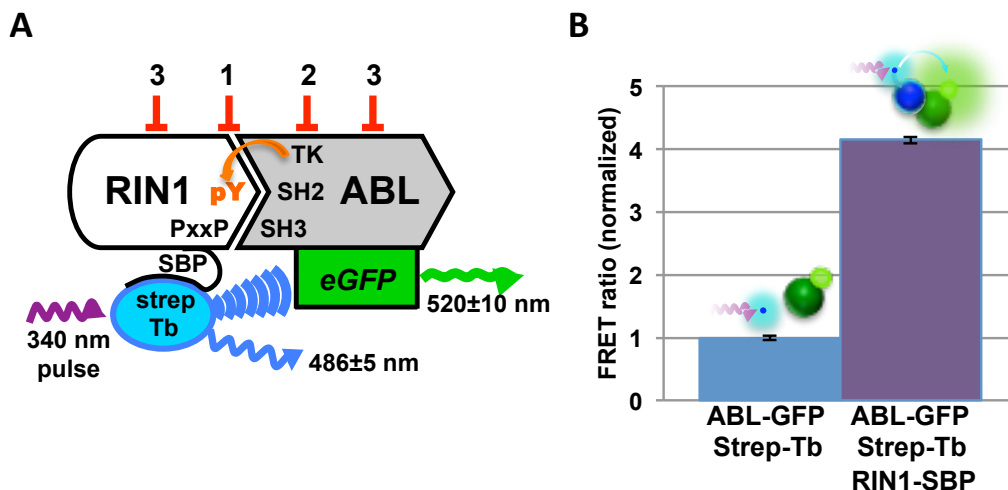
Figure 5-1. TR-FRET screen for RIN1::ABL1 interaction inhibitors. (**A**) Binding between RIN1 and ABL is initiated by a proline rich motif in RIN1 binding to the ABL-SH3 domain. ABL phosphorylates RIN1-Y[36], which then binds the ABL-SH2 domain. For the assay, ABL was fused to eGFP and RIN1 was fused to a streptavidin binding peptide (SBP) that connects to a streptavidin-terbium complex. A 340 nm pulse excites terbium, which can transfer energy to excite the GFP acceptor if the fluorophores are in close proximity, reflecting RIN1::ABL binding. Predicted FRET inhibitor classes: 1. Orthosteric inhibitors, 2. Direct ABL kinase inhibitors and 3. Allosteric inhibitors. (**B**) RIN1::ABL binding was quantified as a FRET ratio: GFP emission at 520 nm to terbium emission at 486 nm. The negative control was donor and acceptor fluorophores only (no RIN1) and was normalized to 1.

99

The assay readout was calculated as a ratio of donor and acceptor emissions, a measurement independent of donor and acceptor concentrations that allows for reliable comparison across assays. Assay components were mixed in kinase buffer and incubated for one hour at room temperature to allow for RIN1-Y^{36} phosphorylation by ABL1 and subsequent formation of a stable divalent interaction between these proteins. Each multi-well assay plate included negative control samples (streptavidin-terbium, ABL-eGFP and ATP *without* RIN1-SBP). Positive control samples (all assay components included) gave robust and reproducible increases in FRET ratio following incubation, reflecting the interaction of RIN1 and ABL1 constructs and subsequent energy transfer from terbium to eGFP (Figure 5-1B).

The assay was validated using several additional controls. Omission of ATP significantly decreased the FRET ratio (Figure 5-2A), reflecting the loss of ABL-mediated RIN1-Y^{36} phosphorylation and resultant loss of ABL-SH2 domain binding. Addition of the ABL kinase inhibitor imatinib also decreased the FRET ratio (Figure 5-2B), as expected if RIN1 tyrosine phosphorylation were blocked. The remaining

Figure 5-2. Validation of TR-FRET screening assay for detection of RIN1::ABL binding. Binding was quantified as a ratio of GFP emission at 520 nm to terbium emission at 486 nm. The negative control was normalized to 1. (**A**) ATP was omitted from the buffer mix to prevent RIN1 phosphorylation by ABL. (**B**) 10 μM or 100 μM imatinib was added to inhibit ABL kinase activity. (**C**) untagged ABL competed with ABL-eGFP (1:1 and 10:1 ratios were used).

signal in both cases is likely due to low affinity binding between the proline-rich motif of RIN1 and the ABL-SH3 domain. Addition of untagged ABL1 into the assay also decreased the FRET ratio in a dose-dependent manner due to competition with the ABL1-eGFP FRET acceptor construct for binding to RIN1 (Figure 5-2C). The Z'-factor of the assay was 0.97±0.03, indicating a high degree of assay sensitivity and reproducibility for high throughput screening.

Based on the assay design and control results, we anticipated identifying three types of inhibitors: 1) compounds that work through steric interference by binding directly to residues at the protein-protein interface, 2) kinase inhibitor compounds that decrease ABL-mediated phosphorylation of RIN1-Y[36] and 3) compounds that work allosterically on one protein to alter conformation and diminish interaction with its partner protein (Figure 5-1A).

High-throughput screening and counter screening

High-throughput screens were carried out at two facilities. At the UCLA Molecular Screening Shared Resource 86,259 compounds were screened at a concentration of 10 μM, with an average Z-factor of 0.64. At the Scripps Research Institute, Florida, 358,484 compounds from the NIH MLSMR small molecule library were screened at 7.35 μM, with an average Z-factor of 0.76 (Table 5-1). Individual plate-based 3-standard deviation decreases in the FRET ratio were used to select hits on a plate per plate basis, with the majority of compounds having no effect in the assay (Figure 5-3). The combined hit rate was 0.36%. In total, 1,637 hits were identified and 708 of these were confirmed by testing in triplicate (Table 5-1).

101

		Molecular Screening Shared Resource (UCLA)	The Scripps Research Institute, Florida
Primary screen	**Compounds tested**	86,259 compounds at 10 μM	358,484 compounds at 7.35 μM
	Average Z'	0.94 ± .03	0.90 ± .01
	Avg. Z-factor	0.64 ± 0.38	0.76 ± 0.38
	hits	202 hits = 0.2%	1435 hits = 0.4%
Confirmation and counter-screens	**confirmed**	78 confirmed	630 confirmed
	quenchers	(7 quenchers)	(93 quenchers)
	Biotin analogs	(4 biotin analogs)	(11 biotin analogs)
	IC$_{50}$ < 10 μM	11 active	82 active
	Selected for further analysis	3 compounds	21 compounds

Table 5-1. High throughput screen results.
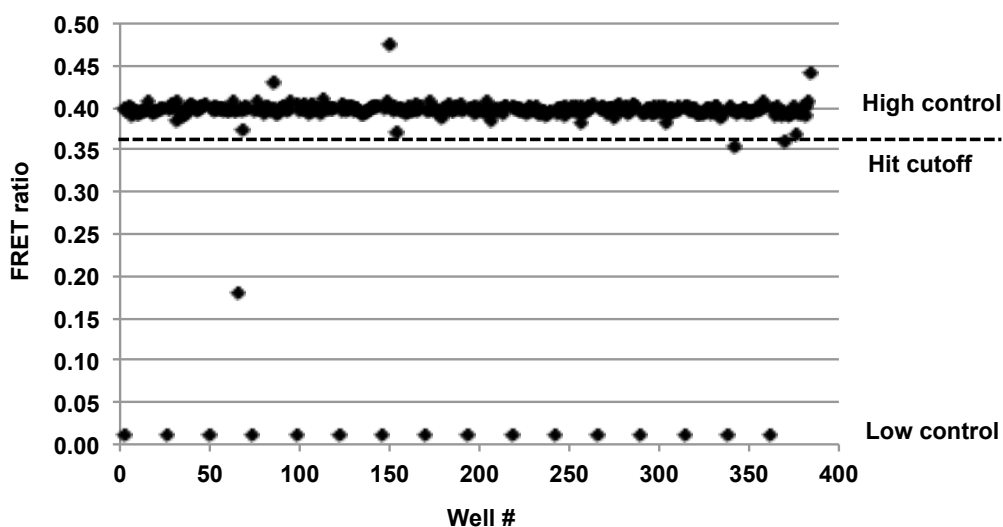
Figure 5-3. Representative data from primary HTS. Example of 384 well plate data presented as a scatterplot. Each plate was screened with high and low controls consisting of streptavidin terbium and ABL-eGFP with and without RIN1-SBP, respectively. The hit cutoff was a plate-based 3-standard deviation decrease in the FRET ratio.

Based on the assay design, two types of false positive inhibitors were predicted: compounds that quench GFP fluorescence, and compounds that bind with high affinity to streptavidin and sequester it from RIN1-SBP (Figure 5-4A). We identified GFP quenchers by incubating compounds with ABL-GFP and measuring fluorescence (Figure 5-4B). Quenchers were defined as compounds that decreased GFP fluorescence by $\geq 50\%$ at 10 µM. To eliminate compounds that might bind with high affinity to streptavidin and sequester it from RIN1-SBP, confirmed hits were examined for structural similarity to biotin (Figure 5-4C). Lastly, we narrowed the list of hits by performing concentration-response curves and giving higher preference to compounds with IC_{50} <10 µM (Figure 5-4D). Confirmed and targeted hits from the UCLA MSSR screen can be found in Table 5-S1, and hits from the TSRI screen at PubChem BioAssay AID 602181 (https://pubchem.ncbi.nlm.nih.gov/assay/assay.cgi?aid=602181).
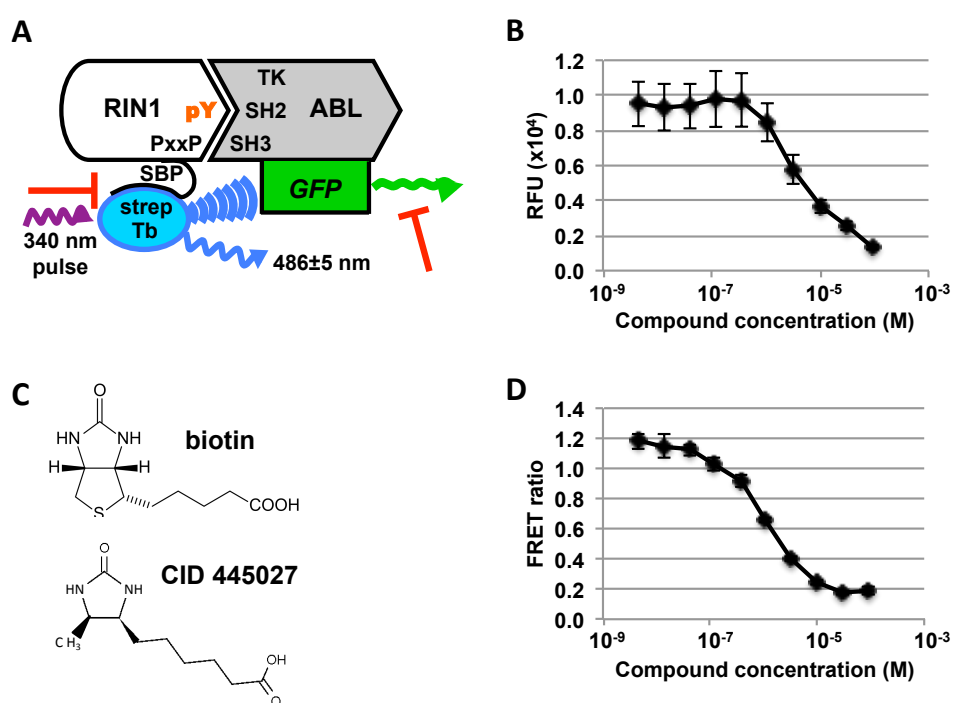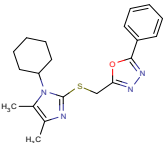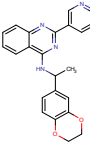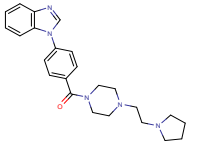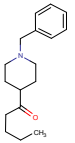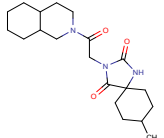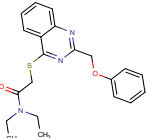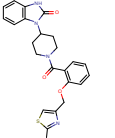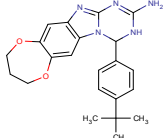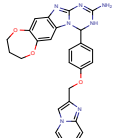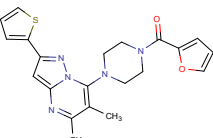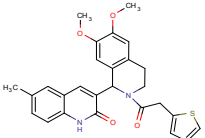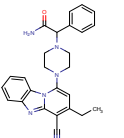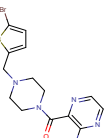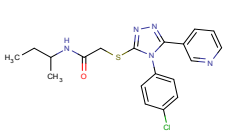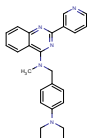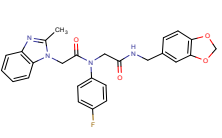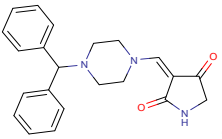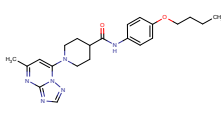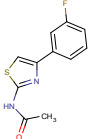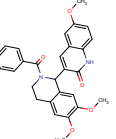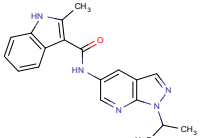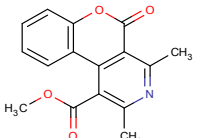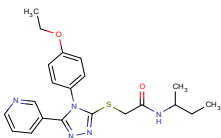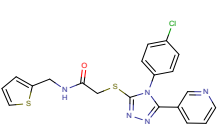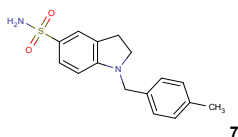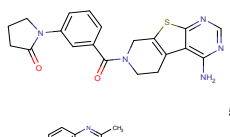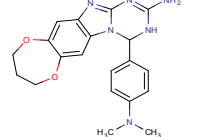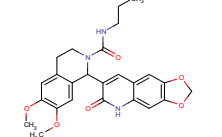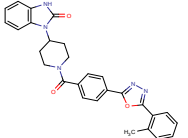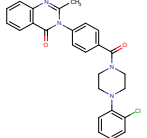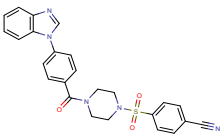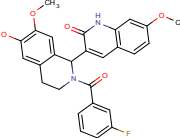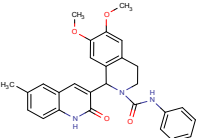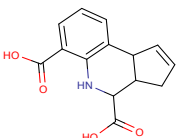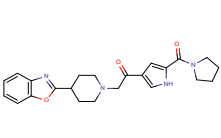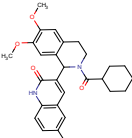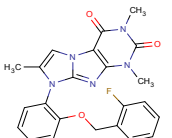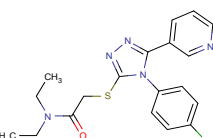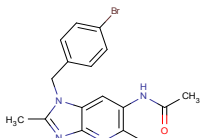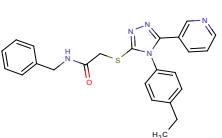
Figure 5-4. Elimination of off-target inhibitors. (**A**) Two types of off-target inhibitors were predicted (red T-bars): compounds that quench GFP fluorescence, and biotin-like compounds that bind and sequester streptavidin. (**B**) Hit compounds were tested in triplicate dose response curves and compounds that reduced RFU (relative fluorescence units) by $\geq 50\%$ at 10 µM were eliminated as quenchers. Concentration response curve data from a representative GFP quencher (methyl 3,4,6-trihydroxy-5-oxo-5H-benzo[7]annulene-8-carboxylate) is shown. (**C**) Biotin mimics were identified by *in silico* screening for structural similarity to biotin. (**D**) Hit compounds were re-tested in the TR-FRET assay in 10-point dose response curves to prioritize those with IC_{50}<10 µM. Data from the representative compound CID 24512426 is shown.

103

Table 5-S1. Confirmed hits from UCLA MSSR screen

Structure	TR-FRET %inhibition at 10 µM	Structure	TR-FRET %inhibition at 10 µM	Structure	TR-FRET %inhibition at 10 µM	Structure	TR-FRET %inhibition at 10 µM
	93.4		65.7		47.6		40.6
	81.7		64.4		47.0		38.9
	79.8		63.7		46.8		38.7
	79.2		62.9		46.0		38.1
	77.4		61.7		44.5		37.3
	74.9		59.2		44.3		34.5
	73.3		58.4		44.2		33.9
	68.8		55.5		42.9		33.2
	68.2		53.0		42.4		29.8
	66.1		52.5		41.5		25.7

104

Although the objective of our TR-FRET assay was to identify a unique class of compounds that disrupt the RIN1::ABL interaction allosterically or by binding to the protein-protein interface, compounds that directly inhibit ABL catalytic activity could also appear as hits (Figure 5-1A). To identify these direct ABL kinase inhibitors, we screened the compounds using an *in vitro* kinase assay. Purified ABL1-eGFP was incubated with CRK, a well-characterized substrate, in kinase buffer containing ATP. CRK and ABL phosphorylation were detected by anti-phosphotyrosine immunoblot, and both were reduced by imatinib. All of the hits were screened, and a representative immunoblot is shown in Figure 5-5. Using this assay we identified one hit compound, theaflavin-3,3'-digallate, that directly inhibits ABL trans-phosphorylation of CRK as well as ABL (Figure 5-5). Although this tea polyphenol has been studied for its antioxidant (287) and anti-cancer effects (288,289), this is the first report of its activity as an ABL kinase inhibitor.
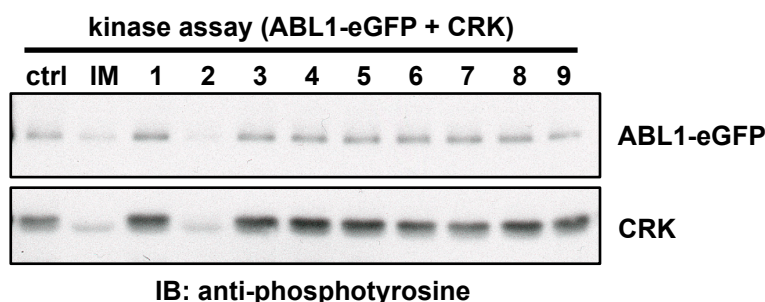
Figure 5-5. Theaflavin-3,3'-digallate is a direct ABL kinase inhibitor. 0.5 nM purified ABL-eGFP was mixed with 2 μM CRK and 10 μM test compound and incubated in kinase buffer for 30 minutes at 30°C. Samples were analyzed by immunoblot using anti-phosphotyrosine. All the hits were screened, and a representative immunoblot is shown here. Test compounds were as follows: DMSO (ctrl), imatinib (IM), CID 16312764 (1), CID 467320 (2), CID 7457610 (3), CID 6084 (4), CID 4844281 (5), IUPAC 1-(4-phenylphenyl)-2-[4-(pyrimidin-2-yl)piperazin-1-yl]ethan-1-ol (6), CID 9291491 (7), CID 3991439 (8) and CID 16350799 (9).

After eliminating off-target inhibitors, the best remaining hits clustered into 7 scaffold groups. Pyridone/pyrimidines, acyl piperidine carboxamides and heterocyclic amides are the largest clusters, with 8, 9 and 17 members, respectively. In addition, we identified three macrocycles, four tetrazoles, one indole alkaloid and one thiadiazole (Figure 5-S1). We selected

21 hits for further analysis (Table 5-S2) based on several criteria: 1) strong inhibition in the TR-FRET assay (IC_{50} <12 μM); 2) high maximal inhibition (>60%); 3) low or moderate hit rate of compounds in other assays reported in pubchem (<10%); 4) chemical tractability; and 5) positive evidence for structure activity relationships in hit scaffolds.

1. pyridone/ pyrimidone
2. N-acyl piperidine-4-carboxamide
3. Heterocyclic amide

4. macrocycle
5. tetrazole
6. indole alkaloid
7. thiadiazole
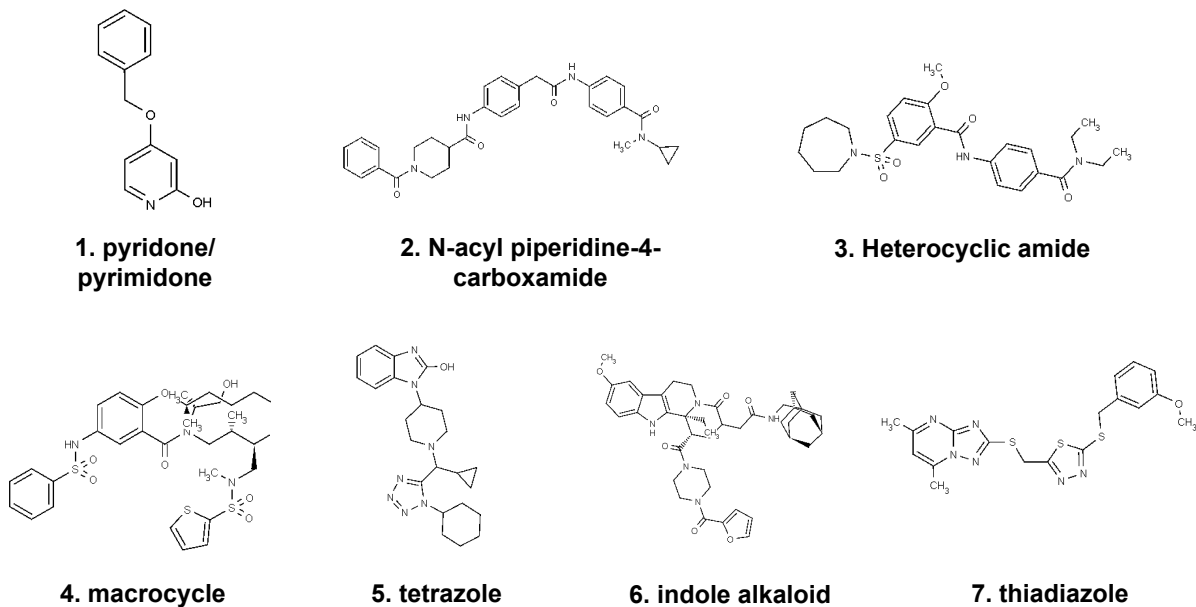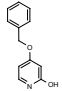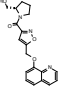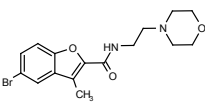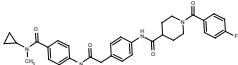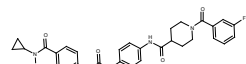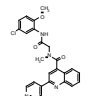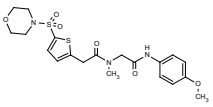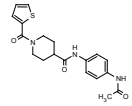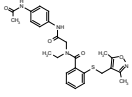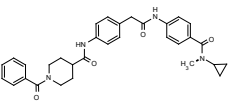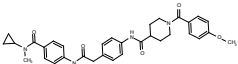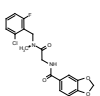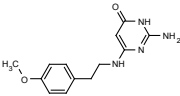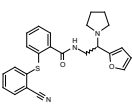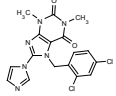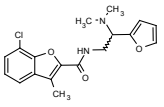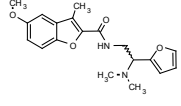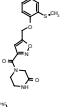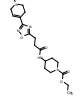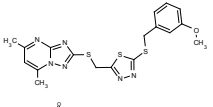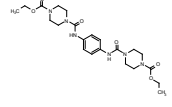
Figure 5-S1. Scaffold clustering of selected hits. After eliminating off-target inhibitors and structures with potential stability, reactivity or promiscuity problems, the remaining best hits clustered into 7 scaffold groups. Pyridone/pyrimidines, acyl piperidine carboxamides and heterocyclic amides are the largest clusters, with 8, 9 and 17 members, respectively. In addition, three compounds are macrocycles, four are tetrazoles and we identified one indole alkaloid (CID 44601827) and one thiadiazole (CID 1818178). Representative compounds are shown for groups 1-5 and their PubChem CID numbers are as follows: (1) 3607724, (2) 44142745, (3) 24686095, (4) 44502732, (5) 51360358.

Table 5-S2. 21 hits selected for cell-based assay

CID	chemical series	IC50 (M) in TR-FRET assay	Max response (%)		Stdev of Max Response (%)
3607724	pyridone/pyrimidinone/pyrimidine	16.1E-9	100.16	±	1.03
42287970	heteroaryl amide	302.3E-9	52.20	±	1.49
8852038	heteroaryl amide	953.9E-9	70.70	±	1.08
56844185	acyl piperidine	1.1E-6	85.16	±	1.13
56844188	acyl piperidine	1.3E-6	86.82	±	0.86
16256008	heteroaryl amide	2.E-6	72.53	±	2.31
16256016	heteroaryl amide	2.E-6	73.84	±	3.19
1081265	acyl piperidine	2.2E-6	80.82	±	0.78
16256082	heteroaryl amide	2.4E-6	78.59	±	0.95
44142745	acyl piperidine	2.5E-6	86.20	±	2.43
56844186	acyl piperidine	3.7E-6	84.85	±	0.99
8009555	heteroaryl amide	3.8E-6	75.86	±	1.05
1532134	pyridone/pyrimidinone/pyrimidine	4.E-6	88.09	±	1.23
16256020	heteroaryl amide	4.1E-6	75.63	±	0.97

1327046	pyridone/pyrimidinone/pyrimidine	4.3E-6	103.21	±	0.21
16257621	heteroaryl amide	4.7E-6	77.54	±	0.95
16257622	heteroaryl amide	5.2E-6	73.40	±	0.63
24793301	acyl piperidine	5.9E-6	86.54	±	0.23
3243211	acyl piperidine	9.4E-6	81.37	±	1.06
1818178	triazole/tertrazole/thiadiazole	9.6E-6	95.67	±	1.09
1103613	diacyl piperazine	11.1E-6	63.66	±	0.75

Five hit compounds decrease MAPK1 phosphorylation

To independently confirm that the hit compounds inhibit RIN1::ABL binding, and to identify those that effectively block signal transduction in cells, we developed a secondary assay to measure the effect of the compounds in the CML cell line K562. We sought to employ ABL substrate phosphorylation as a read-out of RIN1-dependent ABL signaling because of its suitability for cell-based screening. To identify RIN1-dependent ABL substrates, we employed immunoaffinity purification of tyrosine phosphopeptides followed by tandem mass spectrometry to generate phosphotyrosine profiles of previously described K562 cells expressing a control shRNA or a RIN1-targeted shRNA (174). We noted down regulation of many known ABL substrates such as BCR pY[644], ABL1 pY[253], ABL1 pY[257] and ABI1 pY[213], but one of the most robust losses of phosphorylation was seen for MAPK1 pY[187] (Table 5-S3).

Table 5-S3. Phosphotyrosine peptides from K562 ctrl vs. K562 RIN1 knockdown

SEQMOD	Protein	p-Site	log2(KD/CTRL ratio (Rin1 KD/CTRL))		ttest		ttest Bonferroni correc.	SNR
R.IDMpYAMGLVLWELVSR.C_2	ACVR2B	pY387	4.059980684	16.67922886	0.0038094		0.205706124	2.085431
R.NGQpYELIIQLHGK.E_2	Ocrl	pY42	2.459689947	5.500984917	0.0810979		4.379285169	0.936504
R.SGDSEVpYQLGDVSQK.T_2	SSBP1	pY73	1.540761418	2.909480179	0.0002358		0.012733535	3.515055
R.pYHGHSMSDPGVS6YR.T_3	PDHA2	pY287,pS298	1.252715904	2.382895862	0.0576244		3.111716069	0.759112
R.FLFPEpYILDPEPQPTR.E_2	C4orf14	pY77	0.974427338	1.964861113	2.808E-07		1.5163E-05	8.899592
K.LGIPEpYFNFAK.D_2	ACSM3	pY57	0.745418849	1.676460916	0.0005895		0.031831349	2.347638
K.VVQEYIDAFSDpYANFK_3	PTPRA	pY798	0.44908123	1.365170581	0.0476119		2.57104181	0.775213
R.EYDQLpYEEYTR.T_2	PIK3R2	pY464	-0.01439745	0.99007008	0.5048343		27.2610546	-0.03013
R.IYQpYIQSR.F_2	DYRK1B	pY273	-0.03238024	0.977805724	0.6302488		34.03343359	-0.03787
K.NSFNNPAYpYVLEGVPHQLLPPEPPSPAR.A_3	INPPL1	pY923	-0.07666939	0.948244244	0.4100913		22.14492974	-0.15926
K.NSFNNPApYYVLEGVPHQLLPPEPPSPAR.A_3	INPPL1	pY922	-0.09119127	0.938747285	0.4137328		22.34156908	-0.17235
R.GEPNVSpYIC8SR.Y_2	GSK3B	pY216	-0.09602543	0.935607008	0.8203938		44.30126312	-0.3617
K.HIGLVpYSGMGPDYR.V_2	PSMA2	pY75	-0.10168405	0.931944503	0.857685		46.31499083	-0.153
R.LPSSPVpYEDAASFK.A_2	CTTN	pY422	-0.22422908	0.856052343	0.3019745		16.30662152	-0.90352
R.AAVPSGASTGIpYEALELR.D_2	ENO2	pY43	-0.25703919	0.836803512	0.1959434		10.58094584	-1.36773
K.LC8DFGSASHVADNDITPpYLVSR.F_2	PRPF4B	pY849	-0.25738073	0.83660543	0.0995397		5.375145259	-1.21562
K.LC8DFGSASHVADNDITPpYLVSR.F_3	PRPF4B	pY849	-0.2911573	0.817246215	0.0701116		3.786024236	-1.2406
K.TLSEVDpYAPAGPAR.S_2	INPPL1	pY1135	-0.29388392	0.815703122	0.1639121		8.851255029	-1.53926
R.VDpYVVVDQQK.T_2	GAB1	pY659	-0.31140813	0.805854829	0.9239067		49.8909604	-0.34245
R.HTDDEMTGpYVATR.W_2	MAPK14	pY182	-0.33799611	0.791139436	0.676993		36.55762133	-0.64709
K.VVQEYIDAFSDpYANFK_2	PTPRA	pY798	-0.38120824	0.767794305	0.0896895		4.843235464	-1.15585
K.VIpYDFIEK.T_2	WASL	pY256	-0.40831749	0.753501615	0.1368865		7.391870018	-1.06007
K.NSLETLLpYKPVDR.V_3	BCR	pY644	-0.45543383	0.729290834	0.0176072		0.950787821	-1.64572
K.NSLETLLpYKPVDR.V_2	BCR	pY644	-0.46377941	0.725084276	0.0004389		0.023699506	-3.98031
R.YVLDDQpYTSSSGAK.F_2	Tec	pY10	-0.46428479	0.724830318	0.3343523		18.05502182	-1.36973
K.IGEGTpYGVVYK.A_2	CDK3	pY43	-0.5473383	0.68428143	0.0936018		5.054497858	-1.65039
K.IKPSSSANAIpYSLAAR.P_2	CBL	pY674	-0.62687426	0.647577939	0.0082592		0.445996152	-1.96447
R.SAFSNLFGGEPLSpYTR.F_2	TFRC	pY20	-0.64750473	0.638383499	0.0058108		0.313782093	-1.73247
K.REEPEALpYAAVNK.K_2	ITSN2	pY967	-0.66128799	0.632313538	0.0204407		1.103795757	-3.53534
R.ELFDDPSpYVNVQNLDK.A_2	Shc1	pY428	-0.66752746	0.629584765	0.0083389		0.450302313	-1.83401
K.AAASMGDTLSEQQLGDSDIPVIVpYR.C_3	CENTD2	pY735	-0.73064977	0.602632436	0.3941753		21.28546845	-0.53738
R.LLAQAEGEPC8pYIR.D_2	TYK2	pY292	-0.73370031	0.601358854	0.0275042		1.485228983	-2.43792
K.LGGGQpYGEVYEGVWK.K_2	ABL1	pY253	-0.76282854	0.58933974	0.0348845		1.883760338	-1.65474
R.LpYEWISIDKDEAGAK.S_3	INPPL1	pY822	-0.77993574	0.582392731	0.0201064		1.085743182	-1.13007
R.HTDDEMTGpYVATR.W_3	MAPK14	pY182	-0.77994244	0.582390029	0.3800192		20.52103482	-0.84146
R.NEEENIpYSVPHDSTQGK.I_3	GRLF1	pY1105	-0.78879834	0.578826011	0.0912435		4.927147873	-2.0781
R.NEEENIpYSVPHDSTQGK.I_2	GRLF1	pY1105	-0.79402226	0.576733903	2.1830874		117.8867213	-3.37083
R.VQIpYHNPTANSFR.V_2	VASP	pY38	-0.79850853	0.57494325	0.000756		0.040821884	-3.3003
K.PSSSANAIpYSLAAR.P_2	CBL	pY674	-0.83869866	0.559147705	0.0311172		1.680327874	-1.67566
K.LGGGQYGEVpYEGVWK.K_2	ABL1	pY257	-0.86374336	0.549524855	0.0352673		1.904434315	-1.848
R.LpYEWISIDKDEAGAK.S_2	INPPL1	pY822	-0.88649411	0.540927208	0.000244		0.013177117	-2.46307
K.LPPGEQC8EGEEDTEpYMTPSSR.P_3	CBL	pY700	-0.92052175	0.52831792	0.0504783		2.725829411	-1.86995
K.TLEPVKPPTVPNDpYMTSPAR.L_3	ABI1	pY213	-0.93209253	0.524097622	0.053068		2.865671404	-1.05354
K.VVALpYDYMPMNANDLQLR.K_2	BTK	pY222	-0.93825207	0.521864775	0.0112434		0.607141994	-1.72031
K.DASSQDC8pYDIPR.A_2	GAB1	pY406	-0.96363099	0.512764757	0.0621059		3.353721079	-2.09877
R.VGWFPANYVEEDYSEpYC8_2	VAV1	pY844	-1.06520709	0.477904054	0.0004481		0.024200088	-3.5176
R.RLpYPPSAEYPDLR.K_2	CKMT1A	pY47	-1.13795368	0.454403648	0.0002173		0.011731903	-3.20381
R.VGWFPANYVEEDpYS6EYC_2	VAV1	pY841,pS842	-1.14802304	0.451243158	0.0228161		1.232066997	-1.45513
R.APSASVDSSLpYNLPR.S_2	GAB1	pY259	-1.17547434	0.442738168	0.0024096		0.130119604	-2.89381
K.SESVVpYADIR.K_2	MPZL1	pY263	-1.31033595	0.403226973	0.0036202		0.19549255	-3.05404
K.LIpYDFIEDQGGLEAVR.Q_2	WAS	pY290	-1.43656349	0.36944628	2.394E-05		0.001292691	-6.51757
R.YTEFpYHVPTHSDASK.K_3	PDLIM5	pY250	-1.45428695	0.364935411	0.0066544		0.359338526	-4.28062
R.GPVSGTEPEPVpYSMEAADYR.E_2	CTTN	pY447	-1.79353658	0.288464046	0.0002717		0.014673673	-4.28608
R.VADPDHDHTGFLTEpYVATR.W_3	**MAPK1**	**pY186**	**-2.23433645**	**0.212518974**	**0.0005889**		**0.031798658**	**-3.62164**

Down regulation of MAPK1 phosphorylation is a known consequence of imatinib inhibition of BCR-ABL1 in K562 cells, and it is required for imatinib-induced erythroid differentiation (290,291). RIN1 depletion reduced the level of MAPK1/3 phosphorylation by 25 ± 4%. Conversely, RIN1 over-expression increased the level of this phosphorylation by 35 ± 3% (Figure 5-6A). The MAPK1/3 phosphorylation signal decreased rapidly in response to imatinib targeting of BCR-ABL1 (Figure 5-6B). Importantly, the RIN1-dependent decrease in MAPK1/3 phosphorylation was highly reproducible. Cells assayed separately over a weeklong period

showed similar levels of MAPK1/3 phosphorylation (Figure 5-6C). This reproducibility, as well as the responsiveness of MAPK1/3 phosphorylation status to RIN1 expression and BCR-ABL1 activity, made it a useful surrogate for RIN1::ABL binding.
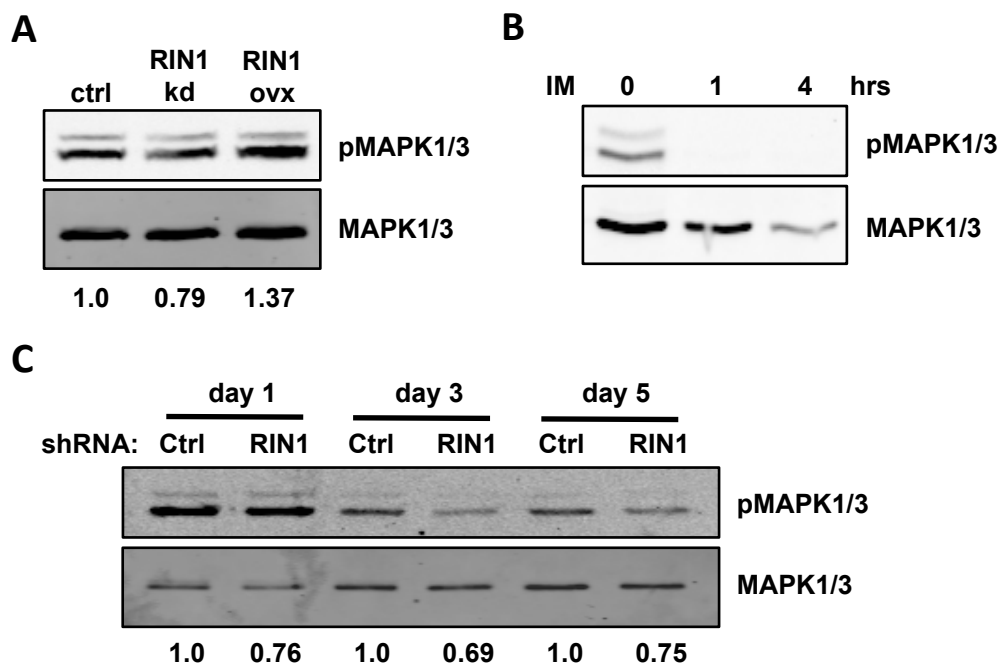
Figure 5-6. MAPK1/3 phosphorylation is RIN1 and BCR-ABL1-dependent in K562 cells. (**A**) K562 cells expressing a control vector, RIN1 shRNA or RIN1 over-expression construct were analyzed by immunoblot with anti-pMAPK1/3 and anti-MAPK1/3 antibodies. (**B**) K562 cells were treated with 1 μM imatinib (IM) for 1 and 4 hours at 37°C, then analyzed by immunoblot as in A. (**C**) K562 cells expressing control or RIN1 shRNA were sampled over a weeklong period and analyzed by immunoblot as in A.

Using this novel assay, we tested our 21 selected hits for their ability to disrupt RIN1-ABL signaling and identified five compounds in two structural classes that significantly decrease MAPK1/3 phosphorylation in K562 cells. One compound is a thiadiazole. The other four compounds are N-acetyl piperidine 4-carboxamides. Levels of inhibition ranged from 25-75% (Figure 5-7).
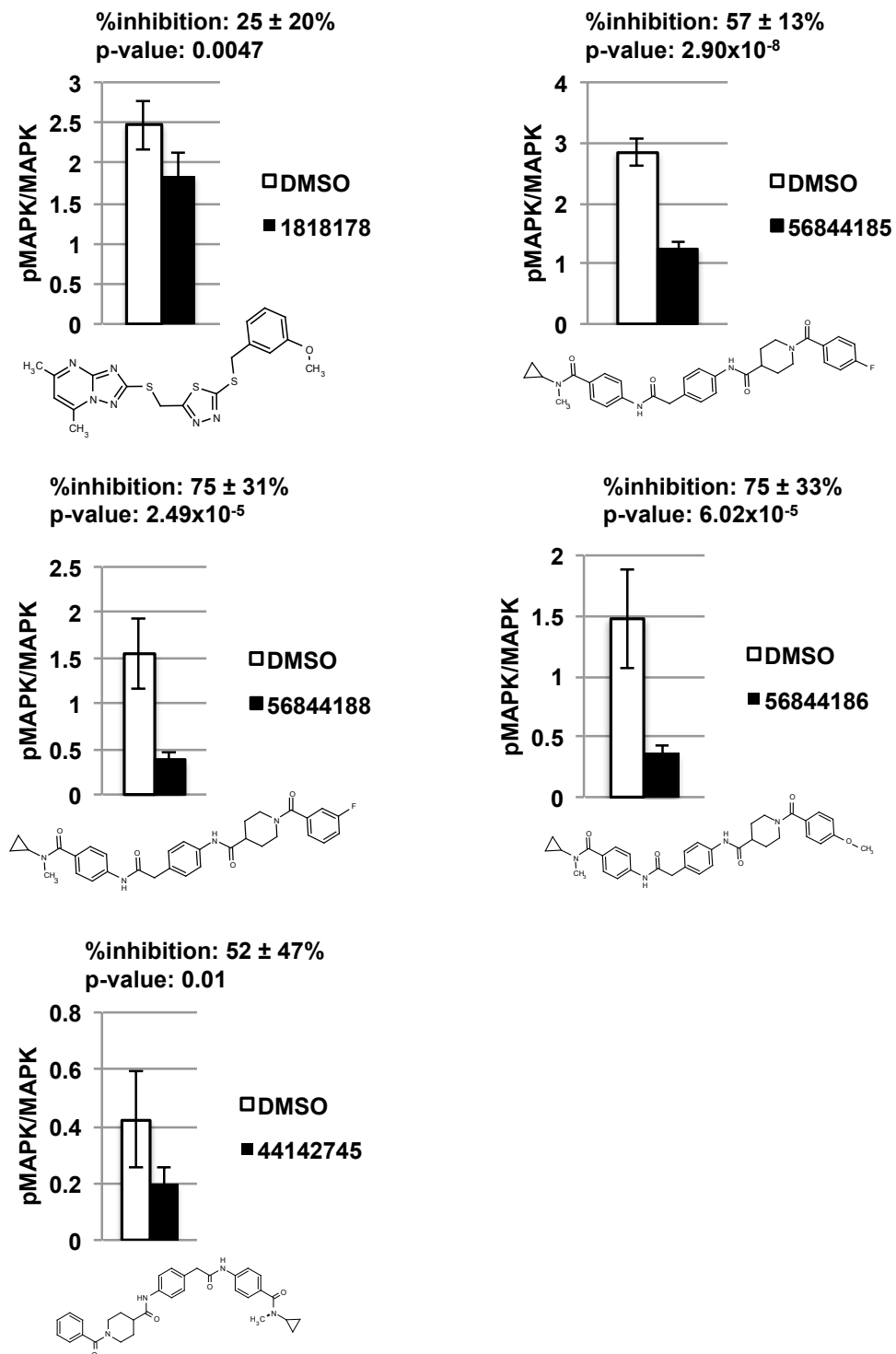
Figure 5-7. Five compounds significantly decrease MAPK1 phosphorylation in K562 cells. DMSO or compound was added to K562 cells at a final concentration of 1% or 10 μM, respectively, and incubated for 4 hours at 37°C before being lysed and analyzed by immunoblot with anti-pMAPK1/3 and anti-MAPK1/3. Each compound was tested with six biological replicates. Band intensity was quantified using LI-COR Odyssey, and the ratio of pMAPK/MAPK signal intensity is graphed for each compound and its DMSO control. Compounds are identified by their PubChem CID number.

5.4 DISCUSSION

Despite the essential role of protein-protein interactions in cell signaling and disease, inhibition of these interactions *via* small molecules remains challenging. Contacts between proteins often involve large and flat interfaces with few apparent openings for high affinity small molecule binding (292). Here we describe the design, validation and results of a robust TR-FRET based HTS to identify inhibitors of the RIN1::ABL1 protein-protein interaction that stimulates tyrosine kinase activity. Two design elements were crucial to the success of the assay. First, the use of the lanthanide element, terbium, contributed to an increased signal to noise ratio by allowing for delayed detection of the emission signal. Secondly, measurement of donor and acceptor emission and calculation of the FRET ratio decreased variability by normalizing for small differences in concentration. The Z' and Z factors of the assay were consistently high, reflecting the large signal range and low well-to-well variability (293).

The primary screen identified 1,637 compounds, of which 708 were confirmed. Serendipitously, two of the hits provided further internal validation of the assay design. Theaflavin-3,3'-digallate was identified as a hit in the primary screen for its ability to significantly decrease the FRET ratio. We also found that theaflavin-3,3'-digallate decreased phosphorylation of CRK and ABL *in vitro*, suggesting that it can function as a direct ABL kinase inhibitor. Its activity as a kinase inhibitor would be expected to destabilize the RIN1::ABL binding interaction by suppressing the RIN1 tyrosine phosphorylation needed for connecting with the ABL SH2 domain. This alone could explain the observed decrease in the FRET ratio. Moreover, theaflavin-3,3'-digallate may also bind RIN1's proline-rich motif and block binding to the ABL SH3 domain, as other tea polyphenols have been shown to have affinity for proline rich regions (294,295).

The screen also identified a compound, 2-amino-6-[2-(4-methoxyphenyl)ethylamino]-1H-pyrimidin-4-one (CID 1532134), that structurally resembles the allosteric BCR-ABL inhibitor GNF-1, and its analogue GNF-2 (Figure 5-S2). GNF-2 binds to the kinase domain myristate pocket of BCR-ABL and thereby stabilizes the catalytically inactive conformation. And just as GNF-2 has no activity against native ABL1 (296,297), CID 1532134 had no activity against native ABL1 in our kinase assay, implying that it interferes with ABL activity but is not an active site competitor. Its structural similarity to GNF-2 suggests that CID 1532134 may inhibit RIN1::ABL complex formation allosterically by binding in the myristate pocket of ABL and stabilizing an inactive conformation.

GNF-2   **GNF-1**   **CID 1532134**
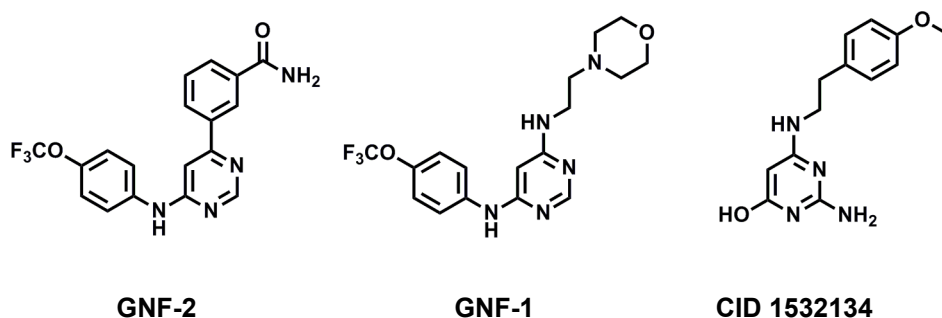
Figure 5-S2. CID 1532134 is structurally similar to known allosteric BCR-ABL kinase inhibitors GNF-1 and GNF-2.

In narrowing our list of hits, we sought to identify lead compounds that were effective in limiting BCR-ABL1 stimulation by RIN1 in cells. The K562 MAPK1/3 phosphorylation assay used here allowed for rapid and reproducible identification of compounds that disrupt RIN1-dependent BCR-ABL1 signaling. This also singled out compounds with favorable characteristics including stability, potency, target selectivity, solubility and cell permeability. Our cell assay identified five lead compounds: one thiadiazole and four structurally similar acyl piperidine carboxamides.

These five lead compounds are notable for their ability to alter BCR-ABL activity by targeting its interaction with the positive regulator RIN1. While BCR-ABL has been extensively targeted with direct kinase inhibitors, this is the first demonstration of selectively altering BCR-ABL kinase activity by interfering with a protein-protein interaction partner. Furthermore, we show that the compounds decrease MAPK1/3 phosphorylation in K562 cells, a down regulation that is required for imatinib-induced apoptosis and differentiation of leukemia cells (291). The results of our high throughput screen and the identification of lead compounds offer a novel tactic for targeting BCR-ABL oncoproteins, and provide new molecular tools for understanding ABL tyrosine kinase regulation by RIN1 binding.

The manner in which these compounds bind and inhibit the formation of a RIN1::ABL complex is unclear. The acyl piperidine carboxamides are distinctly linear and extended molecules, however, perhaps making them well-suited for interaction at a protein-protein interface. There was also strong evidence of a structure-activity relationship in this series (Table 5-S4). Several structural isomers of these hits, such as meta-substituted analogs in the two central phenyl rings and also 3-acyl piperidine analogues, were present in the screening collection. All such positional isomers were inactive in the TR-FRET screening assay (Figure 5-S3), suggesting that a large and elongated conformation is necessary for activity.
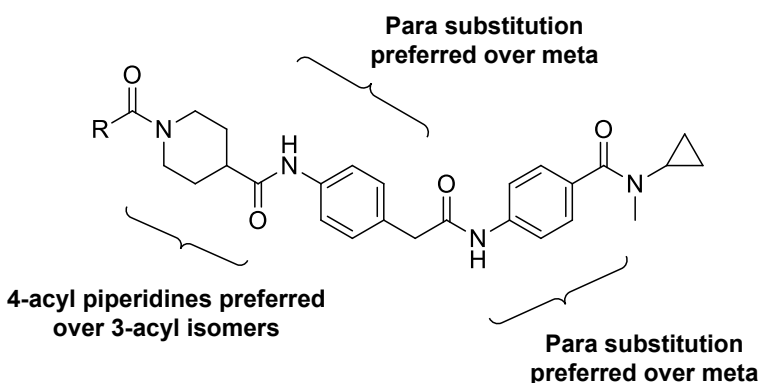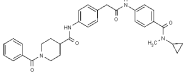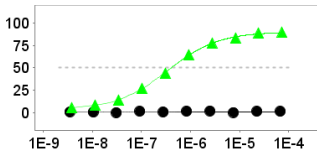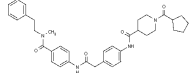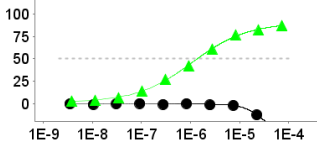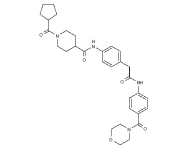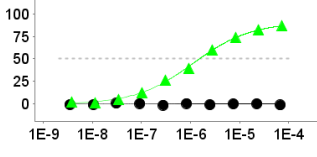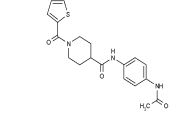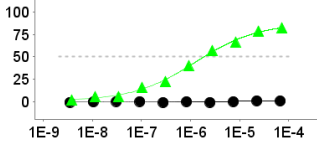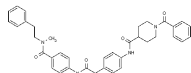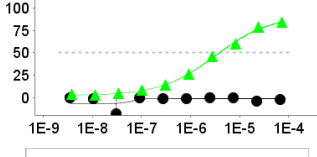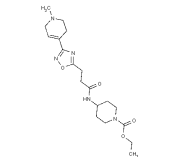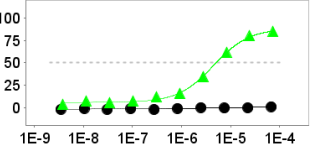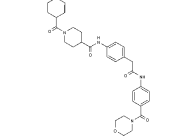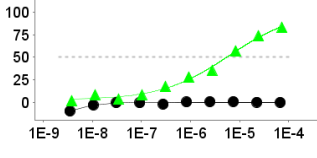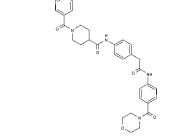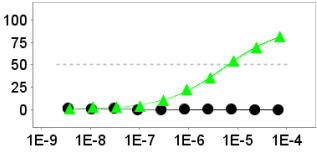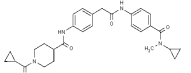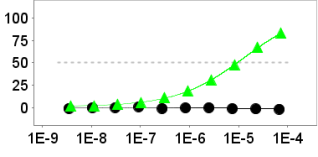
Figure 5-S3. Acyl piperidine carboxamide structure-activity relationship.

114

Table 5-S4. N-acyl piperidine-4-carboxamide Series SAR table

Structure	CID	SID	Dose-response curves Green = RIN1-ABL, black = CS	Max Response (%)	RIN1-ABL IC50 (uM)
	44142745	85146889		89.14	0.407
	44825536	89855047		87.13	1.378
	44825565	89855076		86.36	1.536
	1081265	24780919		82.17	1.899
	44825707	89855218		83.49	3.906
	3243211	87340996		84.52	5.105
	44825553	89855064		82.92	5.51
	44825693	89855204		81.29	6.483
	44142716	85146860		82.72	9.393

115

5.5 MATERIALS AND METHODS

Plasmid construction and baculovirus production

The ABL1 amino terminus was amplified from AblWT1-531 (gift of Dr. John Kuriyan) and cloned into the pKS Bluescript vector. Insertion of the eGFP coding sequence with a His$_6$ tag to the carboxy terminus created a 775 amino acid fusion (Figure 5-S4). This was subsequently moved into pFastBac1 for insect cell expression. The RIN1-SBP construct was generated by connecting a full-length human RIN1 coding sequence to the tandem affinity purification (TAP) tag from pSNSAP1 (PMID: 12574127). This generated a RIN1-SBP (streptavidin binding peptide)-TEV(protease cleavage site)-ProtA(immunoglobulin binding)-Flag(epitope) fusion orf that was cloned into pFastBac1 for insect cell expression. Figure S4 shows the amino acid sequence of each fusion protein construct. Baculovirus stocks were generated using the Life Technologies baculovirus expression system protocol. Briefly, pFastBac1 constructs were transformed into DH10Bac *E. coli* (Life Technologies) to generate recombinant bacmids, which were screened by blue/white selection. Recombinant bacmids were transfected into Sf9 cells using Cellfectin (Life Technologies). Medium containing passage 1 virus was harvested 72 hours post-transfection, clarified by centrifugation at 500*xg*, and stored at 4°C. Baculoviruses were then plaque purified and amplified using the same protocol.

ABL1⁵³¹-GFP MW aprox. 88 kDa

MGQQPGKVLGDQRRPSLPALHFIKGAGKKESSRHGGPHCNVFVEHEALQRPVASDFE
PQGLSEAARWNSKENLLAGPSENDPNLFVALYDFVASGDNTLSITKGEKLRVLGYNHNG
EWCEAQTKNGQGWVPSNYITPVNSLEKHSWYHGPVSRNAAEYLLSSGINGSFLVRESE
SSPGQRSISLRYEGRVYHYRINTASDGKLYVSSESRFNTLAELVHHHSTVADGLITTLHYP
APKRNKPTVYGVSPNYDKWEMERTDITMKHKLGGGQYGEVYEGVWKKYSLTVAVKTLK
EDTMEVEEFLKEAAVMKEIKHPNLVQLLGVCTREPPFYIITEFMTYGNLLDYLRECNRQE
VNAVVLLYMATQISSAMEYLEKKNFIHRDLAARNCLVGENHLVKVADFGLSRLMTGDTYT
AHAGAKFPIKWTAPESLAYNKFSIKSDVWAFGVLLWEIATYGMSPYPGIDLSQVYELLEK
DYRMERPEGCPEKVYELMRACWQWNPSDRPSFAEIHQAFETMFQESSISDEVEKELG
K<mark style="background:#00ff00">MSKGEELFTGVVPILVELDGDVNGHKFSVSGEGEGDATYGKLTLKFICTTGKLPVPWP
TLVTTLTYGVQCFSRYPDHMKQHDFFKSAMPEGYVQERTIFFKDDGNYKTRAEVKFEG
DTLVNRIELKGIDFKEDGNILGHKLEYNYNSHNVYIMADKQKNGIKVNFKIRHNIEDGSVQ
LADHYQQNTPIGDGPVLLPDNHYLSTQSALSKDPNEKRDHMVLLEFVTAAGITHGMDEL
YK</mark>HHHHHH

RIN1-TAP

**MESPGESGAGSPGAPSPSSFTTGHLAREKPAQDPLYDVPNASGGQAGGPQRPGRVV
SLRERLLLTRPVWLQLQANAAAALHMLRTEPPGTFLVRKSNTRQCQALCMRLPEASG
PSFVSSHYILESPGGVSLEGSELMFPDLVQLICAYCHTRDILLLPLQLPRAIHHAATHKE
LEAISHLGIEFWSSSLNIKAQRGPAGGPVLPQLKARSPQELDQGTGAALCFFNPLFPG
DLGPTKREKFKRSFKVRVSTETSSPLSPPAVPPPPVPVLPGAVPSQTERLPPCQLLRR
ESSVGYRVPAGSGPSLPPMPSLQEVDCGSPSSSEEEGVPGSRGSPATSPHLGRRRPL
LRSMSAAFCSLLAPERQVGRAAAALMQDRHTAAGQLVQDLLTQVRDGQRPQELEGIR
QALSRARAMLSAELGPEKLVSPKRLEHVLEKSLHCSVLKPLRPILAARLRRRLAADGS
LGRLAEGLRLARAQGPGAFGSHLSLPSPVELEQVRQKLLQLVRTYSPSAQVKRLLQA
CKLLYMALRTQEGEGSGADGFLPLLSLVLAHCDLPELLLEAEYMSELLEPSLLTGEGG
YYLTSLSASLALLSGLGQAHTLPLSPVQELRRSLSLWEQRRLPATHCFQHLLRVAYQD
PSSGCTSKTLAVPPEASIATLNQLCATKFRVTQPNTFGLFLYKEQGYHRLPPGALAHRL
PTTGYLVYRRAEWPETQGAVTEEEGSGQSEARSRGEEQGCQGDGDAGVKASPRDIR
EQSETTAEGGQGQAQEGPAQPGEPEAEGSRAAEE</mark>SR<mark style="background:#ffff00">MDEKTTGWRGGHVVEGLAG
ELEQLRARLEHHPQGQREP</mark>SGGCKLGLLVPRGSASENLY<mark style="background:#c0c0c0">FQGEL</mark><mark style="background:#00ffff">KTAALAQHDEAVDN
KFNKEQQNAFYEILHLPNLNEEQRNAFIQSLKDDPSQSANLLAEAKKLNDAQAPKVDNK
FNKEQQNAFYEILHLPNLNEEQRNAFIQSLKDDPSQSANLLAEAKKLNGAQAPKVDANS
AGKSTQL</mark>*DYKDDDDK***

<mark style="background:#00ff00">EGFP</mark>
<mark style="background:#ffff00">SBP</mark>
<mark style="background:#c0c0c0">QG</mark> = TEV cleavage
<mark style="background:#00ffff">ProtA</mark>
FLAG epitope tag

Figure 5-S4. ABL-eGFP and RIN1-TAP protein sequences

Purification of Recombinant Proteins

To express protein, 2.5×10^6 Sf9 cells/mL were infected 1:10 with p3-p5 baculovirus. Cells were incubated at 27°C on 150 rpm shaker for 72 hours. Cells were collected and pelleted at 800xg. For ABL-eGFP-His$_6$, cells were sonicated in 20 mM Tris-HCl pH 8, 100 mM NaCl and 5 mM imidazole. The lysate was clarified at 17,000xg for 30 minutes, and then incubated with Ni-NTA agarose (Qiagen) overnight. Beads were washed with 20 mM Tris-HCl pH 8, 250 mM NaCl, 10 mM imidazole and then eluted with 20 mM Tris-HCl pH 8, 250 mM NaCl, 10% glycerol and 100 mM imidazole, followed by 200 mM imidazole. Elutions were dialyzed in 50 mM Tris pH 8, 50 mM NaCl, 1 mM DTT and 10% glycerol. Protein concentration was determined by Bradford assay, and aliquots were frozen at -80°C until use.

For RIN1-SBP, protein was expressed as above. The cell pellet was sonicated in 20 mM Tris-HCl pH 8, 100 mM NaCl and 10% glycerol. The lysate was centrifuged at 17,000xg for 30 minutes, and incubated overnight with IgG sepharose (GE Healthcare Life Sciences). Beads were washed once with 50 mM Tris-HCl pH 8, 150 mM NaCl and .05% Tween. They were then washed twice with TEV cleavage buffer: 50 mM Tris-HCl pH 8, 0.5 mM EDTA and 1 mM DTT. Beads were resuspended in TEV cleavage buffer, and incubated with TEV protease at 15°C overnight. After the supernatant containing RIN1-SBP was collected, beads were resuspended in 50 mM Tris pH 8, 2 M NaCl, 0.5 mM EDTA, 1 mM DTT, 1% NP-40 and 1% BRIJ35 and rotated for 1 hour at 4°C. This was done twice to wash the RIN1-SBP from the beads. Elutions were combined, dialyzed and aliquots frozen at -80°C until use.

TR-FRET assay

For the TR-FRET assay, 75 nM purified ABL1-eGFP was pre-mixed with 100 nM RIN1-SBP and 2.5 nM Streptavidin-terbium (Life Technologies PV3966) in a kinase buffer consisting

of 10 mM Tris pH 7.4, 100 mM NaCl, 10 mM $MgCl_2$, 500 µM ATP, 1 mM DTT, 100 µM Na_3VO_4, 100 µM NaF and 100 µM BSA. For the UCLA MSSR screen, a Multidrop 384 was used to dispense 10 µL/well in a 384-well assay plate (Corning 3673). Compounds were added using Biomek FX, to a final concentration of 10 µM and 1% DMSO. The plates, with lids (Corning 3089), were then incubated for one hour at room temperature. After incubation, plates were read on a Perkin Elmer Victor 3 plate reader using 340 nm pulse, 100 µsec delay and 300 µsec window for signal. Emission filters were 520 ± 10 nm and 486 ± 5 nm.

The assay was further miniaturized to 1536 ultra-HTS format at TSRI, Florida and validated by comparing %inhibition and IC_{50} of a hit from the UCLA MSSR screen, CID 24512426. Details including data analysis methods and hit selection from the TSRI uHTS can be found at PubChem BioAssay AID 588664 (https://pubchem.ncbi.nlm.nih.gov/assay/assay.cgi?aid=588664).

Cheminformatics

Shared scaffolds of active compound families from the confirmation screen and CRC experiments were identified using a Maximum Common Substructure hierarchical clustering (ChemAxon LibraryMCS 5.10.2). The physical properties (i.e. molecular mass, topological polar surface area, chiral atoms, H-bond acceptors/donors, ring count and rotatable bonds) of the compounds tested in dose response format were calculated (ChemAxon Instant JChem 6.2.2).

Chemicals

The MLSMR library was provided by BioFocus DPI (South San Francisco, CA) through the NIH's Roadmap Molecular Libraries Initiative. Details regarding compound selection for this library can be found online at http://mli.nih.gov/mli/compound-repository/mlsmr-compounds/. Briefly, this library is a highly diversified collection of small molecules (more than 50% in the

119

molecular weight range 350-410 g/mol) and is comprised of both synthetic and natural products, from either commercial or academic sources, that can be grouped into the 4 following categories: (1) specialty sets of known bioactive compounds such as drugs and toxins (0.65%), (2) focused libraries aimed at specific target classes (2.85%), (3) non-commercial sources (7.4%) and (4) diversity sets covering a large area of the chemical space (89.1%).

In vitro kinase assay for direct ABL inhibitors

The kinase assay to identify direct ABL kinase inhibitors from UCLA MSSR and TSRI hits was performed as described in PubChem BioAssay AID 624303 (https://pubchem.ncbi.nlm.nih.gov/assay/assay.cgi?aid=624303). Purified His_6-CrkII was expressed and purified as previously described (144).

Mass spectrometry and phosphopeptide identification by fragmentation spectra sequencing and chromatography alignment

K562 (298) cells were cultured in RPMI with 10% FBS and 1% Pen/Strep. K562 with control and RIN1 shRNA were previously described (174). K562 cells expressing control shRNA or RIN1-shRNA were grown, processed and analyzed by MS twice independently. Cells were cultured in the presence of antibiotic during expansion before MS analysis, and were lysed by sonication in urea buffer (8 M urea, 50 mM Tris-HCl pH 7.5, 1 mM vanadate). Phosphotyrosine peptide were immunoprecipitated with anti-phosphotyrosine antibodies (Millipore, clone 4G10) using $2x10^8$ cells as previously described (199).

Phosphorylated peptides were analyzed by LC-MS/MS using an autosampler coupled with Nano2DLC pump (Eksigent) and LTQ-Orbitrap (Thermo Fisher Scientific). The samples were loaded onto an analytical column (10 cm ×75 μm i.d.) packed with 5 μm Integrafit Proteopep2 300 Å C18 (New Objective). Peptides were eluted into the mass spectrometer using

a HPLC gradient of 5−40% Buffer B in 45 min followed by a quick gradient of 40−90% Buffer B in 10 min, where Buffer A contains 0.1% formic acid in water and Buffer B contains 0.1% formic acid in acetonitrile (Ultima Gold, Fisher Scientific). Mass spectra were collected in positive ion mode using the Orbitrap for parent mass determination and the LTQ for data-dependent MS/MS acquisition of the top five most abundant peptides. Each sample was analyzed twice (replicate runs), and in each run, one-half of the sample was injected.

MS/MS fragmentation spectra were searched with SEQUEST (Version v.27, rev. 12, Thermo Fisher Scientific) against a database containing the human International Protein Index (IPI) protein database (ftp.ebi.ac.uk). Search parameters included carboxyamidomethylation of cysteine as static modification. Dynamic modifications included phosphorylation on tyrosine, and oxidation on methionine. Results derived from database searching were filtered using the following criteria: Xcorr >1.0(+1), 1.5(+2), 2(+3); peptide probability score <0.001; dCn >0.1; and mass accuracy <5 ppm (parts per million) with Bioworks version 3.2 (Thermo Electron Corp.). We estimated the false-positive rate of sequence assignments at 0.5% on the basis of a composite target-reversed decoy database search strategy (200). The Ascore algorithm was used to more accurately localize the phosphate on the peptide (http://ascore.med.harvard.edu) (201).

As is common in data-dependent MS2 fragmentation sequencing, some peptides identified by sequencing in one sample may not be sequenced or identified in another sample even if the peak is present. Peptide peaks sequenced in some samples but not in others were located in the remaining samples by aligning the chromatogram elution profiles by means of a dynamic time warping algorithm (202). An extended explanation of the strategy used in this work, and example performance results, can be found in the supporting information of Zimman *et al* (199).

Antibodies

The following antibodies were used: monoclonal rabbit-anti-pERK1 pY^{204}/ERK2 pY^{187} 1:500 (Epitomics, 2219-1), monoclonal mouse-anti-ERK1/2 1:5000 (BD, 610123), monoclonal mouse-anti-RIN1 1:500 (Colicelli lab, clone C9E11, Abpro), polyclonal rabbit-anti-ABL 1:1000 (Santa Cruz Biotechnology, sc-131), monoclonal mouse-anti-BCR 1:1000 (Santa Cruz Biotechnology, sc-48422), mouse-anti-tubulin 1:5000 (Sigma-Aldrich, T6074), goat-anti-rabbit-IRDye 800 1:5000 (Li-Cor Biosciences, 926-32211) and goat-anti-mouse-IRDye 680 1:5000 (Li-Cor Biosciences, 926-32220). Membranes were scanned and quantified using a Li-Cor Odyssey scanner.

pMAPK in K562

K562 with vector or RIN1 overexpression lentivirus were previously described (174). To analyze MAPK1 phosphorylation, confluent K562 cells were lysed in NP-40 buffer and immunoblotted. To test the effect of imatinib on MAPK phosphorylation, K562 cells were seeded $5x10^5$/well in a 12-well plate and incubated overnight at 37°C and 5% CO_2. Cells were treated with 1 μM imatinib for 1 or 4 hours. Cells from each well were harvested, lysed in 400 μL NP-40 and immunoblotted.

To test each compound, $5x10^5$ K562 cells were plated on a 10 cm tissue culture plate and incubated for 3 days. Cells were harvested and the volume brought to 12 mLs with fresh medium. 1 mL of the cells was distributed into each well of a 12-well tissue culture plate. In 6 of the wells, 10 μL of 1 mM compound was added per well. 10 μL of DMSO was added to the remaining wells and mixed by pipetting up and down. Cells were incubated at 37°C and 5% CO_2 for 4 hours. After incubation, cells were harvested from each well, lysed in 150 μL of RIPA buffer and analyzed as above.

CHAPTER 6. CONCLUSIONS, SIGNIFICANCE AND FUTURE DIRECTIONS

6.1 TYROSINE PHOSPHORYLATION OF RAS

We demonstrate in Chapter Two that RAS can be phosphorylated by ABL on Y137, and that overexpression of the RAS effector and ABL activator, RIN1, enhances phosphorylation at this site. Phosphomimetic mutation of this residue allosterically reduces RAF1-dependent hydrolysis. RAF1-RBD binds preferentially to RAS-pY^{137} compared to unphosphorylated RAS, consistent with impairment in hydrolysis and a prolonged GTP-bound state. Posttranslational regulation of RAS activity adds another level of complexity to RAS signaling. Moreover, RIN1-dependent enhancement of RAS phosphorylation suggests that RAS binding to RIN1 may trigger feedback regulation of RAS activity. Y137 is unique, though, because it *allosterically* regulates RAS and the data presented here experimentally validate a recent computational modeling study indicating allosteric "hot spots" on the surface of RAS (198). That Y137 is remote from the active site, but can allosterically modulate activity, makes the cleft that it resides in an interesting target for rational drug design, particularly since efforts to target the active site of RAS have been unsuccessful thus far (reviewed in (299)).

In the present study, we were unable to purify RAS-pY^{137}, impeding our ability to examine the intrinsic hydrolysis rate of the phosphorylated protein. This could be addressed, however, by using an orthogonal pair of amber suppressor tRNA and aminoacyl tRNA synthase to site-specifically incorporate the phosphotyrosine analog *p*-Carboxymethyl-L-phenylalanine (*p*CMF) at position 137. This method has previously been used to study the effect of phosphorylation of STAT1 (300) and RAD52 (301) and could be used to produce Y137-*p*CMF-RAS for biochemical studies. In addition, examining binding to additional effectors such as

RIN1 and PI3K could enhance our understanding of the effect of Y137 phosphorylation on activity and effector binding.

Of the 15 RAS-posttranslational modifications that have been detected by mass spectrometry and recorded on PhosphoSitePlus, only four have been characterized. Of those that are yet to be studied, one stands out – phosphorylation of Y64. The endogenous phosphorylated Y64 peptide has been detected by mass spectrometry in multiple cell lines and has been reported as a SRC substrate (77). Phosphorylation at this residue is particularly interesting because Y64 is part of Switch II, a series of residues that mediate effector binding. Mutation of Y64 to alanine or glycine abolishes binding to RASSF5, PI3K and neurofibromin, but not RAF1 (302) (303,304), suggesting that the tyrosine side chain mediates effector binding preference. Additionally, the mutant NRAS^{Y64N} has been reported in melanoma, and is thought to collaborate with a weakly activating BRAF mutation to promote activation of the MAPK pathway (305). The existing structural and mutational data suggest that Y64 phosphorylation would significantly and directly alter RAS function.

One particularly surprising, albeit peripheral, finding from this study was evidence of RAS dimerization. RAS dimers have long been suspected, largely because RAF requires plasma membrane recruitment and dimerization for activation. However *in vivo* data has been lacking. Recent studies using quantitative physical techniques on *in vitro* membrane-anchored NRAS have proposed several residues involved in the dimerization interface: D47, E49, R135, R161, and R164 (196). Coincidentally, Y64 has been proposed as an allosteric regulator of dimerization (197), and it is intriguing to hypothesize that Y64 phosphorylation may regulate RAS dimerization. These studies provide useful starting points for identifying the dimer interface and studying the effect of dimerization on RAS signaling.

6.2 NUCLEAR LOCALIZATION OF RIN1

In Chapter Three we reported the cell cycle-dependent nuclear localization of RIN1, and its regulation by three nuclear localization sequences and three serine residues. RIN1 has long been considered to be an exclusively cytoplasmic protein, and is best characterized for its roles as RAS effector and mediator of RTK endocytosis and signaling. However, growing numbers of endocytic proteins have been found in the nucleus in recent years including RAB5 effectors APPL1 and APPL2 (235), clathrin (234), eps15, CALM (236), epsin (237) and EDH2 (306). The nuclear function of most of these proteins is still unclear, but in general they appear to influence transcription and chromatin remodeling (reviewed in (307)). With the exception of APPL1 and APPL2, there is no clear link between their endocytic functions and nuclear localization.

Although we examined cell cycle progression, we did not find a distinct cell cycle phenotype associated with shRNA-mediated RIN1 knockdown. However, it is possible that overexpression of RIN1 mutants that are retained in or excluded from the nucleus could have a dominant negative effect. RIN1 also has a naturally expressed slice variant, RIN1Δ, with a 62aa internal deletion encompassing one of the nuclear localization sequences (86,117). Examining its subcellular localization could offer additional insight into regulation of nuclear translocation.

The RIN1 binding partners identified using MudPIT also offer leads to understanding nuclear function. The most abundant proteins included several known binding partners including 14-3-3 isoforms, ABL1 and ABL2. However RIN1 interaction partners were also enriched in RNA-binding proteins, particularly those involved in post-transcriptional regulation of gene expression. These included ELAVL1, HNRNPA3, DDX1, RBMX, TAF15 and DKC1. A possible role for RIN1 in regulating splicing could be probed using a splicing reporter in RIN1

knockdown or mutant cells. CLIP-seq could be used to identify the targets of these RIN1-associated RNA binding proteins, which could then be analyzed for pathway enrichment.

RIN1 belongs to a family of proteins that share related structures and domains, as well as functions. Cell cycle-dependent nuclear localization of RIN1 raises the question of whether other family members localize to the nucleus, as well as whether they might be functionally redundant. RIN2 is particularly interesting because RIN2 mutations and deficiency lead to RIN2 syndrome (a.k.a. Macrocephaly, Alopecia, Cutis Laxa and Scoliosis syndrome) (103-105). RIN2 is expressed ubiquitously, has been implicated in regulation of cell adhesion by modulating E-cadherin and integrin endocytosis (87,308), and sequence analysis reveals two putative nuclear localization sequences. How RIN2 deficiency results in skeletal and elastic tissue abnormalities remains to be elucidated.

6.3 RIN1 REGULATION OF BCR-ABL1

Chapter Four extended the work of previous studies in the lab that identified RIN1 as a positive regulator of ABL (112,309) and an accelerator of BCR-ABL-induced leukemia (111). Here, we demonstrated that RIN1 is required for BCR-ABL transformation of murine bone marrow cells to growth factor independence *ex vivo*, and that RIN1 silencing sensitizes leukemia cells to imatinib. Surprisingly, however, RIN1 is not required for BCR-ABL-induced leukemogenesis in *in vivo* mouse models of lymphoid and myeloid leukemia.

Although the BCR-ABL retroviral bone marrow transduction/transplantation model that we used is generally considered to be the most accurate and informative model for CML, a major drawback is the expression of BCR-ABL from the retroviral LTR instead of the BCR promoter. In addition to expression by the strong viral promoter, multiple copies can be integrated into the same cell, driving high expression of BCR-ABL, and leading to a shorter latent period than in

human CML. Strong expression of BCR-ABL may check the effect of or requirement for RIN1 in leukemogenesis, a possibility which could be studied using BCR-ABL transgenic mice (reviewed in (310)).

Based on the existing literature, it appears that *in vivo*, the "constitutively active" BCR-ABL1 oncogene remains responsive to positive regulation by RIN1, but does not *require* RIN1 for leukemogenesis. This is also supported by *in vitro* data from leukemia cells and cell lines, where RIN1 overexpression significantly enhances phosphorylation of BCR-ABL substrates, but RIN1 silencing has mild to undetectable effects. Additionally, although RIN1 silencing enhances the sensitivity of cells to imatinib, RIN1 is not required for the proliferation or survival of leukemia cells and cell lines in the absence of drug. These data suggest that RIN1 modulates and fine-tunes BCR-ABL activity, but is not required for basal ABL and BCR-ABL function. This fine-tuning ability also appears to be the case in RIN1's functions in modulating endocytosis and cytoskeleton remodeling and suggests that RIN1 plays a role akin to a "coregulator."

That RIN1 silencing enhances sensitivity of BCR-ABL^{T315I} cells to imatinib is an important observation in the context of the drug resistance that often arises in patients treated in the blast phase of CML. However, further studies need to be done to clarify the mechanism of sensitization. Based on our knowledge of RIN1::BCR-ABL1 binding, one possibility is that loss of RIN1 binding shifts ABL1 toward the inactive conformation which imatinib binds, and away from the active conformation that RIN1 stabilizes. This hypothesis could be tested using a mutant RIN1^{QM} that exhibits reduced binding to ABL because of mutations in four tyrosine residues. Furthermore, the *in vivo* role of RIN1 in mediating imatinib sensitivity could be tested using mouse models of leukemia. Together these experiments would help to clarify the

therapeutic usefulness of targeting both RIN1::BCR-ABL1 binding and the BCR-ABL1 active site in combination.

In Chapter Five we reported the design and implementation of a TR-FRET-based high-throughput screening assay to identify inhibitors of the RIN1-ABL1 binding interaction, which yielded two lead scaffolds. Interest in targeting protein-protein interaction interfaces has increased in recent years, although they are difficult to target because of the large, flat surfaces and lack of natural ligands. We used TR-FRET to measure the interaction between RIN1-ABL *in vitro* and optimized the assay for robustness as well as time and cost-efficiency. This design could be applied to the study and targeting of other protein-protein interactions in cancer (i.e. MDM2-p53, MYC-MAX) and infections diseases (i.e. CD4-gp120).

6.4 OVERALL SUMMARY

In this work we examined the structure, function and regulation of the components of the RAS-RIN1-ABL signaling pathway. Members of this pathway are commonly activated or overexpressed in cancer. While some RAS effector pathways, such as RAS-RAF and RAS-PI3K, have been extensively studied, the RAS-RIN1-ABL axis is less well-understood. Our work provides new insights into RAS regulation and RIN1 subcellular localization. We also clarify the role of RIN1 in regulating BCR-ABL1 activity in leukemia, and report a high-throughput screening assay that can be used to identify protein-protein interaction inhibitors.

REFERENCES

1.   HARVEY, J. J. AN UNIDENTIFIED VIRUS WHICH CAUSES THE RAPID PRODUCTION OF TUMOURS IN MICE. *Nature* **204**, 1104–1105 (1964).

2.   Kirsten, W. H. & Mayer, L. A. Malignant lymphomas of extrathymic origin induced in rats by murine erythroblastosis virus. *J. Natl. Cancer Inst.* **43**, 735–746 (1969).

3.   Scolnick, E. M., Rands, E., Williams, D. & Parks, W. P. Studies on the nucleic acid sequences of Kirsten sarcoma virus: a model for formation of a mammalian RNA-containing sarcoma virus. *J. Virol.* **12**, 458–463 (1973).

4.   Stehelin, D., Varmus, H. E., Bishop, J. M. & Vogt, P. K. DNA related to the transforming gene(s) of avian sarcoma viruses is present in normal avian DNA. *Nature* **260**, 170–173 (1976).

5.   Ellis, R. W. *et al.* The p21 src genes of Harvey and Kirsten sarcoma viruses originate from divergent members of a family of normal vertebrate genes. *Nature* **292**, 506–511 (1981).

6.   Chang, E. H., Gonda, M. A., Ellis, R. W., Scolnick, E. M. & Lowy, D. R. Human genome contains four genes homologous to transforming genes of Harvey and Kirsten murine sarcoma viruses. *Proc. Natl. Acad. Sci. U.S.A.* **79**, 4848–4852 (1982).

7.   Papageorge, A., Lowy, D. & Scolnick, E. M. Comparative biochemical properties of p21 ras molecules coded for by viral and cellular ras genes. *J. Virol.* **44**, 509–519 (1982).

8.   Wennerberg, K., Rossman, K. L. & Der, C. J. The Ras superfamily at a glance. *J. Cell. Sci.* **118**, 843–846 (2005).

9.   Bourne, H. R., Sanders, D. A. & McCormick, F. The GTPase superfamily: conserved structure and molecular mechanism. *Nature* **349**, 117–127 (1991).

10.   Neal, S. E., Eccleston, J. F., Hall, A. & Webb, M. R. Kinetic analysis of the hydrolysis of GTP by p21N-ras. The basal GTPase mechanism. *J. Biol. Chem.* **263**, 19718–19722 (1988).

11.   Gibbs, J. B., Schaber, M. D., Allard, W. J., Sigal, I. S. & Scolnick, E. M. Purification of ras GTPase activating protein from bovine brain. *Proc. Natl. Acad. Sci. U.S.A.* **85**, 5026–5030 (1988).

12.   Boguski, M. S. & McCormick, F. Proteins regulating Ras and its relatives. *Nature* **366**, 643–654 (1993).

13.   Scheffzek, K. *et al.* The Ras-RasGAP complex: structural basis for GTPase activation and its loss in oncogenic Ras mutants. *Science* **277**, 333–338 (1997).

14.   Boriack-Sjodin, P. A., Margarit, S. M., Bar-Sagi, D. & Kuriyan, J. The structural basis of the activation of Ras by Sos. *Nature* **394**, 337–343 (1998).

15. Van Dyke, K. *et al.* An analysis of nucleotides and catecholamines in bovine medullary granules by anion exchange high pressure liquid chromatography and fluorescence. Evidence that most of the catecholamines in chromaffin granules are stored without associated ATP. *Pharmacology* **15**, 377–391 (1977).

16. Buday, L. & Downward, J. Many faces of Ras activation. *Biochim. Biophys. Acta* **1786**, 178–187 (2008).

17. Stacey, D. W. & Kung, H. F. Transformation of NIH 3T3 cells by microinjection of Ha-ras p21 protein. *Nature* **310**, 508–511 (1984).

18. Mulcahy, L. S., Smith, M. R. & Stacey, D. W. Requirement for ras proto-oncogene function during serum-stimulated growth of NIH 3T3 cells. *Nature* **313**, 241–243 (1985).

19. Simon, M. A., Bowtell, D. D., Dodson, G. S., Laverty, T. R. & Rubin, G. M. Ras1 and a putative guanine nucleotide exchange factor perform crucial steps in signaling by the sevenless protein tyrosine kinase. *Cell* **67**, 701–716 (1991).

20. Rogge, R. D., Karlovich, C. A. & Banerjee, U. Genetic dissection of a neurodevelopmental pathway: Son of sevenless functions downstream of the sevenless and EGF receptor tyrosine kinases. *Cell* **64**, 39–48 (1991).

21. Bonfini, L., Karlovich, C. A., Dasgupta, C. & Banerjee, U. The Son of sevenless gene product: a putative activator of Ras. *Science* **255**, 603–606 (1992).

22. Lowenstein, E. J. *et al.* The SH2 and SH3 domain-containing protein GRB2 links receptor tyrosine kinases to ras signaling. *Cell* **70**, 431–442 (1992).

23. Egan, S. E. *et al.* Association of Sos Ras exchange protein with Grb2 is implicated in tyrosine kinase signal transduction and transformation. *Nature* **363**, 45–51 (1993).

24. Li, N. *et al.* Guanine-nucleotide-releasing factor hSos1 binds to Grb2 and links receptor tyrosine kinases to Ras signalling. *Nature* **363**, 85–88 (1993).

25. Rajalingam, K., Schreck, R., Rapp, U. R. & Albert, S. Ras oncogenes and their downstream targets. *Biochim. Biophys. Acta* **1773**, 1177–1195 (2007).

26. Rapp, U. R. *et al.* Structure and biological activity of v-raf, a unique oncogene transduced by a retrovirus. *Proc. Natl. Acad. Sci. U.S.A.* **80**, 4218–4222 (1983).

27. Kolch, W., Heidecker, G., Lloyd, P. & Rapp, U. R. Raf-1 protein kinase is required for growth of induced NIH/3T3 cells. *Nature* **349**, 426–428 (1991).

28. Vojtek, A. B., Hollenberg, S. M. & Cooper, J. A. Mammalian Ras interacts directly with the serine/threonine kinase Raf. *Cell* **74**, 205–214 (1993).

29. Koide, H., Satoh, T., Nakafuku, M. & Kaziro, Y. GTP-dependent association of Raf-1 with Ha-Ras: identification of Raf as a target downstream of Ras in mammalian cells. *Proc. Natl. Acad. Sci. U.S.A.* **90**, 8683–8686 (1993).

30. Warne, P. H., Viciana, P. R. & Downward, J. Direct interaction of Ras and the amino-

terminal region of Raf-1 in vitro. *Nature* **364**, 352–355 (1993).

31.   Zhang, X. F. *et al.* Normal and oncogenic p21ras proteins bind to the amino-terminal regulatory domain of c-Raf-1. *Nature* **364**, 308–313 (1993).

32.   Robinson, M. J. & Cobb, M. H. Mitogen-activated protein kinase pathways. *Curr. Opin. Cell Biol.* **9**, 180–186 (1997).

33.   Roberts, P. J. & Der, C. J. Targeting the Raf-MEK-ERK mitogen-activated protein kinase cascade for the treatment of cancer. *Oncogene* **26**, 3291–3310 (2007).

34.   Rodriguez-Viciana, P. *et al.* Phosphatidylinositol-3-OH kinase as a direct target of Ras. *Nature* **370**, 527–532 (1994).

35.   Rodriguez-Viciana, P., Warne, P. H., Vanhaesebroeck, B., Waterfield, M. D. & Downward, J. Activation of phosphoinositide 3-kinase by interaction with Ras and by point mutation. *EMBO J.* **15**, 2442–2451 (1996).

36.   Samuels, Y. *et al.* High frequency of mutations of the PIK3CA gene in human cancers. *Science* **304**, 554–554 (2004).

37.   Urano, T., Emkey, R. & Feig, L. A. Ral-GTPases mediate a distinct downstream signaling pathway from Ras that facilitates cellular transformation. *EMBO J.* **15**, 810–816 (1996).

38.   Lambert, J. M. *et al.* Tiam1 mediates Ras activation of Rac by a PI(3)K-independent mechanism. *Nat. Cell Biol.* **4**, 621–625 (2002).

39.   Khokhlatchev, A. *et al.* Identification of a novel Ras-regulated proapoptotic pathway. *Curr. Biol.* **12**, 253–265 (2002).

40.   Kelley, G. G., Reks, S. E., Ondrako, J. M. & Smrcka, A. V. Phospholipase C(epsilon): a novel Ras effector. *EMBO J.* **20**, 743–754 (2001).

41.   Hill, M. & Hillova, J. Recombinational events between exogenous mouse DNA and newly synthesized DNA strands of chicken cells in culture. *Nature New Biol.* **231**, 261–265 (1971).

42.   Wigler, M., Pellicer, A., Silverstein, S. & Axel, R. Biochemical transfer of single-copy eucaryotic genes using total cellular DNA as donor. *Cell* **14**, 725–731 (1978).

43.   Shih, C., Shilo, B. Z., Goldfarb, M. P., Dannenberg, A. & Weinberg, R. A. Passage of phenotypes of chemically transformed cells via transfection of DNA and chromatin. *Proc. Natl. Acad. Sci. U.S.A.* **76**, 5714–5718 (1979).

44.   Krontiris, T. G. & Cooper, G. M. Transforming activity of human tumor DNAs. *Proc. Natl. Acad. Sci. U.S.A.* **78**, 1181–1184 (1981).

45.   Murray, M. J. *et al.* Three different human tumor cell lines contain different oncogenes. *Cell* **25**, 355–361 (1981).

46. Perucho, M. *et al.* Human-tumor-derived cell lines contain common and different transforming genes. *Cell* **27**, 467–476 (1981).

47. Parada, L. F., Tabin, C. J., Shih, C. & Weinberg, R. A. Human EJ bladder carcinoma oncogene is homologue of Harvey sarcoma virus ras gene. *Nature* **297**, 474–478 (1982).

48. Santos, E., Tronick, S. R., Aaronson, S. A., Pulciani, S. & Barbacid, M. T24 human bladder carcinoma oncogene is an activated form of the normal human homologue of BALB- and Harvey-MSV transforming genes. *Nature* **298**, 343–347 (1982).

49. Der, C. J., Krontiris, T. G. & Cooper, G. M. Transforming genes of human bladder and lung carcinoma cell lines are homologous to the ras genes of Harvey and Kirsten sarcoma viruses. *Proc. Natl. Acad. Sci. U.S.A.* **79**, 3637–3640 (1982).

50. Taparowsky, E. *et al.* Activation of the T24 bladder carcinoma transforming gene is linked to a single amino acid change. *Nature* **300**, 762–765 (1982).

51. Reddy, E. P., Reynolds, R. K., Santos, E. & Barbacid, M. A point mutation is responsible for the acquisition of transforming properties by the T24 human bladder carcinoma oncogene. *Nature* **300**, 149–152 (1982).

52. Tabin, C. J. *et al.* Mechanism of activation of a human oncogene. *Nature* **300**, 143–149 (1982).

53. Gremer, L., Gilsbach, B., Ahmadian, M. R. & Wittinghofer, A. Fluoride complexes of oncogenic Ras mutants to study the Ras-RasGap interaction. *Biol. Chem.* **389**, 1163–1171 (2008).

54. Prior, I. A., Lewis, P. D. & Mattos, C. A comprehensive survey of Ras mutations in cancer. *Cancer Res.* **72**, 2457–2467 (2012).

55. Vageli, D. *et al.* Transcriptional activation of H-ras, K-ras and N-ras proto-oncogenes in human bladder tumors. *Cancer Lett.* **107**, 241–247 (1996).

56. Taya, Y. *et al.* A novel combination of K-ras and myc amplification accompanied by point mutational activation of K-ras in a human lung cancer. *EMBO J.* **3**, 2943–2946 (1984).

57. Graham, K. A., Richardson, C. L., Minden, M. D., Trent, J. M. & Buick, R. N. Varying degrees of amplification of the N-ras oncogene in the human breast cancer cell line MCF-7. *Cancer Res.* **45**, 2201–2205 (1985).

58. Fernández-Medarde, A. & Santos, E. Ras in cancer and developmental diseases. *Genes Cancer* **2**, 344–358 (2011).

59. Aoki, Y. *et al.* Germline mutations in HRAS proto-oncogene cause Costello syndrome. *Nat. Genet.* **37**, 1038–1040 (2005).

60. Razzaque, M. A. *et al.* Characterization of a novel KRAS mutation identified in Noonan syndrome. *Am. J. Med. Genet. A* **158A**, 524–532 (2012).

61. Willumsen, B. M., Christensen, A., Hubbert, N. L., Papageorge, A. G. & Lowy, D. R. The p21 ras C-terminus is required for transformation and membrane association. *Nature* **310**, 583–586 (1984).

62. Buss, J. E. & Sefton, B. M. Direct identification of palmitic acid as the lipid attached to p21ras. *Mol. Cell. Biol.* **6**, 116–122 (1986).

63. Clarke, S., Vogel, J. P., Deschenes, R. J. & Stock, J. Posttranslational modification of the Ha-ras oncogene protein: evidence for a third class of protein carboxyl methyltransferases. *Proc. Natl. Acad. Sci. U.S.A.* **85**, 4643–4647 (1988).

64. Hancock, J. F., Magee, A. I., Childs, J. E. & Marshall, C. J. All ras proteins are polyisoprenylated but only some are palmitoylated. *Cell* **57**, 1167–1177 (1989).

65. Casey, P. J., Solski, P. A., Der, C. J. & Buss, J. E. p21ras is modified by a farnesyl isoprenoid. *Proc. Natl. Acad. Sci. U.S.A.* **86**, 8323–8327 (1989).

66. Wright, L. P. & Philips, M. R. Thematic review series: lipid posttranslational modifications. CAAX modification and membrane targeting of Ras. *J. Lipid Res.* **47**, 883–891 (2006).

67. Silvius, J. R. & l'Heureux, F. Fluorimetric evaluation of the affinities of isoprenylated peptides for lipid bilayers. *Biochemistry* **33**, 3014–3022 (1994).

68. Choy, E. *et al.* Endomembrane trafficking of ras: the CAAX motif targets proteins to the ER and Golgi. *Cell* **98**, 69–80 (1999).

69. Laude, A. J. & Prior, I. A. Palmitoylation and localisation of RAS isoforms are modulated by the hypervariable linker domain. *J. Cell. Sci.* **121**, 421–427 (2008).

70. Apolloni, A., Prior, I. A., Lindsay, M., Parton, R. G. & Hancock, J. F. H-ras but not K-ras traffics to the plasma membrane through the exocytic pathway. *Mol. Cell. Biol.* **20**, 2475–2487 (2000).

71. Rocks, O. *et al.* An acylation cycle regulates localization and activity of palmitoylated Ras isoforms. *Science* **307**, 1746–1752 (2005).

72. Hancock, J. F., Paterson, H. & Marshall, C. J. A polybasic domain or palmitoylation is required in addition to the CAAX motif to localize p21ras to the plasma membrane. *Cell* **63**, 133–139 (1990).

73. Bivona, T. G. *et al.* PKC regulates a farnesyl-electrostatic switch on K-Ras that promotes its association with Bcl-XL on mitochondria and induces apoptosis. *Mol. Cell* **21**, 481–493 (2006).

74. Williams, J. G., Pappu, K. & Campbell, S. L. Structural and biochemical studies of p21Ras S-nitrosylation and nitric oxide-mediated guanine nucleotide exchange. *Proc. Natl. Acad. Sci. U.S.A.* **100**, 6376–6381 (2003).

75. Sasaki, A. T. *et al.* Ubiquitination of K-Ras enhances activation and facilitates binding

to select downstream effectors. *Sci Signal* **4**, ra13 (2011).

76.   Jeong, W.-J. *et al.* Ras stabilization through aberrant activation of Wnt/β-catenin signaling promotes intestinal tumorigenesis. *Sci Signal* **5**, ra30 (2012).

77.   Bunda, S. *et al.* Src promotes GTPase activity of Ras via tyrosine 32 phosphorylation. *Proc. Natl. Acad. Sci. U.S.A.* **111**, E3785–94 (2014).

78.   Colicelli, J. *et al.* Expression of three mammalian cDNAs that interfere with RAS function in Saccharomyces cerevisiae. *Proc. Natl. Acad. Sci. U.S.A.* **88**, 2913–2917 (1991).

79.   Han, L. & Colicelli, J. A human protein selected for interference with Ras function interacts directly with Ras and competes with Raf1. *Mol. Cell. Biol.* **15**, 1318–1323 (1995).

80.   Saito, K. *et al.* A novel binding protein composed of homophilic tetramer exhibits unique properties for the small GTPase Rab5. *Journal of Biological Chemistry* **277**, 3412–3418 (2002).

81.   Kajiho, H. *et al.* Characterization of RIN3 as a guanine nucleotide exchange factor for the Rab5 subfamily GTPase Rab31. *J. Biol. Chem.* **286**, 24364–24373 (2011).

82.   Woller, B. *et al.* Rin-like, a novel regulator of endocytosis, acts as guanine nucleotide exchange factor for Rab5a and Rab22. *Biochim. Biophys. Acta* **1813**, 1198–1210 (2011).

83.   Ponting, C. P. & Benjamin, D. R. A novel family of Ras-binding domains. *Trends Biochem. Sci.* **21**, 422–425 (1996).

84.   Wang, Y. *et al.* The RAS effector RIN1 directly competes with RAF and is regulated by 14-3-3 proteins. *Mol. Cell. Biol.* **22**, 916–926 (2002).

85.   Tall, G. G., Barbieri, M. A., Stahl, P. D. & Horazdovsky, B. F. Ras-activated endocytosis is mediated by the Rab5 guanine nucleotide exchange activity of RIN1. *Dev. Cell* **1**, 73–82 (2001).

86.   Han, L. *et al.* Protein binding and signaling properties of RIN1 suggest a unique effector function. *Proc. Natl. Acad. Sci. U.S.A.* **94**, 4954–4959 (1997).

87.   Sandri, C. *et al.* The R-Ras/RIN2/Rab5 complex controls endothelial cell adhesion and morphogenesis via active integrin endocytosis and Rac signaling. *Cell Res.* **22**, 1479–1501 (2012).

88.   Janson, C., Kasahara, N., Prendergast, G. C. & Colicelli, J. RIN3 is a negative regulator of mast cell responses to SCF. *PLoS ONE* **7**, e49615 (2012).

89.   Kajiho, H. *et al.* RIN3: a novel Rab5 GEF interacting with amphiphysin II involved in the early endocytic pathway. *J. Cell. Sci.* **116**, 4159–4168 (2003).

90.   Barbieri, M. A., Kong, C., Chen, P.-I., Horazdovsky, B. F. & Stahl, P. D. The SRC homology 2 domain of Rin1 mediates its binding to the epidermal growth factor receptor

and regulates receptor endocytosis. *Journal of Biological Chemistry* **278**, 32027–32036 (2003).

91.   Deininger, K. *et al.* The Rab5 guanylate exchange factor Rin1 regulates endocytosis of the EphA4 receptor in mature excitatory neurons. *Proc. Natl. Acad. Sci. U.S.A.* **105**, 12539–12544 (2008).

92.   Hu, H. *et al.* Integration of transforming growth factor beta and RAS signaling silences a RAB5 guanine nucleotide exchange factor and enhances growth factor-directed cell migration. *Mol. Cell. Biol.* **28**, 1573–1583 (2008).

93.   Balaji, K., French, C. T., Miller, J. F. & Colicelli, J. The RAB5-GEF Function of RIN1 Regulates Multiple Steps During Listeria monocytogenes Infection. *Traffic* n/a–n/a (2014).doi:10.1111/tra.12204

94.   Hunker, C. M., Galvis, A., Veisaga, M. L. & Barbieri, M. A. Rin1 is a negative regulator of the IL3 receptor signal transduction pathways. *Anticancer Res.* **26**, 905–916 (2006).

95.   Balaji, K. *et al.* RIN1 orchestrates the activation of RAB5 GTPases and ABL tyrosine kinases to determine the fate of EGFR. *J. Cell. Sci.* **125**, 5887–5896 (2012).

96.   Shan, G.-Y. *et al.* Overexpression of RIN1 associates with tumor grade and progression in patients of bladder urothelial carcinoma. *Tumour Biol.* **33**, 847–855 (2012).

97.   Wang, Q. *et al.* Prognostic significance of RIN1 gene expression in human non-small cell lung cancer. *Acta Histochem.* **114**, 463–468 (2012).

98.   Tomshine, J. C. *et al.* Cell proliferation and epidermal growth factor signaling in non-small cell lung adenocarcinoma cell lines are dependent on Rin1. *J. Biol. Chem.* **284**, 26331–26339 (2009).

99.   Yu, H.-F. *et al.* High RIN1 expression is associated with poor prognosis in patients with gastric adenocarcinoma. *Tumour Biol.* **33**, 1557–1563 (2012).

100.   Fang, P., Zhao, Z., Tian, H. & Zhang, X. RIN1 exhibits oncogenic property to suppress apoptosis and its aberrant accumulation associates with poor prognosis in melanoma. *Tumour Biol.* **33**, 1511–1518 (2012).

101.   He, H. *et al.* Low RIN1 expression in HCC is associated with tumor invasion and unfavorable prognosis. *Am. J. Clin. Pathol.* **140**, 73–81 (2013).

102.   Milstein, M. *et al.* RIN1 is a breast tumor suppressor gene. *Cancer Res.* **67**, 11510–11516 (2007).

103.   Syx, D. *et al.* The RIN2 syndrome: a new autosomal recessive connective tissue disorder caused by deficiency of Ras and Rab interactor 2 (RIN2). *Hum. Genet.* **128**, 79–88 (2010).

104.   Aslanger, A. D. *et al.* Newly described clinical features in two siblings with MACS syndrome and a novel mutation in RIN2. *Am. J. Med. Genet. A* **164A**, 484–489 (2014).

105. Basel-Vanagaite, L. *et al.* RIN2 deficiency results in macrocephaly, alopecia, cutis laxa, and scoliosis: MACS syndrome. *Am. J. Hum. Genet.* **85**, 254–263 (2009).

106. Albagha, O. M. E. *et al.* Genome-wide association identifies three new susceptibility loci for Paget's disease of bone. *Nat. Genet.* **43**, 685–689 (2011).

107. Chung, P. Y. J. & Van Hul, W. Paget's disease of bone: evidence for complex pathogenetic interactions. *Semin. Arthritis Rheum.* **41**, 619–641 (2012).

108. Kemp, J. P. *et al.* Phenotypic dissection of bone mineral density reveals skeletal site specificity and facilitates the identification of novel loci in the genetic regulation of bone mass attainment. *PLoS Genet.* **10**, e1004423 (2014).

109. Rosenthal, S. L. & Kamboh, M. I. Late-Onset Alzheimer's Disease Genes and the Potentially Implicated Pathways. *Curr Genet Med Rep* **2**, 85–101 (2014).

110. Dhaka, A. *et al.* The RAS effector RIN1 modulates the formation of aversive memories. *J. Neurosci.* **23**, 748–757 (2003).

111. Afar, D. E. *et al.* Regulation of the oncogenic activity of BCR-ABL by a tightly bound substrate protein RIN1. *Immunity* **6**, 773–782 (1997).

112. Hu, H., Bliss, J. M., Wang, Y. & Colicelli, J. RIN1 is an ABL tyrosine kinase activator and a regulator of epithelial-cell adhesion and migration. *Curr. Biol.* **15**, 815–823 (2005).

113. Dzudzor, B. *et al.* Regulated expression of the Ras effector Rin1 in forebrain neurons. *Molecular and Cellular Neuroscience* **43**, 108–116 (2010).

114. Bliss, J. M., Gray, E. E., Dhaka, A., O'Dell, T. J. & Colicelli, J. Fear learning and extinction are linked to neuronal plasticity through Rin1 signaling. *J. Neurosci. Res.* **88**, 917–926 (2010).

115. Barbieri, M. A., Kong, C., Chen, P.-I., Horazdovsky, B. F. & Stahl, P. D. The SRC homology 2 domain of Rin1 mediates its binding to the epidermal growth factor receptor and regulates receptor endocytosis. *J. Biol. Chem.* **278**, 32027–32036 (2003).

116. Kong, C., Su, X., Chen, P.-I & Stahl, P. D. Rin1 interacts with signal-transducing adaptor molecule (STAM) and mediates epidermal growth factor receptor trafficking and degradation. *J. Biol. Chem.* **282**, 15294–15301 (2007).

117. Hunker, C. M. *et al.* Rin1 regulates insulin receptor signal transduction pathways. *Exp. Cell Res.* **312**, 1106–1118 (2006).

118. Balaji, K. & Colicelli, J. RIN1 regulates cell migration through RAB5 GTPases and ABL tyrosine kinases. *Commun Integr Biol* **6**, e25421 (2013).

119. Ziegler, S. *et al.* A novel protein kinase D phosphorylation site in the tumor suppressor Rab interactor 1 is critical for coordination of cell migration. *Mol. Biol. Cell* **22**, 570–580 (2011).

120. Abelson, H. T. & Rabstein, L. S. Lymphosarcoma: virus-induced thymic-independent

disease in mice. *Cancer Res.* **30**, 2213–2222 (1970).

121.   Collett, M. S., Purchio, A. F. & Erikson, R. L. Avian sarcoma virus-transforming protein, pp60src shows protein kinase activity specific for tyrosine. *Nature* **285**, 167–169 (1980).

122.   Witte, O. N., Rosenberg, N., Paskind, M., Shields, A. & Baltimore, D. Identification of an Abelson murine leukemia virus-encoded protein present in transformed fibroblast and lymphoid cells. *Proc. Natl. Acad. Sci. U.S.A.* **75**, 2488–2492 (1978).

123.   Witte, O. N., Rosenberg, N. E. & Baltimore, D. A normal cell protein cross-reactive to the major Abelson murine leukaemia virus gene product. *Nature* **281**, 396–398 (1979).

124.   Witte, O. N., Dasgupta, A. & Baltimore, D. Abelson murine leukaemia virus protein is phosphorylated in vitro to form phosphotyrosine. *Nature* **283**, 826–831 (1980).

125.   Sefton, B. M., Hunter, T. & Raschke, W. C. Evidence that the Abelson virus protein functions in vivo as a protein kinase that phosphorylates tyrosine. *Proc. Natl. Acad. Sci. U.S.A.* **78**, 1552–1556 (1981).

126.   Jackson, P. & Baltimore, D. N-terminal mutations activate the leukemogenic potential of the myristoylated form of c-abl. *EMBO J.* **8**, 449–456 (1989).

127.   Van Etten, R. A. *et al.* The COOH terminus of the c-Abl tyrosine kinase contains distinct F- and G-actin binding domains with bundling activity. *J. Cell Biol.* **124**, 325–340 (1994).

128.   Feller, S. M., Knudsen, B. & Hanafusa, H. c-Abl kinase regulates the protein binding activity of c-Crk. *EMBO J.* **13**, 2341–2351 (1994).

129.   Shafman, T. *et al.* Interaction between ATM protein and c-Abl in response to DNA damage. *Nature* **387**, 520–523 (1997).

130.   Goga, A. *et al.* p53 dependent growth suppression by the c-Abl nuclear tyrosine kinase. *Oncogene* **11**, 791–799 (1995).

131.   Kipreos, E. T. & Wang, J. Y. Cell cycle-regulated binding of c-Abl tyrosine kinase to DNA. *Science* **256**, 382–385 (1992).

132.   Wang, Y., Miller, A. L., Mooseker, M. S. & Koleske, A. J. The Abl-related gene (Arg) nonreceptor tyrosine kinase uses two F-actin-binding domains to bundle F-actin. *Proc. Natl. Acad. Sci. U.S.A.* **98**, 14865–14870 (2001).

133.   Van Etten, R. A., Jackson, P. & Baltimore, D. The mouse type IV c-abl gene product is a nuclear protein, and activation of transforming ability is associated with cytoplasmic localization. *Cell* **58**, 669–678 (1989).

134.   Taagepera, S. *et al.* Nuclear-cytoplasmic shuttling of C-ABL tyrosine kinase. *Proc. Natl. Acad. Sci. U.S.A.* **95**, 7457–7462 (1998).

135.   Colicelli, J. ABL tyrosine kinases: evolution of function, regulation, and specificity. *Sci Signal* **3**, re6 (2010).

136. Meltser, V., Ben-Yehoyada, M. & Shaul, Y. c-Abl tyrosine kinase in the DNA damage response: cell death and more. *Cell Death Differ.* **18**, 2–4 (2011).

137. Nagar, B. *et al.* Structural basis for the autoinhibition of c-Abl tyrosine kinase. *Cell* **112**, 859–871 (2003).

138. Hantschel, O. *et al.* A myristoyl/phosphotyrosine switch regulates c-Abl. *Cell* **112**, 845–857 (2003).

139. Pluk, H., Dorey, K. & Superti-Furga, G. Autoinhibition of c-Abl. *Cell* **108**, 247–259 (2002).

140. Courtneidge, S. A. Cancer: Escape from inhibition. *Nature* **422**, 827–828 (2003).

141. Dorey, K. *et al.* Phosphorylation and structure-based functional studies reveal a positive and a negative role for the activation loop of the c-Abl tyrosine kinase. *Oncogene* **20**, 8075–8084 (2001).

142. Tanis, K. Q., Veach, D., Duewel, H. S., Bornmann, W. G. & Koleske, A. J. Two distinct phosphorylation pathways have additive effects on Abl family kinase activation. *Mol. Cell. Biol.* **23**, 3884–3896 (2003).

143. Plattner, R., Kadlec, L., DeMali, K. A., Kazlauskas, A. & Pendergast, A. M. c-Abl is activated by growth factors and Src family kinases and has a role in the cellular response to PDGF. *Genes Dev.* **13**, 2400–2411 (1999).

144. Cao, X., Tanis, K. Q., Koleske, A. J. & Colicelli, J. Enhancement of ABL kinase catalytic efficiency by a direct binding regulator is independent of other regulatory mechanisms. *J. Biol. Chem.* **283**, 31401–31407 (2008).

145. Miyoshi-Akiyama, T., Aleman, L. M., Smith, J. M., Adler, C. E. & Mayer, B. J. Regulation of Cbl phosphorylation by the Abl tyrosine kinase and the Nck SH2/SH3 adaptor. *Oncogene* **20**, 4058–4069 (2001).

146. Cong, F. *et al.* Cytoskeletal protein PSTPIP1 directs the PEST-type protein tyrosine phosphatase to the c-Abl kinase to mediate Abl dephosphorylation. *Mol. Cell* **6**, 1413–1423 (2000).

147. Echarri, A. & Pendergast, A. M. Activated c-Abl is degraded by the ubiquitin-dependent proteasome pathway. *Curr. Biol.* **11**, 1759–1765 (2001).

148. NOWELL, P. C. & HUNGERFORD, D. A. Chromosome studies on normal and leukemic human leukocytes. *J. Natl. Cancer Inst.* **25**, 85–109 (1960).

149. NOWELL, P. C. Legacy of the Philadelphia Chromosome. at <http://www.uphs.upenn.edu/news/features/philadelphia-chromosome/history/nowell-personal-perspective.html>

150. NOWELL, P. C. & HUNGERFORD, D. A. A minute chromosome in human chronic granulocytic leukemia. *Science* 1488–1501 (1960).

151. Rowley, J. D. Letter: A new consistent chromosomal abnormality in chronic myelogenous leukaemia identified by quinacrine fluorescence and Giemsa staining. *Nature* **243**, 290–293 (1973).

152. Heisterkamp, N. *et al.* Chromosomal localization of human cellular homologues of two viral oncogenes. *Nature* **299**, 747–749 (1982).

153. Heisterkamp, N. & Groffen, J. Philadelphia-positive leukemia: a personal perspective. *Oncogene* **21**, 8536–8540 (2002).

154. de Klein, A. *et al.* A cellular oncogene is translocated to the Philadelphia chromosome in chronic myelocytic leukaemia. *Nature* **300**, 765–767 (1982).

155. Ben-Neriah, Y., Daley, G. Q., Mes-Masson, A. M., Witte, O. N. & Baltimore, D. The chronic myelogenous leukemia-specific P210 protein is the product of the bcr/abl hybrid gene. *Science* **233**, 212–214 (1986).

156. Hermans, A. *et al.* Unique fusion of bcr and c-abl genes in Philadelphia chromosome positive acute lymphoblastic leukemia. *Cell* **51**, 33–40 (1987).

157. Kantarjian, H. M. *et al.* Significance of the P210 versus P190 molecular abnormalities in adults with Philadelphia chromosome-positive acute leukemia. *Blood* **78**, 2411–2418 (1991).

158. Pane, F. *et al.* Neutrophilic-chronic myeloid leukemia: a distinct disease with a specific molecular marker (BCR/ABL with C3/A2 junction). *Blood* **88**, 2410–2414 (1996).

159. McWhirter, J. R., Galasso, D. L. & Wang, J. Y. A coiled-coil oligomerization domain of Bcr is essential for the transforming function of Bcr-Abl oncoproteins. *Mol. Cell. Biol.* **13**, 7587–7595 (1993).

160. Pendergast, A. M., Gishizky, M. L., Havlik, M. H. & Witte, O. N. SH1 domain autophosphorylation of P210 BCR/ABL is required for transformation but not growth factor independence. *Mol. Cell. Biol.* **13**, 1728–1736 (1993).

161. Wong, S. & Witte, O. N. The BCR-ABL story: bench to bedside and back. *Annu. Rev. Immunol.* **22**, 247–306 (2004).

162. Mandanas, R. A. *et al.* Role of p21 RAS in p210 bcr-abl transformation of murine myeloid cells. *Blood* **82**, 1838–1847 (1993).

163. Sawyers, C. L., McLaughlin, J. & Witte, O. N. Genetic requirement for Ras in the transformation of fibroblasts and hematopoietic cells by the Bcr-Abl oncogene. *J. Exp. Med.* **181**, 307–313 (1995).

164. Zimmermann, J. *et al.* Phenylamino-pyrimidine (PAP) derivatives: a new class of potent and selective inhibitors of protein kinase C (PKC). *Arch. Pharm. (Weinheim)* **329**, 371–376 (1996).

165. Capdeville, R., Buchdunger, E., Zimmermann, J. & Matter, A. Glivec (STI571, imatinib),

a rationally developed, targeted anticancer drug. *Nat Rev Drug Discov* **1**, 493–502 (2002).

166.   Druker, B. J. *et al.* Effects of a selective inhibitor of the Abl tyrosine kinase on the growth of Bcr-Abl positive cells. *Nat. Med.* **2**, 561–566 (1996).

167.   Druker, B. J. *et al.* Efficacy and safety of a specific inhibitor of the BCR-ABL tyrosine kinase in chronic myeloid leukemia. *N. Engl. J. Med.* **344**, 1031–1037 (2001).

168.   Gorre, M. E. *et al.* Clinical resistance to STI-571 cancer therapy caused by BCR-ABL gene mutation or amplification. *Science* **293**, 876–880 (2001).

169.   Shah, N. P. *et al.* Overriding imatinib resistance with a novel ABL kinase inhibitor. *Science* **305**, 399–401 (2004).

170.   Weisberg, E. *et al.* Characterization of AMN107, a selective inhibitor of native and mutant Bcr-Abl. *Cancer Cell* **7**, 129–141 (2005).

171.   O'Hare, T. *et al.* AP24534, a Pan-BCR-ABL Inhibitor for Chronic Myeloid Leukemia, Potently Inhibits the T315I Mutant and Overcomes Mutation-Based Resistance. *Cancer Cell* **16**, 401–412 (2009).

172.   Cortes, J. E. *et al.* A phase 2 trial of ponatinib in Philadelphia chromosome-positive leukemias. *N. Engl. J. Med.* **369**, 1783–1796 (2013).

173.   Zabriskie, M. S. *et al.* BCR-ABL1 Compound Mutations Combining Key Kinase Domain Positions Confer Clinical Resistance to Ponatinib in Ph Chromosome-Positive Leukemia. *Cancer Cell* (2014).doi:10.1016/j.ccr.2014.07.006

174.   Thai, M. *et al.* ABL fusion oncogene transformation and inhibitor sensitivity are mediated by the cellular regulator RIN1. *Leukemia* **25**, 290–300 (2011).

175.   Chardin, P. *et al.* Human Sos1: a guanine nucleotide exchange factor for Ras that binds to GRB2. *Science* **260**, 1338–1343 (1993).

176.   Quilliam, L. A., Rebhun, J. F. & Castro, A. F. A growing family of guanine nucleotide exchange factors is responsible for activation of Ras-family GTPases. *Prog. Nucleic Acid Res. Mol. Biol.* **71**, 391–444 (2002).

177.   Colicelli, J. Human RAS superfamily proteins and related GTPases. *Sci. STKE* **2004**, RE13 (2004).

178.   Wittinghofer, A. & Herrmann, C. Ras-effector interactions, the problem of specificity. *FEBS Lett.* **369**, 52–56 (1995).

179.   Trahey, M. & McCormick, F. A cytoplasmic protein stimulates normal N-ras p21 GTPase, but does not affect oncogenic mutants. *Science* **238**, 542–545 (1987).

180.   Ahmadian, M. R., Stege, P., Scheffzek, K. & Wittinghofer, A. Confirmation of the arginine-finger hypothesis for the GAP-stimulated GTP-hydrolysis reaction of Ras. *Nat. Struct. Biol.* **4**, 686–689 (1997).

181.   Barceló, C. *et al.* Phosphorylation at Ser-181 of oncogenic KRAS is required for tumor growth. *Cancer Res.* **74**, 1190–1199 (2014).

182.   Wang, Y. & Colicelli, J. RAS interaction with effector target RIN1. *Meth. Enzymol.* **332**, 139–151 (2001).

183.   Hu, H. *et al.* Integration of transforming growth factor beta and RAS signaling silences a RAB5 guanine nucleotide exchange factor and enhances growth factor-directed cell migration. *Mol. Cell. Biol.* **28**, 1573–1583 (2008).

184.   Carroll, W. L. *et al.* Pediatric acute lymphoblastic leukemia. *Hematology Am Soc Hematol Educ Program* 102–131 (2003).

185.   Faderl, S., Kantarjian, H. M., Talpaz, M. & Estrov, Z. Clinical significance of cytogenetic abnormalities in adult acute lymphoblastic leukemia. *Blood* **91**, 3995–4019 (1998).

186.   Zhang, K. *et al.* Suppression of c-ras transformation by GTPase-activating protein. *Nature* **346**, 754–756 (1990).

187.   Webb, Y., Hermida-Matsumoto, L. & Resh, M. D. Inhibition of protein palmitoylation, raft localization, and T cell signaling by 2-bromopalmitate and polyunsaturated fatty acids. *J. Biol. Chem.* **275**, 261–270 (2000).

188.   Gibbs, J. B., Sigal, I. S., Poe, M. & Scolnick, E. M. Intrinsic GTPase activity distinguishes normal and oncogenic ras p21 molecules. *Proc. Natl. Acad. Sci. U.S.A.* **81**, 5704–5708 (1984).

189.   Ito, Y. *et al.* Regional polysterism in the GTP-bound form of the human c-Ha-Ras protein. *Biochemistry* **36**, 9109–9119 (1997).

190.   Buhrman, G., Holzapfel, G., Fetics, S. & Mattos, C. Allosteric modulation of Ras positions Q61 for a direct role in catalysis. *Proc. Natl. Acad. Sci. U.S.A.* **107**, 4931–4936 (2010).

191.   Johnson, C. W. & Mattos, C. The allosteric switch and conformational states in Ras GTPase affected by small molecules. *Enzymes* **33 Pt A**, 41–67 (2013).

192.   Buhrman, G., Kumar, V. S. S., Cirit, M., Haugh, J. M. & Mattos, C. Allosteric modulation of Ras-GTP is linked to signal transduction through RAF kinase. *J. Biol. Chem.* **286**, 3323–3331 (2011).

193.   Li, L. *et al.* Prediction of phosphotyrosine signaling networks using a scoring matrix-assisted ligand identification approach. *Nucleic Acids Res.* **36**, 3263–3273 (2008).

194.   Lock, P., Casagranda, F. & Dunn, A. R. Independent SH2-binding sites mediate interaction of Dok-related protein with RasGTPase-activating protein and Nck. *J. Biol. Chem.* **274**, 22775–22784 (1999).

195.   Hunter, T. & Sefton, B. M. Transforming gene product of Rous sarcoma virus

phosphorylates tyrosine. *Proc. Natl. Acad. Sci. U.S.A.* **77**, 1311–1315 (1980).

196.   Güldenhaupt, J. *et al.* N-Ras forms dimers at POPC membranes. *Biophys. J.* **103**, 1585–1593 (2012).

197.   Lin, W.-C. *et al.* H-Ras forms dimers on membrane surfaces via a protein-protein interface. *Proc. Natl. Acad. Sci. U.S.A.* **111**, 2996–3001 (2014).

198.   Buhrman, G. *et al.* Analysis of binding site hot spots on the surface of Ras GTPase. *J. Mol. Biol.* **413**, 773–789 (2011).

199.   Zimman, A. *et al.* Activation of aortic endothelial cells by oxidized phospholipids: a phosphoproteomic analysis. *J. Proteome Res.* **9**, 2812–2824 (2010).

200.   Elias, J. E., Haas, W., Faherty, B. K. & Gygi, S. P. Comparative evaluation of mass spectrometry platforms used in large-scale proteomics investigations. *Nat. Methods* **2**, 667–675 (2005).

201.   Beausoleil, S. A., Villén, J., Gerber, S. A., Rush, J. & Gygi, S. P. A probability-based approach for high-throughput protein phosphorylation analysis and site localization. *Nat. Biotechnol.* **24**, 1285–1292 (2006).

202.   Prakash, A. *et al.* Signal maps for mass spectrometry-based comparative proteomics. *Mol. Cell Proteomics* **5**, 423–432 (2006).

203.   Kearney, B. M., Johnson, C. W., Roberts, D. M., Swartz, P. & Mattos, C. DRoP: a water analysis program identifies Ras-GTP-specific pathway of communication between membrane-interacting regions and the active site. *J. Mol. Biol.* **426**, 611–629 (2014).

204.   Buhrman, G., de Serrano, V. & Mattos, C. Organic solvents order the dynamic switch II in Ras crystals. *Structure* **11**, 747–751 (2003).

205.   Otwinowski, Z. & Minor, W.in *Methods in Enzymology* (Carter, C. W., Jr & Sweet, R. M.) **276**, 307–326 (Academic Press, 1997).

206.   Adams, P. D. *et al.* PHENIX: a comprehensive Python-based system for macromolecular structure solution. *Acta Crystallogr. D Biol. Crystallogr.* **66**, 213–221 (2010).

207.   Emsley, P. & Cowtan, K. Coot: model-building tools for molecular graphics. *Acta Crystallogr. D Biol. Crystallogr.* **60**, 2126–2132 (2004).

208.   Kaiser, P. & Wohlschlegel, J. Identification of ubiquitination sites and determination of ubiquitin-chain architectures by mass spectrometry. *Meth. Enzymol.* **399**, 266–277 (2005).

209.   Wohlschlegel, J. A. Identification of SUMO-conjugated proteins and their SUMO attachment sites using proteomic mass spectrometry. *Methods Mol. Biol.* **497**, 33–49 (2009).

210.   Xu, T. *et al.* ProLuCID, a fast and sensitive tandem mass spectra-based protein

identification program. *Mol. Cell Proteomics* **5**, S174 (2006).

211.   Tabb, D. L., McDonald, W. H. & Yates, J. R. DTASelect and Contrast: tools for assembling and comparing protein identifications from shotgun proteomics. *J. Proteome Res.* **1**, 21–26 (2002).

212.   Elias, J. E. & Gygi, S. P. Target-decoy search strategy for increased confidence in large-scale protein identifications by mass spectrometry. *Nat. Methods* **4**, 207–214 (2007).

213.   Florens, L. *et al.* Analyzing chromatin remodeling complexes using shotgun proteomics and normalized spectral abundance factors. *Methods* **40**, 303–311 (2006).

214.   Senda, K., Goi, T., Hirono, Y., Katayama, K. & Yamaguchi, A. Analysis of RIN1 gene expression in colorectal cancer. *Oncol. Rep.* **17**, 1171–1175 (2007).

215.   Mustafi, S., Rivero, N., Olson, J. C., Stahl, P. D. & Barbieri, M. A. Regulation of Rab5 function during phagocytosis of live Pseudomonas aeruginosa in macrophages. *Infect. Immun.* **81**, 2426–2436 (2013).

216.   Leevers, S. J., Paterson, H. F. & Marshall, C. J. Requirement for Ras in Raf activation is overcome by targeting Raf to the plasma membrane. *Nature* **369**, 411–414 (1994).

217.   Brunet, A. *et al.* 14-3-3 transits to the nucleus and participates in dynamic nucleocytoplasmic transport. *J. Cell Biol.* **156**, 817–828 (2002).

218.   Sekimoto, T., Fukumoto, M. & Yoneda, Y. 14-3-3 suppresses the nuclear localization of threonine 157-phosphorylated p27(Kip1). *EMBO J.* **23**, 1934–1942 (2004).

219.   Kumagai, A. & Dunphy, W. G. Binding of 14-3-3 proteins and nuclear export control the intracellular localization of the mitotic inducer Cdc25. *Genes Dev.* **13**, 1067–1072 (1999).

220.   Lopez-Girona, A., Furnari, B., Mondesert, O. & Russell, P. Nuclear localization of Cdc25 is regulated by DNA damage and a 14-3-3 protein. *Nature* **397**, 172–175 (1999).

221.   Johnson, C. *et al.* Bioinformatic and experimental survey of 14-3-3-binding sites. *Biochem. J.* **427**, 69–78 (2010).

222.   Kosugi, S. *et al.* Six classes of nuclear localization signals specific to different binding grooves of importin alpha. *Journal of Biological Chemistry* **284**, 478–485 (2009).

223.   Kumari, G., Singhal, P. K., Rao, M. R. K. S. & Mahalingam, S. Nuclear transport of Ras-associated tumor suppressor proteins: different transport receptor binding specificities for arginine-rich nuclear targeting signals. *J. Mol. Biol.* **367**, 1294–1311 (2007).

224.   O'Connell, M. J., Walworth, N. C. & Carr, A. M. The G2-phase DNA-damage checkpoint. *Trends Cell Biol.* **10**, 296–303 (2000).

225.   Voigt, W. *et al.* Topoisomerase-I inhibitor SN-38 can induce DNA damage and chromosomal aberrations independent from DNA synthesis. *Anticancer Res.* **18**, 3499–

3505 (1998).

226. Naetar, N. *et al.* PP2A-mediated regulation of Ras signaling in G2 is essential for stable quiescence and normal G1 length. *Mol. Cell* **54**, 932–945 (2014).

227. Bogerd, H. P., Fridell, R. A., Benson, R. E., Hua, J. & Cullen, B. R. Protein sequence requirements for function of the human T-cell leukemia virus type 1 Rex nuclear export signal delineated by a novel in vivo randomization-selection assay. *Mol. Cell. Biol.* **16**, 4207–4214 (1996).

228. Scott, M. S., Troshin, P. V. & Barton, G. J. NoD: a Nucleolar localization sequence detector for eukaryotic and viral proteins. *BMC Bioinformatics* **12**, 317 (2011).

229. Fu, H., Subramanian, R. R. & Masters, S. C. 14-3-3 proteins: structure, function, and regulation. *Annu. Rev. Pharmacol. Toxicol.* **40**, 617–647 (2000).

230. Hart, G. W., Slawson, C., Ramirez-Correa, G. & Lagerlof, O. Cross talk between O-GlcNAcylation and phosphorylation: roles in signaling, transcription, and chronic disease. *Annu. Rev. Biochem.* **80**, 825–858 (2011).

231. Sayat, R., Leber, B., Grubac, V., Wiltshire, L. & Persad, S. O-GlcNAc-glycosylation of beta-catenin regulates its nuclear localization and transcriptional activity. *Exp. Cell Res.* **314**, 2774–2787 (2008).

232. Majumdar, G. *et al.* Insulin stimulates and diabetes inhibits O-linked N-acetylglucosamine transferase and O-glycosylation of Sp1. *Diabetes* **53**, 3184–3192 (2004).

233. Milstein, M. *et al.* RIN1 is a breast tumor suppressor gene. *Cancer Res.* **67**, 11510–11516 (2007).

234. Enari, M., Ohmori, K., Kitabayashi, I. & Taya, Y. Requirement of clathrin heavy chain for p53-mediated transcription. *Genes Dev.* **20**, 1087–1099 (2006).

235. Miaczynska, M. *et al.* APPL proteins link Rab5 to nuclear signal transduction via an endosomal compartment. *Cell* **116**, 445–456 (2004).

236. Vecchi, M. *et al.* Nucleocytoplasmic Shuttling of Endocytic Proteins. *J. Cell Biol.* **153**, 1511–1518 (2001).

237. Hyman, J., Chen, H., Di Fiore, P. P., De Camilli, P. & Brunger, A. T. Epsin 1 undergoes nucleocytosolic shuttling and its eps15 interactor NH(2)-terminal homology (ENTH) domain, structurally similar to Armadillo and HEAT repeats, interacts with the transcription factor promyelocytic leukemia Zn(2)+ finger protein (PLZF). *J. Cell Biol.* **149**, 537–546 (2000).

238. Mills, I. G. *et al.* Huntingtin interacting protein 1 modulates the transcriptional activity of nuclear hormone receptors. *J. Cell Biol.* **170**, 191–200 (2005).

239. Juven-Gershon, T. *et al.* The Mdm2 Oncoprotein Interacts with the Cell Fate Regulator

Numb. *Mol. Cell. Biol.* **18**, 3974–3982 (1998).

240. Niehr, F. *et al.* Combination therapy with vemurafenib (PLX4032/RG7204) and metformin in melanoma cell lines with distinct driver mutations. *J Transl Med* **9**, 76 (2011).

241. Papadopoulos, P., Ridge, S. A., Boucher, C. A., Stocking, C. & Wiedemann, L. M. The novel activation of ABL by fusion to an ets-related gene, TEL. *Cancer Res.* **55**, 34–38 (1995).

242. Iijima, Y. *et al.* A new ETV6/TEL partner gene, ARG (ABL-related gene or ABL2), identified in an AML-M3 cell line with a t(1;12)(q25;p13) translocation. *Blood* **95**, 2126–2131 (2000).

243. Deininger, M. The development of imatinib as a therapeutic agent for chronic myeloid leukemia. *Blood* **105**, 2640–2653 (2005).

244. O'Hare, T. *et al.* AP24534, a pan-BCR-ABL inhibitor for chronic myeloid leukemia, potently inhibits the T315I mutant and overcomes mutation-based resistance. *Cancer Cell* **16**, 401–412 (2009).

245. Shah, N. P. *et al.* Sequential ABL kinase inhibitor therapy selects for compound drug-resistant BCR-ABL mutations with altered oncogenic potency. *J. Clin. Invest.* **117**, 2562–2569 (2007).

246. Bueno, M. J. *et al.* Genetic and Epigenetic Silencing of MicroRNA-203 Enhances ABL1 and BCR-ABL1 Oncogene Expression. *Cancer Cell* **13**, 496–506 (2008).

247. Chen, R., Gandhi, V. & Plunkett, W. A sequential blockade strategy for the design of combination therapies to overcome oncogene addiction in chronic myelogenous leukemia. *Cancer Res.* **66**, 10959–10966 (2006).

248. Kawano, T. *et al.* MUC1 oncoprotein regulates Bcr-Abl stability and pathogenesis in chronic myelogenous leukemia cells. *Cancer Res.* **67**, 11576–11584 (2007).

249. Wu, L. X. *et al.* Disruption of the Bcr-Abl/Hsp90 protein complex: a possible mechanism to inhibit Bcr-Abl-positive human leukemic blasts by novobiocin. *Leukemia* **22**, 1402–1409 (2008).

250. Dierks, C. *et al.* Expansion of Bcr-Abl-Positive Leukemic Stem Cells Is Dependent on Hedgehog Pathway Activation. *Cancer Cell* **14**, 238–249 (2008).

251. Gregory, M. A. *et al.* Wnt/Ca2+/NFAT Signaling Maintains Survival of Ph+ Leukemia Cells upon Inhibition of Bcr-Abl. *Cancer Cell* **18**, 74–87 (2010).

252. Hess, P., Pihan, G., Sawyers, C. L., Flavell, R. A. & Davis, R. J. Survival signaling mediated by c-Jun NH2-terminal kinase in transformed B lymphoblasts. *Nat. Genet.* **32**, 201–205 (2002).

253. Zhao, C. *et al.* Hedgehog signalling is essential for maintenance of cancer stem cells in

myeloid leukaemia. *Nature* **458**, 776–779 (2009).

254. Nagar, B. *et al.* Organization of the SH3-SH2 Unit in Active and Inactive Forms of the c-Abl Tyrosine Kinase. *Mol. Cell* **21**, 787–798 (2006).

255. Brasher, B. B. & Van Etten, R. A. c-Abl has high intrinsic tyrosine kinase activity that is stimulated by mutation of the Src homology 3 domain and by autophosphorylation at two distinct regulatory tyrosines. *Journal of Biological Chemistry* **275**, 35631–35637 (2000).

256. Golub, T. R. *et al.* Oligomerization of the ABL tyrosine kinase by the Ets protein TEL in human leukemia. *Mol. Cell. Biol.* **16**, 4107–4116 (1996).

257. Deininger, M. W., Goldman, J. M. & Melo, J. V. The molecular biology of chronic myeloid leukemia. *Blood* **96**, 3343–3356 (2000).

258. Smith, K. M., Yacobi, R. & Van Etten, R. A. Autoinhibition of Bcr-Abl through Its SH3 Domain. *Mol. Cell* **12**, 27–37 (2003).

259. Kelliher, M. A., McLaughlin, J., Witte, O. N. & Rosenberg, N. Induction of a chronic myelogenous leukemia-like syndrome in mice with v-abl and BCR/ABL. *Proc. Natl. Acad. Sci. U.S.A.* **87**, 6649–6653 (1990).

260. Schindler, T. *et al.* Structural mechanism for STI-571 inhibition of abelson tyrosine kinase. *Science* **289**, 1938–1942 (2000).

261. Miranda, M. B. & Johnson, D. E. Signal transduction pathways that contribute to myeloid differentiation. *Leukemia* **21**, 1363–1377 (2007).

262. McLaughlin, J., Chianese, E. & Witte, O. N. In vitro transformation of immature hematopoietic cells by the P210 BCR/ABL oncogene product of the Philadelphia chromosome. *Proc. Natl. Acad. Sci. U.S.A.* **84**, 6558–6562 (1987).

263. Wong, S. *et al.* IL-3 receptor signaling is dispensable for BCR-ABL-induced myeloproliferative disease. *Proc. Natl. Acad. Sci. U.S.A.* **100**, 11630–11635 (2003).

264. Okabe, M. *et al.* Establishment and characterization of a cell line, TOM-1, derived from a patient with Philadelphia chromosome-positive acute lymphocytic leukemia. *Blood* **69**, 990–998 (1987).

265. de Vos, S. *et al.* Gene Expression Profile of Serial Samples of Transformed B-Cell Lymphomas. *Lab Invest* **83**, 271–285 (2003).

266. Skaggs, B. J. *et al.* Phosphorylation of the ATP-binding loop directs oncogenicity of drug-resistant BCR-ABL mutants. *Proc. Natl. Acad. Sci. U.S.A.* **103**, 19466–19471 (2006).

267. Gross, A. W., Zhang, X. & Ren, R. Bcr-Abl with an SH3 deletion retains the ability To induce a myeloproliferative disease in mice, yet c-Abl activated by an SH3 deletion induces only lymphoid malignancy. *Mol. Cell. Biol.* **19**, 6918–6928 (1999).

268. Skorski, T. *et al.* The SH3 domain contributes to BCR/ABL-dependent leukemogenesis in vivo: role in adhesion, invasion, and homing. *Blood* **91**, 406–418 (1998).

269. Clark, S. S., Chen, E., Fizzotti, M., Witte, O. N. & Malkovska, V. BCR-ABL and v-abl oncogenes induce distinct patterns of thymic lymphoma involving different lymphocyte subsets. *J. Virol.* **67**, 6033–6046 (1993).

270. Chen, S., O'Reilly, L. P., Smithgall, T. E. & Engen, J. R. Tyrosine Phosphorylation in the SH3 Domain Disrupts Negative Regulatory Interactions within the c-Abl Kinase Core. *J. Mol. Biol.* **383**, 414–423 (2008).

271. Weng, A. P. *et al.* Activating mutations of NOTCH1 in human T cell acute lymphoblastic leukemia. *Science* **306**, 269–271 (2004).

272. Talora, C., Sgroi, D. C., Crum, C. P. & Dotto, G. P. Specific down-modulation of Notch1 signaling in cervical cancer cells is required for sustained HPV-E6/E7 expression and late steps of malignant transformation. *Genes Dev.* **16**, 2252–2263 (2002).

273. Azam, M., Latek, R. R. & Daley, G. Q. Mechanisms of Autoinhibition and STI-571/Imatinib Resistance Revealed by Mutagenesis of BCR-ABL. *Cell* **112**, 831–843 (2003).

274. Sherbenou, D. W. *et al.* BCR-ABL SH3-SH2 domain mutations in chronic myeloid leukemia patients on imatinib. *Blood* **116**, 3278–3285 (2010).

275. Hardy, R. R. & Hayakawa, K. B-lineage differentiation stages resolved by multiparameter flow cytometry. *Annals of the New York Academy of Sciences* **764**, 19–24 (1995).

276. Klemm, L. *et al.* The B Cell Mutator AID Promotes B Lymphoid Blast Crisis and Drug Resistance in Chronic Myeloid Leukemia. *Cancer Cell* **16**, 232–245 (2009).

277. Mardiney, M. & Malech, H. L. Enhanced engraftment of hematopoietic progenitor cells in mice treated with granulocyte colony-stimulating factor before low-dose irradiation: implications for gene therapy. *Blood* **87**, 4049–4056 (1996).

278. Kurzrock, R., Gutterman, J. U. & Talpaz, M. The molecular genetics of Philadelphia chromosome-positive leukemias. *N. Engl. J. Med.* **319**, 990–998 (1988).

279. Shah, N. P. *et al.* Multiple BCR-ABL kinase domain mutations confer polyclonal resistance to the tyrosine kinase inhibitor imatinib (STI571) in chronic phase and blast crisis chronic myeloid leukemia. *Cancer Cell* **2**, 117–125 (2002).

280. Druker, B. J., Guilhot, F., O'Brien, S., Larson, R. A.IRIS Long-term benefits of imatinib (IM) for patients newly diagnosed with chronic myelogenous leukemia in chronic phase (CML-CP): The 5-year update from the IRIS study. *Journal of Clinical Oncology* **24**, 338S–338S (2006).

281. Kantarjian, H. M. *et al.* Nilotinib (formerly AMN107), a highly selective BCR-ABL tyrosine kinase inhibitor, is effective in patients with Philadelphia chromosome-positive

chronic myelogenous leukemia in chronic phase following imatinib resistance and intolerance. *Blood* **110**, 3540–3546 (2007).

282. Khoury, H. J. *et al.* Bosutinib is active in chronic phase chronic myeloid leukemia after imatinib and dasatinib and/or nilotinib therapy failure. *Blood* **119**, 3403–3412 (2012).

283. Cortes, J. E. *et al.* Ponatinib in refractory Philadelphia chromosome-positive leukemias. *N. Engl. J. Med.* **367**, 2075–2088 (2012).

284. Smith, K. M., Yacobi, R. & Van Etten, R. A. Autoinhibition of Bcr-Abl through its SH3 domain. *Mol. Cell* **12**, 27–37 (2003).

285. Dixon, A. S., Constance, J. E., Tanaka, T., Rabbitts, T. H. & Lim, C. S. Changing the subcellular location of the oncoprotein Bcr-Abl using rationally designed capture motifs. *Pharm. Res.* **29**, 1098–1109 (2012).

286. Yuan, J. & Wang, G. Lanthanide complex-based fluorescence label for time-resolved fluorescence bioassay. *J Fluoresc* **15**, 559–568 (2005).

287. Miller, N. J., Castelluccio, C., Tijburg, L. & RiceEvans, C. The antioxidant properties of theaflavins and their gallate esters - Radical scavengers or metal chelators? *FEBS Lett.* **392**, 40–44 (1996).

288. Hibasami, H. *et al.* Black tea theaflavins induce programmed cell death in cultured human stomach cancer cells. *Int. J. Mol. Med.* **1**, 725–727 (1998).

289. Liang, Y. C. *et al.* Suppression of extracellular signals and cell proliferation by the black tea polyphenol, theaflavin-3,3 '-digallate (vol 20, pg 733, 1999). *Carcinogenesis* **20**, 1383–1383 (1999).

290. Jacquel, A. *et al.* Imatinib induces mitochondria-dependent apoptosis of the Bcr-Abl-positive K562 cell line and its differentiation toward the erythroid lineage. *FASEB J.* **17**, 2160–2162 (2003).

291. Kawano, T. *et al.* Inactivation of ERK accelerates erythroid differentiation of K562 cells induced by herbimycin A and STI571 while activation of MEK1 interferes with it. *Mol. Cell. Biochem.* **258**, 25–33 (2004).

292. Jin, L., Wang, W. & Fang, G. Targeting protein-protein interaction by small molecules. *Annu. Rev. Pharmacol. Toxicol.* **54**, 435–456 (2014).

293. Zhang, J., Chung, T. & Oldenburg, K. A Simple Statistical Parameter for Use in Evaluation and Validation of High Throughput Screening Assays. *J Biomol Screen* **4**, 67–73 (1999).

294. Baxter, N. J., Lilley, T. H., Haslam, E. & Williamson, M. P. Multiple interactions between polyphenols and a salivary proline-rich protein repeat result in complexation and precipitation. *Biochemistry* **36**, 5566–5577 (1997).

295. Charlton, A. J. *et al.* Tannin interactions with a full-length human salivary proline-rich

protein display a stronger affinity than with single proline-rich repeats. *FEBS Lett.* **382**, 289–292 (1996).

296. Adrián, F. J. *et al.* Allosteric inhibitors of Bcr-abl-dependent cell proliferation. *Nat. Chem. Biol.* **2**, 95–102 (2006).

297. Zhang, J. *et al.* Targeting Bcr-Abl by combining allosteric with ATP-binding-site inhibitors. *Nature* **463**, 501–506 (2010).

298. Klein, E. *et al.* Properties of the K562 cell line, derived from a patient with chronic myeloid leukemia. *Int. J. Cancer* **18**, 421–431 (1976).

299. Cox, A. D., Fesik, S. W., Kimmelman, A. C., Luo, J. & Der, C. J. Drugging the undruggable RAS: Mission possible? *Nat Rev Drug Discov* **13**, 828–851 (2014).

300. Xie, J., Supekova, L. & Schultz, P. G. A genetically encoded metabolically stable analogue of phosphotyrosine in Escherichia coli. *ACS Chem. Biol.* **2**, 474–478 (2007).

301. Honda, M., Okuno, Y., Yoo, J., Ha, T. & Spies, M. Tyrosine phosphorylation enhances RAD52-mediated annealing by modulating its DNA binding. *EMBO J.* **30**, 3368–3382 (2011).

302. Stieglitz, B. *et al.* Novel type of Ras effector interaction established between tumour suppressor NORE1A and Ras switch II. *EMBO J.* **27**, 1995–2005 (2008).

303. Pacold, M. E. *et al.* Crystal structure and functional analysis of Ras binding to its effector phosphoinositide 3-kinase gamma. *Cell* **103**, 931–943 (2000).

304. Vetter, I. R. *et al.* Structural and biochemical analysis of Ras-effector signaling via RalGDS. *FEBS Lett.* **451**, 175–180 (1999).

305. Gorden, A. *et al.* Analysis of BRAF and N-RAS mutations in metastatic melanoma tissues. *Cancer Res.* **63**, 3955–3957 (2003).

306. Pekar, O. *et al.* EHD2 shuttles to the nucleus and represses transcription. *Biochem. J.* **444**, 383–394 (2012).

307. Pilecka, I., Banach-Orlowska, M. & Miaczynska, M. Nuclear functions of endocytic proteins. *Eur. J. Cell Biol.* **86**, 533–547 (2007).

308. Kimura, T., Sakisaka, T., Baba, T., Yamada, T. & Takai, Y. Involvement of the Ras-Ras-activated Rab5 guanine nucleotide exchange factor RIN2-Rab5 pathway in the hepatocyte growth factor-induced endocytosis of E-cadherin. *Journal of Biological Chemistry* **281**, 10598–10609 (2006).

309. Cao, X., Tanis, K. Q., Koleske, A. J. & Colicelli, J. Enhancement of ABL kinase catalytic efficiency by a direct binding regulator is independent of other regulatory mechanisms. *Journal of Biological Chemistry* **283**, 31401–31407 (2008).

310. Van Etten, R. A. Models of chronic myeloid leukemia. *Curr Oncol Rep* **3**, 228–237 (2001).